AD-A231 782 Progress Report

EXPERIMENTAL AND THEORETICAL STUDIES OF HIGH POWER PLASMA FILLED BACKWARD WAVE OSCILLATORS

For the Period
August 1, 1990 to January 31, 1991

Principal Investigators

T.M. Antonsen, Jr., Y. Carmel, W.W. Destler,
V.L. Granatstein, and B. Levush

Laboratory for Plasma Research
and
Electrical Engineering Department
University of Maryland, College Park, MD 20742

February 1991

MAR 06

i

91 2 19 180

Progress Report

EXPERIMENTAL AND THEORETICAL STUDIES OF HIGH POWER PLASMA FILLED BACKWARD WAVE OSCILLATORS

For the Period
August 1, 1990 to January 31, 1991

Principal Investigators

T.M. Antonsen, Jr., Y. Carmel, W.W. Destler,
V.L. Granatstein, and B. Levush

Laboratory for Plasma Research
and
Electrical Engineering Department
University of Maryland, College Park, MD 20742

February 1991

Statement "A" per telecon Dr. Charles
Roberson. INR/Code 1112AI

VHG   3/6/91

A-1

Contents

1 Executive Summary

This progress report summarizes the work done under the Grant No. N00014-89-K-2030 entitled "Experimental and Theoretical Studies of High Power Plasma Filled Backward Wave Oscillators" during the period August 1, 1989 to January 31, 1991.

Relativistic Backward Wave Oscillators (BWOs) have proven to be relatively efficient, high power microwave sources at the centimeter and millimeter wavelength range. It consists of a relativistic electron beam, a strong guiding magnetic field and a slow wave structure. Our approach for increasing the power generating capabilities of relativistic BWO's is to introduce plasma into the device. It is expected that in this way very large electron beam currents (well above the vacuum space charge limit) may be propagated, resulting in extremely high power microwave generation. Also, the plasma is expected to reduce the ac space charge in the beam, resulting in enhanced axial bunching and possibly enhancement in efficiency.

Previously, it was found experimentally that peak efficiency in the presence of the plasma can be greatly enhanced, by a factor of 8 (to about 40%). Also, we found that the plasma can be externally generated and then injected into the device. The experimental configuration is shown in Fig. 1. For a detailed drawing of the slow wave structure see Fig. 2.

The purpose of the research covered during this period was to study the behavior of a plasma loaded BWO when driven by large beam current approaching the vacuum space charge limiting value inside the device. The main results are:

1. The plasma indeed allows injection of large current into the BWO. Currents as high as 75% of the vacuum space charge limit were successfully propagated.

2. In plasma loaded BWO, in contrast to the vacuum case, the enhanced efficiency can be maintained even for large beam currents (approaching the vacuum limit). It is anticipated that this might hold even well beyond the vacuum limit.

3. The output frequency is only slightly shifted (1%-5%) by the presence of the plasma.

4. A foilless field emission diode can be operate successfully in a background of low density plasma.

5. An important parameter, the start oscillation current was measured for the first time in vacuum BWO for various beam voltages and geometries. For example, at 600 kV the start current is under 140 A.

6. Initial indications are that the plasma increases the microwave pulse duration.

7. A novel field emission cathode design (new geometries and materials) allows for continuous control of the beam current in the range of 50-6000 Amps. Turn on fields below 50 kV/cm were achieved.

8. Linear theory for a plasma loaded BWO was developed (using a simplified model).

9. A nonlinear theory for a finite length device was developed.

We achieved considerable progress on the experimental and theoretical aspects of microwave plasma electronics, as summarized below and reported in greater detail in Section 2 of this report.
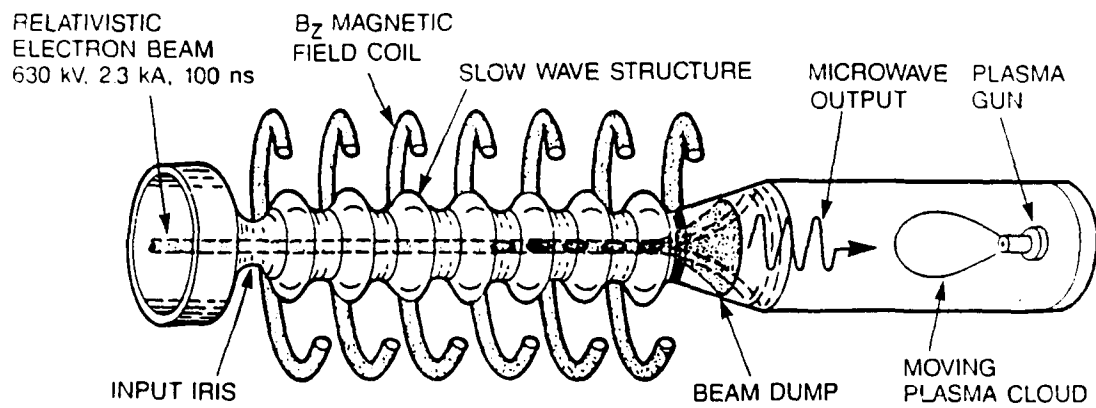
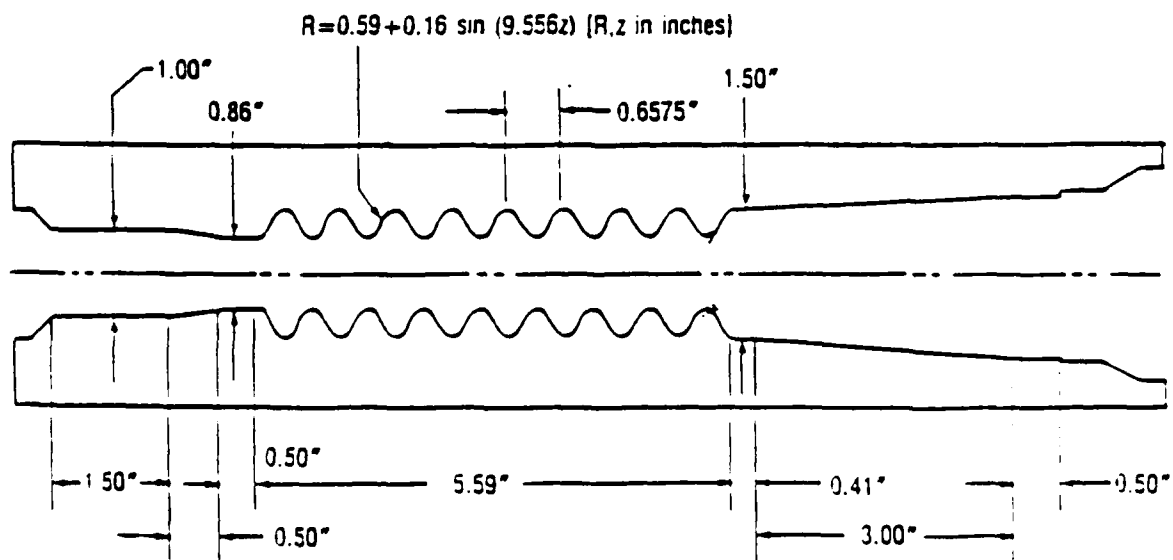Figure 1: Schematic diagram of the plasma loaded BWO experiment.

Figure 2: The rippled-wall slow-wave structure used in our plasma loaded BWO.

Novel Method for Determining the Electromagnetic Dispersion Relation of Periodic Slow Wave Structures A novel method for calculating the dispersion relation of electromagnetic modes in arbitrary periodic slow wave structures was found. In this method it is sufficient to know the frequencies corresponding to three special wave number values, with other points calculated using an approximate analytical expression. This technique was successfully applied to determine the dispersion relation of TM_{01} mode in a variety of slow wave structures. The results are in excellent agreement (within 0.15%) with other numerical and analytical techniques. (See Section 2.1.)

Studies of Novel Field Emission Guns for BWOs Experimental studies of novel non-planar, magnetically insulated, foilless, explosive emission guns were successfully completed. New geometries and materials were evaluated, resulting in the development of guns which turn on at very low average electric fields (about 50 kV/cm). These geometries include annular, single cathode design and annular, cylindrically symmetric double cathode design. Additional studies investigated the effects of several cathode emitting surfaces. We can now vary the beam current in the range of 50 A to 6 kA reproducibly. (See Section 2.2.)

The Physics of Relativistic Electron Beams Close to the Vacuum Space Charge Limiting Current This topic is important in the understanding of intense beam interaction in BWOs. It was found that the potential depression due to dc space charge drastically change the behavior of the space charge waves supported by the beams. (These waves are responsible for the interaction in a BWO.) For example, the phase velocity of the slow space charge wave vanishes at the limiting current. It was also found that the beam can support four space charge waves. A complete, fully relativistic dispersion relation for a thin, annular beam in an infinitely large magnetic field was analyzed numerically. (See Section 2.3.)

Plasma Characterization Measurements were made of plasma density, drift velocity and temperature as a function of time, space and magnetic field. Langmuir probes and interferometric techniques were used to characterize two kinds of plasma guns. (See Section 2.4.)

Experimental Studies of the Starting Current in a Relativistic Vacuum BWO The vacuum BWO was studied experimentally over wide range of beam currents, from the threshold (starting current) to 75% of the limiting current and over wide range of voltages and magnetic fields. Frequency, power and pulse shape were analyzed. For a 600 kV beam, the experimentally measured start current is under 140 A. (See Section 2.5.)

Frequency Pulling in Relativistic Vacuum BWOs The frequency of a vacuum BWO can be tuned by varying the beam voltage. Since the beam's space charge waves are drastically modified by space charge effects close to the limiting current, the exact relativistic dispersion relation was used to calculate the new interaction frequency. This frequency is defined here as the intersection of the slow space charge beam wave with the cold structure dispersion relation. The difference between the two is called "frequency pulling". It was calculated numerically for the cases of interest. (See Section 2.6.)

Experimental Studies of Plasma Loaded BWOs A plasma filled relativistic BWO was driven by an intense relativistic electron beam with current approaching the vacuum space charge limiting value. The beam propagation in plasma as well as the BWO characteristics such as power, frequency, and pulse duration were measured. Initial results indicate that the presence of plasma causes small frequency shifts (compared with the vacuum case) in addition to efficiency enhancement. It also helps to extend the pulse duration. Above a critical plasma density the interaction is quenched. (See Section 2.7.)

Finite Length Effects in BWOs When finite length effects (such as reflection coefficients at the ends) are taken into accounts, the slow wave structure behave much like a cavity with discrete axial resonances for a fixed transverse mode. The number of these resonances is equal to the number of periods in the slow wave structure plus one. We have designed and fabricated a cold test system to measure these resonances as well as the reflection coefficient and the dispersion relation of the TM_{01} mode in the actual structure. These resonances are due to various axial modes. (See Section 2.8.)

Linear Theory of Plasma Loaded BWO Linear theory of plasma loaded BWO was developed (for infinitely strong guiding magnetic field, solid beam and neglecting electron plasma waves). It shows that below some critical background plasma density the instability is absolute (BWO), while above it is convective (TWT) in nature. Growth rates were also calculated. The linear theory will have to be expanded to better explain the experimental results. (See Section 2.9.)

Theory of Relativistic BWOs As a first step in the development of a comprehensive theory of plasma loaded relativistic BWO, we have developed a linear and nonlinear theory for a vacuum relativistic BWO of a finite length. The main result of our investigations is the discovery of regions in parameter space of single and multimode BWO operation. We found that the start oscillation current and the efficiency of a single frequency operation are sensitive to the choice of a operation point of a BWO. The operation point in stationary regime is modified by the presence of a low density plasma. However, preliminary estimates indicate that Maryland BWO is operating in overbunch unstable region (multimode regime). The effect of plasma in this regime will be a subject of the future investigations. (See Section 2.10.)

Open Research Topics We achieved considerable progress on both the experimental and theoretical aspects of plasma loaded BWO. Additional research is needed, however in order to take full benefit of the innovative approach of plasma microwave electronics. In particular we need to address such questions as operation well and above the vacuum space charge limiting current, over moded systems and understanding the operating regimes and pulse duration. (See Section 2.11.)

Our results were extensively documented, published in a timely manner, and caused considerable scientific interest. Fifteen papers of various kinds were published, including two in *Physical Review Letters* and three invited talks. (See Section 2.13.)

1

2 Research Progress

2.1 Novel Method for Determining the Electromagnetic Dispersion Relation of Periodic Slow Wave Structures

It is important to accurately know the dispersion relation of the slow wave structure in order to synchronize the phase velocity of the electromagnetic wave with the electron beam to produce efficient interaction. There are few techniques to calculate the dispersion relation of a slow wave structure. One technique relies on an equivalent lumped-element circuit model. Others are analytical and are suitable for sinusoidally or square wall small perturbations. Numerical techniques (like the code SUPERFISH) require considerable effort and time in order to accurately calculate the dispersion relation everywhere in the ω–k plane. Here, we developed a novel, accurate and simple method for calculating the dispersion relation of a slow wave structure of arbitrary geometry.

- **Basic Principle.** For any periodic slow wave structure with n periods, when shorted at both ends, there are $(n + 1)$ discrete resonant frequencies with a phase shift per period equally spaced between 0 and π. Instead of using a large number of points to accurately calculate the periodic dispersion relation in the range 0 to π, we calculate the resonant frequencies corresponding to three special normalized wavenumber values and then use an analytically expression to produce the complete dispersion curve.

- **Results.** For our sinusoidally corrugated slow wave structure (see Fig. 2); the radius is described by $R = R_0[1 + h\cos(2\pi z/L)]$ where R_0 is the average radius, h is the normalized corrugation amplitude, and L is the structure period. Superfish modeling yielded (with proper boundary conditions) the three special resonance frequencies f_0, $f_{\pi/2}$, f_π in the lower passband. The results are tabulate in Table 1. The corresponding mode patterns (electric field lines) are shown in Fig. 3.

The approximate form of the dispersion relation is given by $f = A - B\cos\beta L - C\cos^2\beta L$, where $A = f_{\pi/2}$; $B = (f_\pi - f_0)/2$; $C = f_{\pi/2} - (f_\pi + f_0)/2$. The calculated dispersion relation is plotted in Fig. 4.

In order to estimate the accuracy of this technique, we first calculate additional points on the dispersion curve using SUPERFISH. As an independent check, the dispersion relation derived here was compared to that derived by other techniques for the same structure. Both are in excellent agreement (within 0.15%) over the entire frequency band.
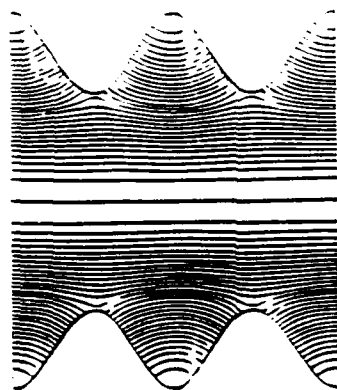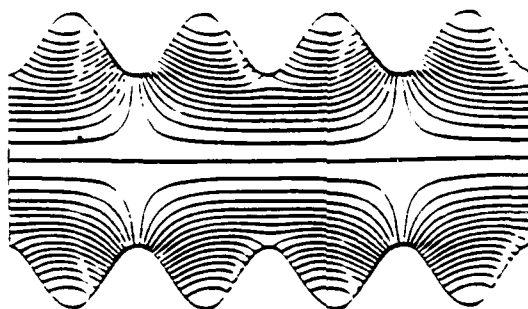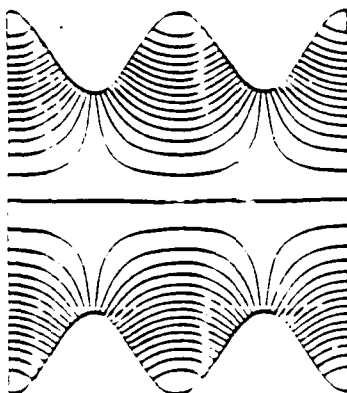
Figure 3: Mode patterns (electric field lines) corresponding to (a) zero phase-shift, (b) $\pi/2$ phase shift, and (c) π phase shift in the TM_{01} lower pass band of sinusoidally corrugated waveguide.

Table 1: The resonance frequencies (GHz) of a sinusoidally corrugated waveguide cavity
($R_0 = 1.5$ cm, $L = 1.67$ cm, $h = 0.273$).

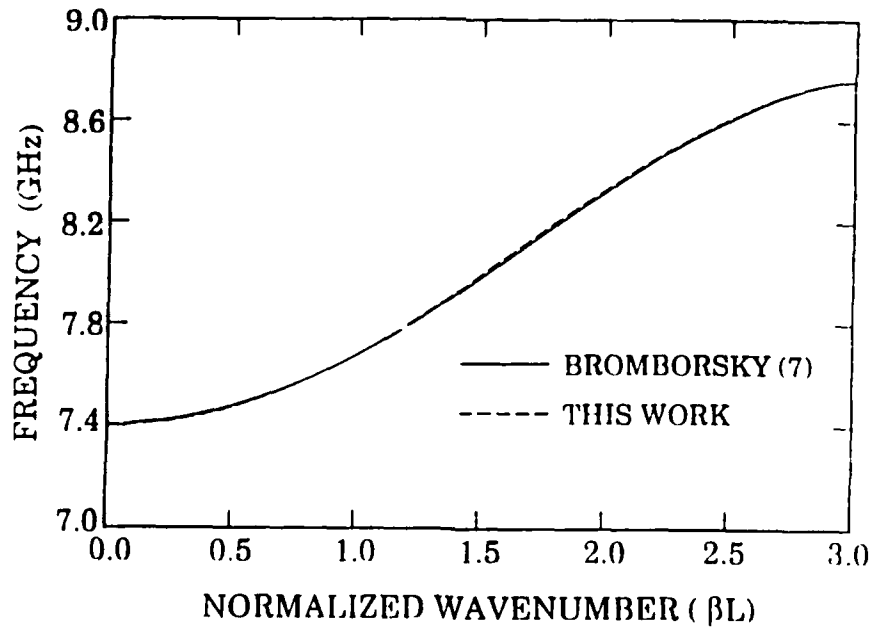| Resonance Frequency	2 period cavity	4 period cavity
$f_0 = f(\beta L = 0)$	4.404	7.412
$f(\beta L = \pi/4)$	N/A	7.589
$f_{\pi/2} = f(\beta L = \pi/2)$	8.046	8.046
$f(\beta L = 3\pi/4)$	N/A	8.557
$f_\pi = f(\beta L = \pi)$	8.773	8.754

Figure 4: Comparison of the TM_{01} dispersion curve of other technique (solid line) and this work (dotted line) for a sinusoidally corrugated waveguide.

2.2 Studies of Novel Field Emission Guns for BWOs

Explosive emission diodes are often used to generate the intense relativistic electron beams used in high power microwave devices. In contrast to typical explosive emission guns which produce beams with current densities on the order 10 kA/cm², we have studied cathode designs in which the beam current density is tunable over a wide range (200 A/cm²-12,000 A/cm²). This is necessary in order to access different operating regime of BWO, from the threshold (starting current) and up.

Purpose of This Work

- Use magnetically insulated, foilless emission explosive diodes to generate a hollow relativistic electron beam in a BWO slow wave structure. The beam radii are 7.75 mm and 2.6 mm with thicknesses 0.1 to 0.2 cm.

- Carefully analyze the operation of explosive emission diodes to determine how the microwave output power and resonant frequency depend on the parameters of the beam.

- Study the characteristics of the gun injection and beam propagation in magnetized BWO structures.

- Scan a wide range of currents from the BWO start oscillation current to the space charge limiting current. Both single and double cathode geometries are employed (see Fig. 5).

- Analyze the beam uniformity.

- Study cathode coating techniques to reduce the average electric field required for emission.

The Relativistic Diode Analysis
Suppose that the anode potential is zero, while the cathode is at potential of $\mathcal{O}_0$. Conservation of energy implies that

$$\gamma = 1 + \frac{e\mathcal{O}}{m_0 c^2}. \tag{1}$$

By solving Poisson's equation with the boundary condition:

$$\frac{d^2\mathcal{O}}{dz^2} = -\frac{J}{\epsilon_0 v_0} \tag{2}$$

We get the following relationship between current density and the applied voltage for the relativistic planar diode:

$$J = \frac{m_0 c^3 \epsilon_0}{2 e d^2} \left[F(\delta, 1/\sqrt{2}) - 2E(\delta, 1/\sqrt{2}) + \frac{2\gamma(\gamma^2 - 1)^{1/4}}{1 + (\gamma^2 - 1)^{1/2}} \right]^2 \tag{3}$$

where

$$\delta = \cos^{-1}\left[\frac{1 - (\gamma^2 - 1)^{1/2}}{1 + (\gamma^2 - 1)^{1/2}}\right]$$ (4)

and F and E are elliptic integrals of the first and second kind. In the limit of nonrelativistic beam, $e\phi/m_0c^2 \ll 1$, Eq.(3) reduces to the familiar Child-Langmuir expression:

$$J = \frac{4\sqrt{2}\epsilon_0}{9}\left(\frac{e}{m_0}\right)^{1/2}\frac{\phi^{3/2}}{d^2}$$ (5)

In the ultra-relativistic limit, $\gamma \gg 1$, Eq.(3) reduces to

$$U\zeta^{-2} = 1/2$$ (6)

where $U = e\phi/m_0c^2$ and $\zeta^2 = ed^2 J/m_0c^3\epsilon_0$.

A comparison of the normalized diode impedance for the relativistic and non-relativistic solution is presented in Fig. 6. The diode impedance decreases as the applied potential is increased. And also, the calculated current as a function of diode voltage is shown in Fig. 9 for a certain AK gap (12.5 mm).

Conclusions

1. The gun followed a Child-Langmuir-like law ($I \sim V^\alpha$). The experimentally measured power coefficient varies from 1 to 1.5 for different gun geometries, compared with 1.5 for the non-relativistic Child Langmuir law. Figures 7 and 8 show the experimental V-I characteristic of different gun geometries.

2. Using both single and double cathode configurations (see Fig. 5), the beam current ranges from 100 A to 6 kA (current density from 200 A/cm^2 to 12 kA/cm^2). Beam energies from 200 keV to 800 keV were generated.

3. The effective emission area is larger than the physical cathode area. For example, for AK Gap=12.5 mm, $A_{eff} = 10.8A_{phys}$ (see Fig. 9).

4. Graphite/epoxy cathode coating reduced the average electric field required for uniform emission to about 50 kV/cm. With the coating, we obtain a uniform beam at 150 A, while without the coating, this value was 350 A (400 kV) and the beam was filamented.

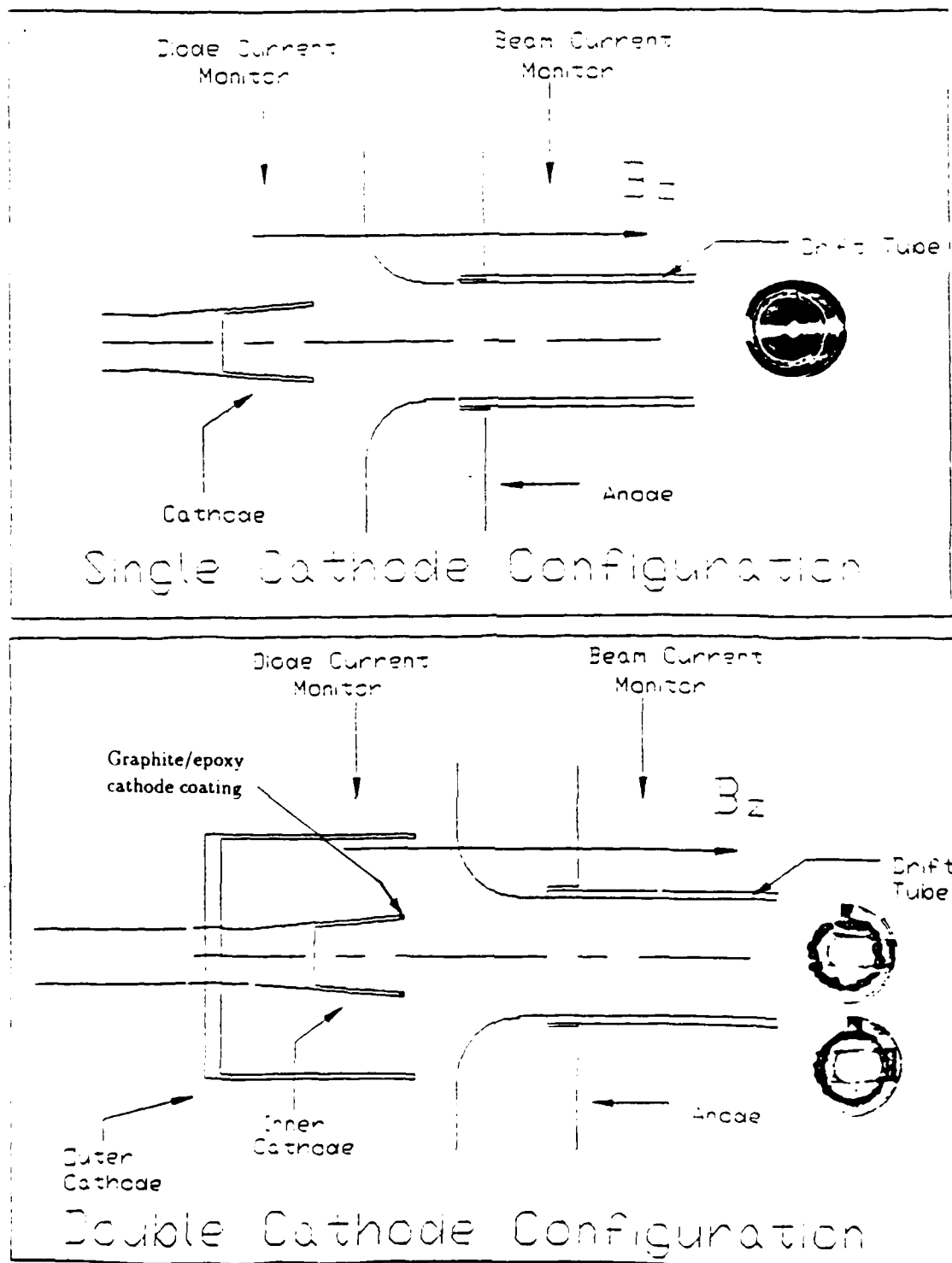Figure 5: Schematic diagram of the gun geometries as well as representative damage patterns

Planar Diode Gun Calculation
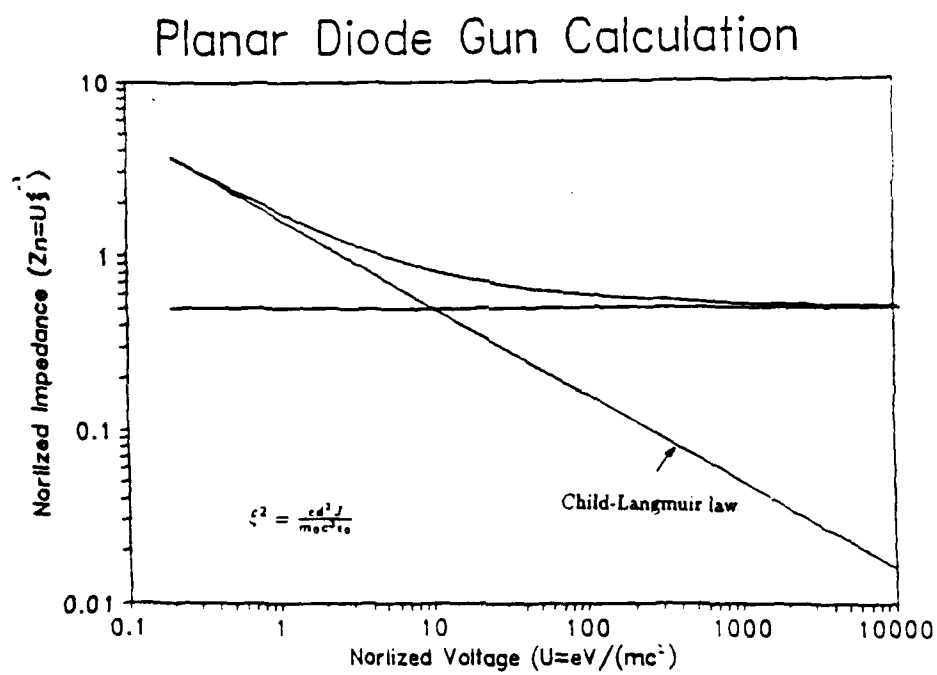
Figure 6: A comparison of the relativistic and nonrelativistic solution for the impedance of a one-dimensional planar diode.

11

DIODE CHARACTERISTICS
(Single Cathode)

beam radius=7.75mm

$I_4=V_1^{1.11118}*0.00316209$

$I_3=V_1^{1.11159}*0.00106943$

$I_2=V_1^{1.11112}*0.000627244$

$I_1=V_1^{1.11633}*0.000943586$

BEAM CHARACTERISTICS
(Single Cathode)

$I_5=V_1^{1.17315}*0.00438954$

$I_5=V_1^{1.12811}*0.00137086$

$I_5=V_1^{1.12281}*0.000483971$

$I_5=V_1^{1.11135}*0.000604031$

Figure 7: Experimental V-I characteristics for single cathode diodes (AK gap: 5.4: 7.5: 12.5: 31 mm).

GUN CHARACTERISTICS
(Double Cathode)

beam radius=7.75mm   w/o graphite/epoxy coating
$I_d = V_d^{1.399986} \cdot 0.00945993$

beam radius=7.75mm   w/ graphite/epoxy coating
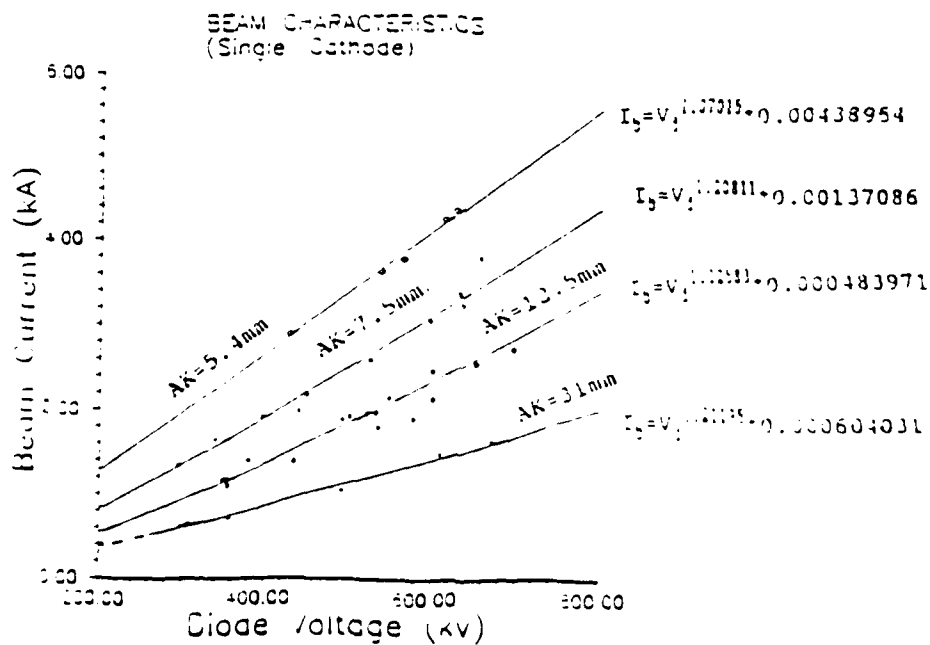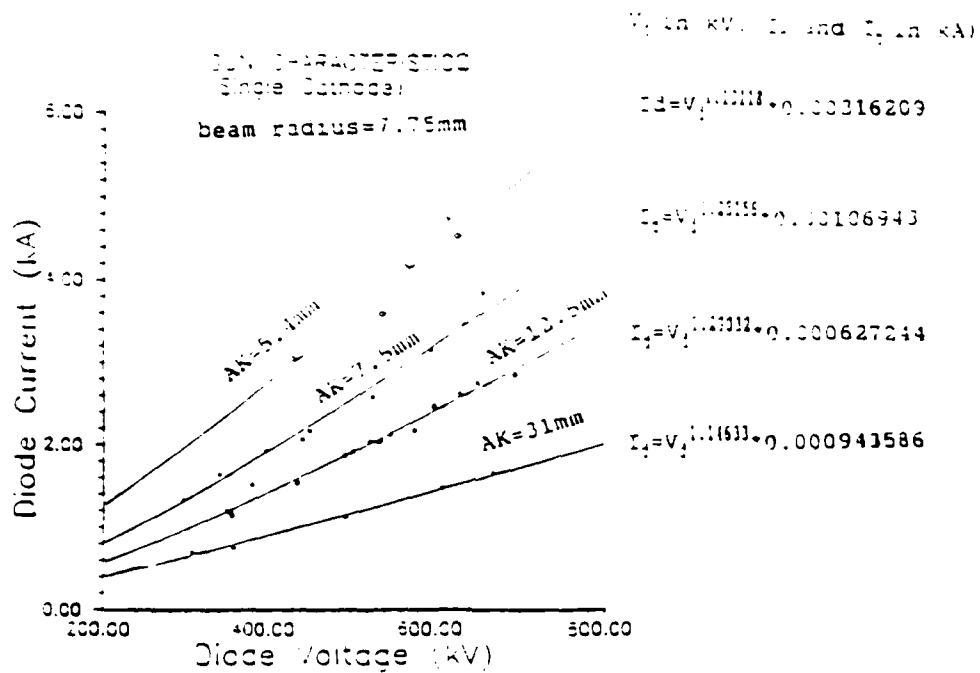$I_d = V_d^{1.22137} \cdot 0.00155513$

beam radius=2.6mm   w/ graphite/epoxy coating
$I_d = V_d^{1.36284} \cdot 0.000496272$

BEAM CHARACTERISTICS
(Double Cathode)

AKI/O=37/45mm $I_b = V_d^{1.22151} \cdot 0.00012273$

AKI/O=35/55mm $I_b = V_d^{1.65375} \cdot 1.31407E-5$

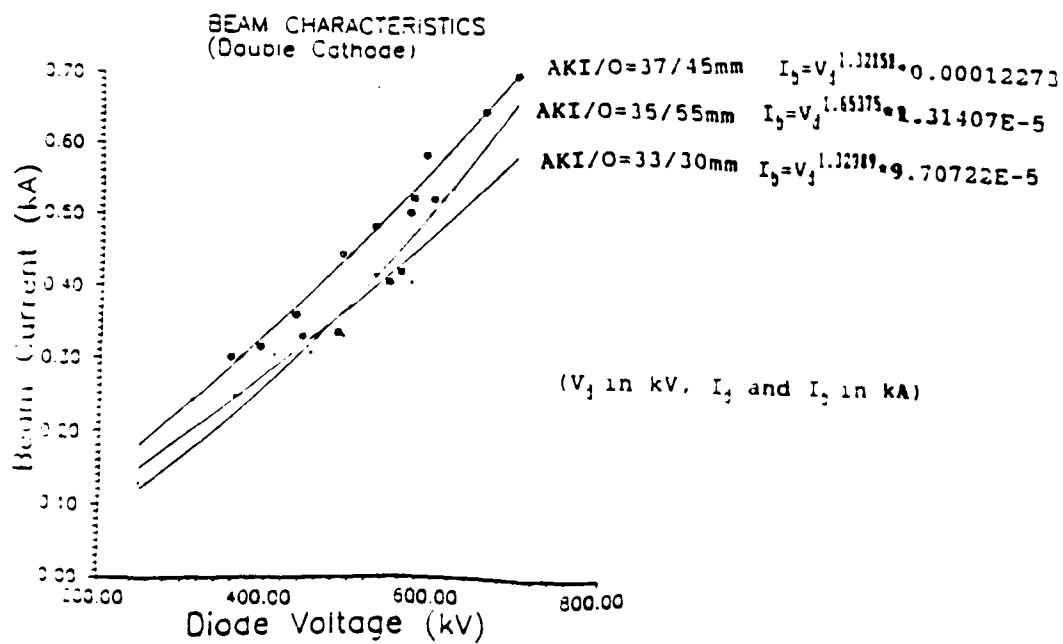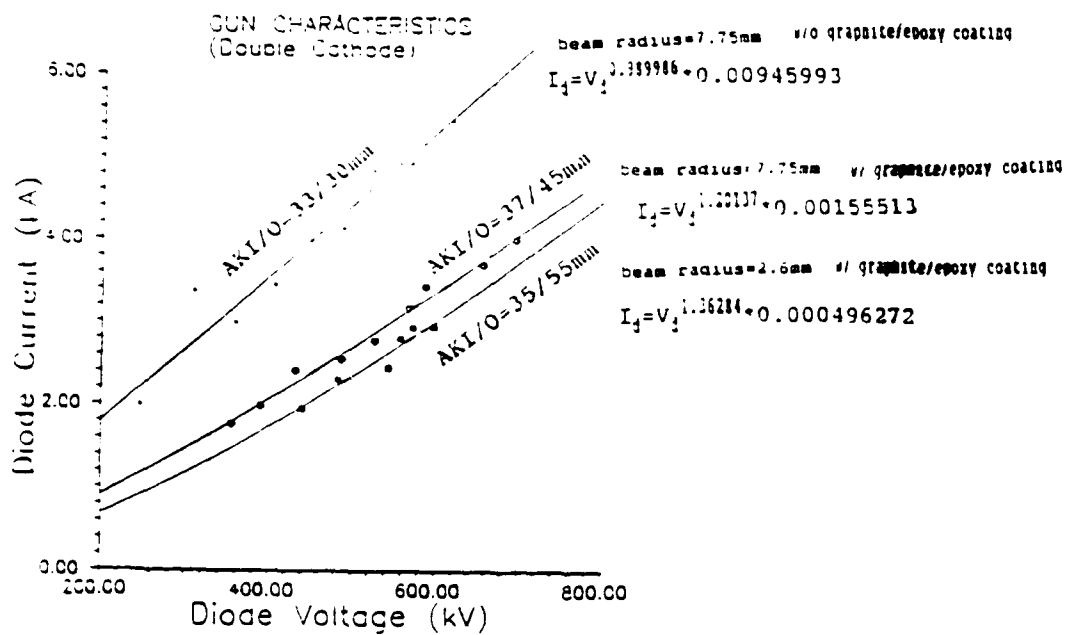AKI/O=33/30mm $I_b = V_d^{1.32389} \cdot 9.70722E-5$

(V_d in kV, I_d and I_b in kA)

Figure 8: Experimental V-I characteristics for double cathode diodes (AKI/O: 33/30: 37/45: 35/55 mm).

13

Effective Area Calculation
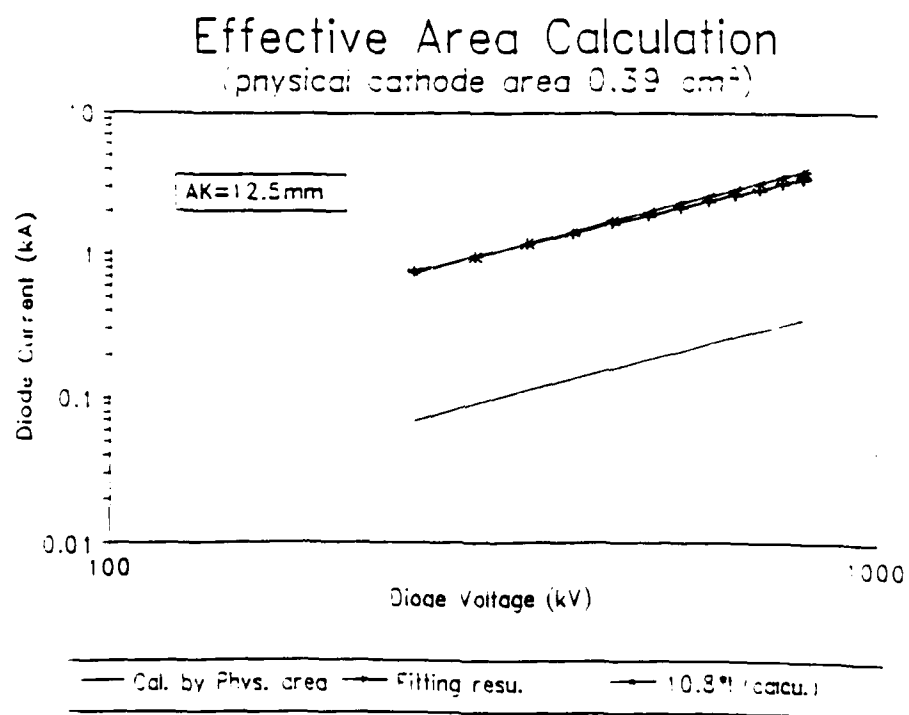## (pnysicai cathode area 0.39 cm²)

Figure 9: Effective area calculation for single cathod diode (AK gap: 12.5 mm).

2.3 The Physics of Relativistic Electron Beams Close to the Vacuum Space Charge Limiting Current

This subject is important for the understanding of intense beams interaction in BWOs, especially when the beam current approach the limiting value. This is clearly the case here, since under these condition we might expect to maximize the microwave output power (the plasma, of course, is expected to drastically change the beam behavior).

The electron beam drift energy is influenced by the diode potential (γ_c), beam current density (I_b) and the beam geometry. By solving Poisson's equation with the appropriate boundary condition, we get the well known dependence of I_{beam} on the effective beam energy γ_b is as follows

$$I_b = \frac{I_A}{2ln(r_0/r_b)}(\gamma_b^2 - 1)^{1/2}(\gamma_c/\gamma_b - 1) \tag{7}$$

where r_0 is the drift tube radius and r_b is the beam radius. Maximizing this expression with respect to the injection energy yield the absolute maximum current which can stably propagate under the ideal condition of infinitely large guiding magnetic field. This maximum value is plotted in Fig. 11, while the beam geometry is defined in Fig. 10.

When an electron beam is injected into the slow wave structure (instead of a smooth wall waveguide/drift tube) it may excite an unstable interaction. This instability occurs when a normal mode of structure having positive energy, interacts with the negative energy, slow space-charge wave of electron beam. By varying the slope of the slow space-charge wave of the electron beam, the interaction point is shifted along the dispersion curve of the structure. To accurately predict the operating frequency of the BWO, an understanding of dispersive characteristics of the slow space wave of the beam close to the vacuum space charge limiting current is necessary.

The dispersion relation for the space charge waves derived by the linear wave analysis for an annular, infinitely thin relativistic electron beam could be expressed as follows:

$$J_0(\Gamma r_0) + \alpha \left(\frac{\Gamma c}{\omega - kv_b}\right)^2 J_0(\Gamma r_b) [J_0(\Gamma r_b)N_0(\Gamma r_0) - J_0(\Gamma r_0)N_0(\Gamma r_b)] = 0 \tag{8}$$

where $\alpha \equiv \pi I_b/\beta_b\gamma_b^3 I_A$, $\Gamma^2 = \omega^2/c^2 - k^2$ and J_0, N_0 are the zeroth order Bessel functions of the first and second kind, respectively. α represents the space charge parameter.

Solving this equation numerically, we could get the ω vs k curves for the two space charge wave, the fast (positive energy) and the slow (negative energy). In Fig. 12, we show only the slow space charge wave (labeled SSCW) for various beam currents. We clearly see from this figure that as the current is increased (α is larger), the phase velocity ω/k decreases for the same injection energy. This phase velocity ($\omega/k|_{k\to 0}$) is plotted versus the beam current and it vanishes when the beam current exactly equals the space charge limiting value in vacuum (see Fig. 13). Furthermore, this phase velocity can also be negative. To understand this seemingly strange phenomena let's look at Fig. 14a, which is a plot of I_b vs γ_b. For a given cathode potential and a certain current, γ_b has two equilibrium solutions. One corresponds to a higher density and a lower velocity. Another corresponds to a lower density and high velocity. These two equilibrium solutions merges when the beam current exactly equals the vacuum space charge limiting value (i.e., the peak in I_b). At this point, the beam drift energy

(γ_b) equals to

$$\gamma_b = \gamma_c^{1/3} \tag{9}$$

We see that there are two equilibrium solution for a beam in a smooth drift section (i.e. waveguide), and therefore the beam can support two pairs of space charge waves. As an example, lets look at the 4 waves supported by a 2 kA beam with an injection energy of 600 kV. The conventional fast and slow wave are recovered for $\gamma_b > \gamma_c^{1/3}$ (Fig. 15) and a second pair exists for $\gamma_b < \gamma_c^{1/3}$ (Fig. 16). The solution which correspond to higher beam density and lower velocity is usually labeled as unstable. In this region, the electrostatic potential energy of each electron is larger than its kinetic energy. As indicated earlier, when the beam current exactly equal to the space charge limiting current, the two solutions merge (see Fig. 17). The consequences of this analysis will be further discussed in Section 2.6.
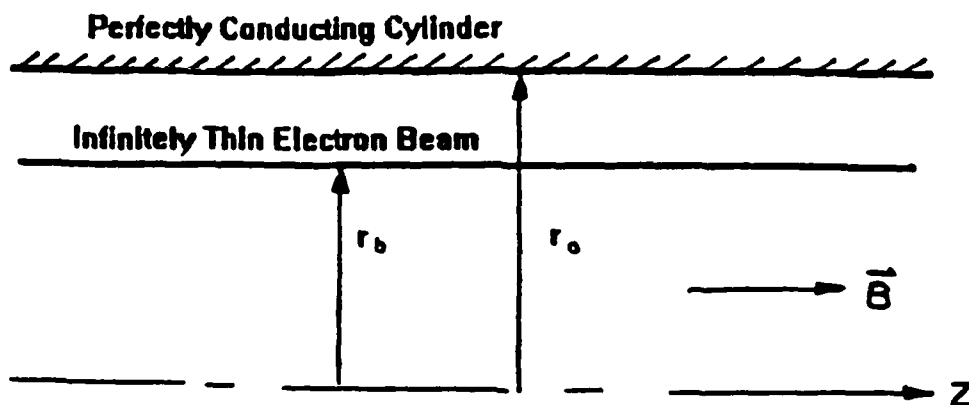
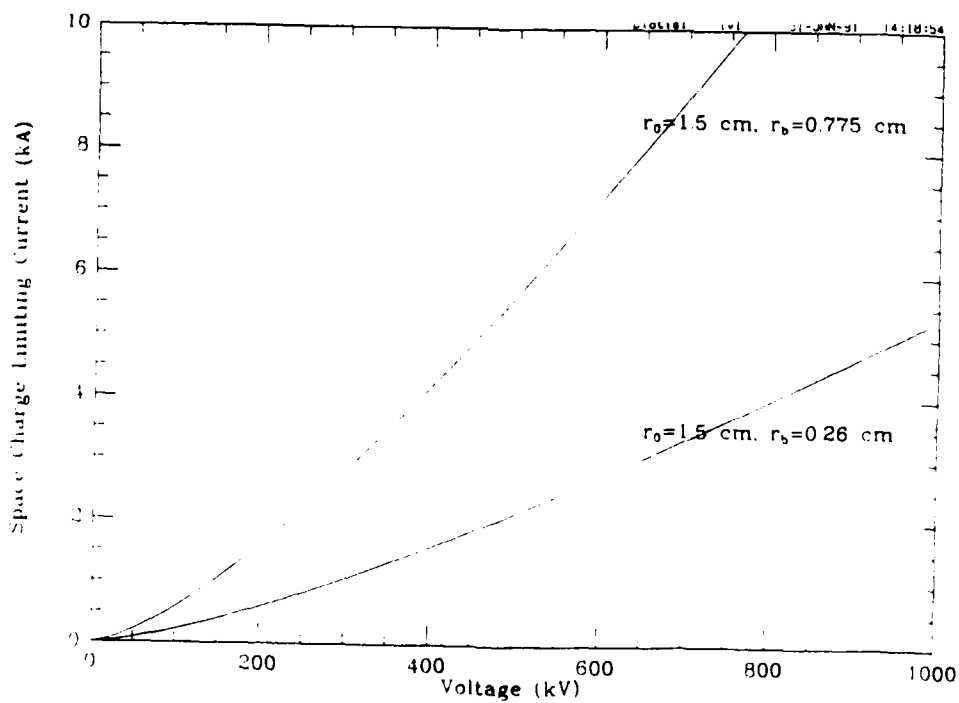Figure 10: The configuration of the beam geometry under consideration.

Figure 11: Space charge limiting current vs diode voltage with drift tube radius of 1.5 cm. beam radius of 0.775 cm and 0.26 cm (annular beam).
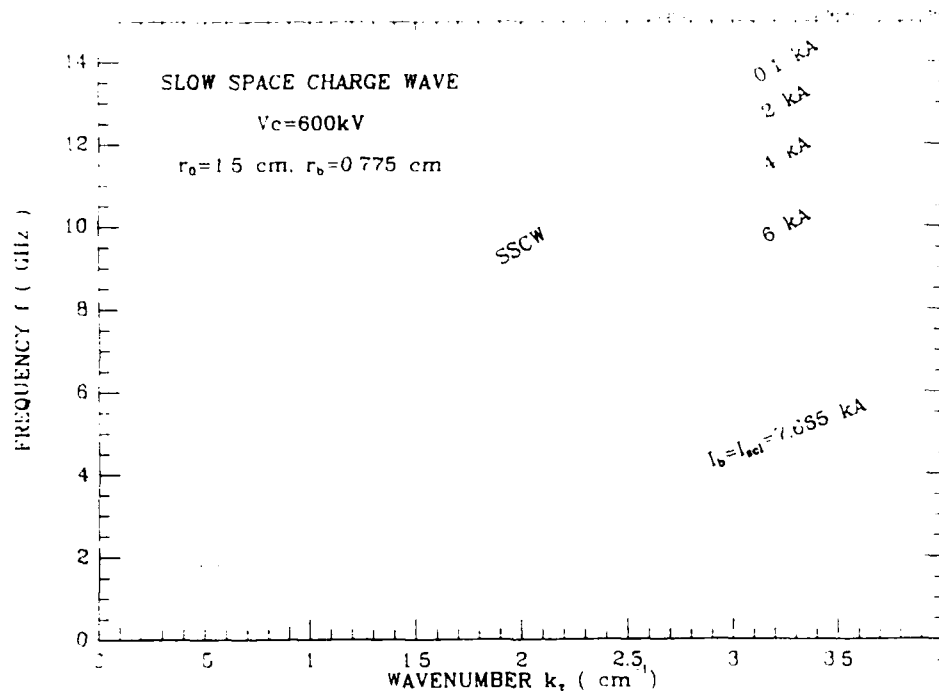
Figure 12: The dispersion characteristics of the slow space charge wave for different beam currents at 600 kV.
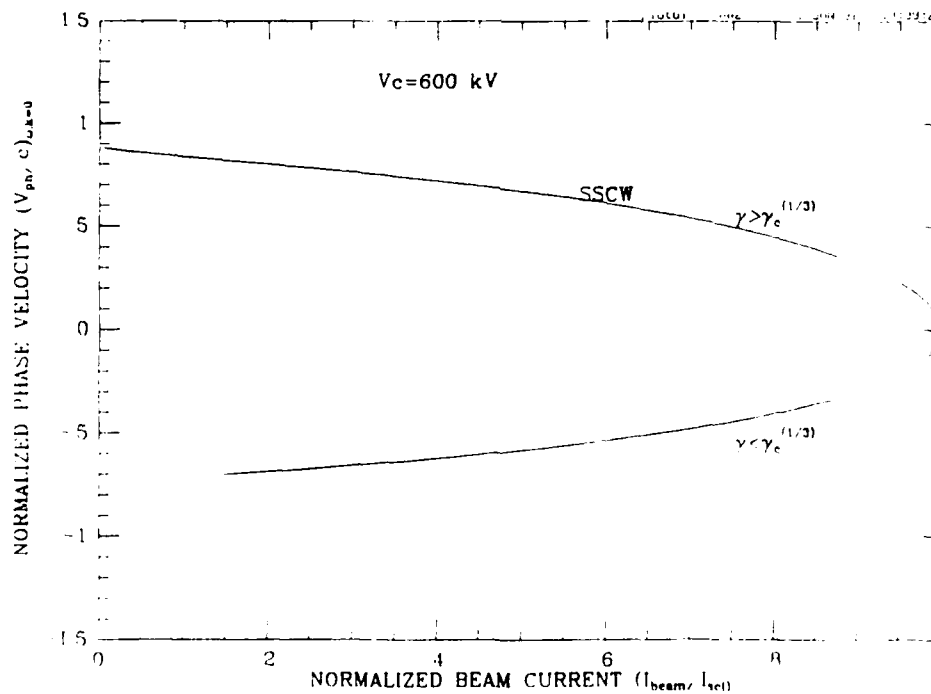
Figure 13: Normalized phase velocity of slow space charge vs normalized beam current.

18
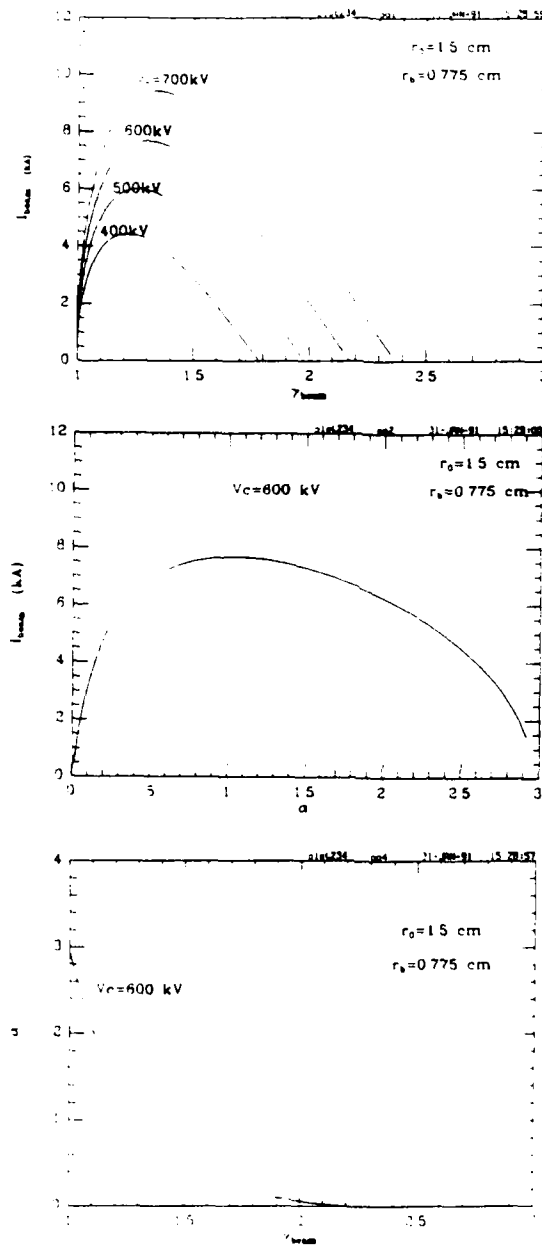
Figure 14: The relation between the beam current, the space charge parameter (α), and γ_b.

19
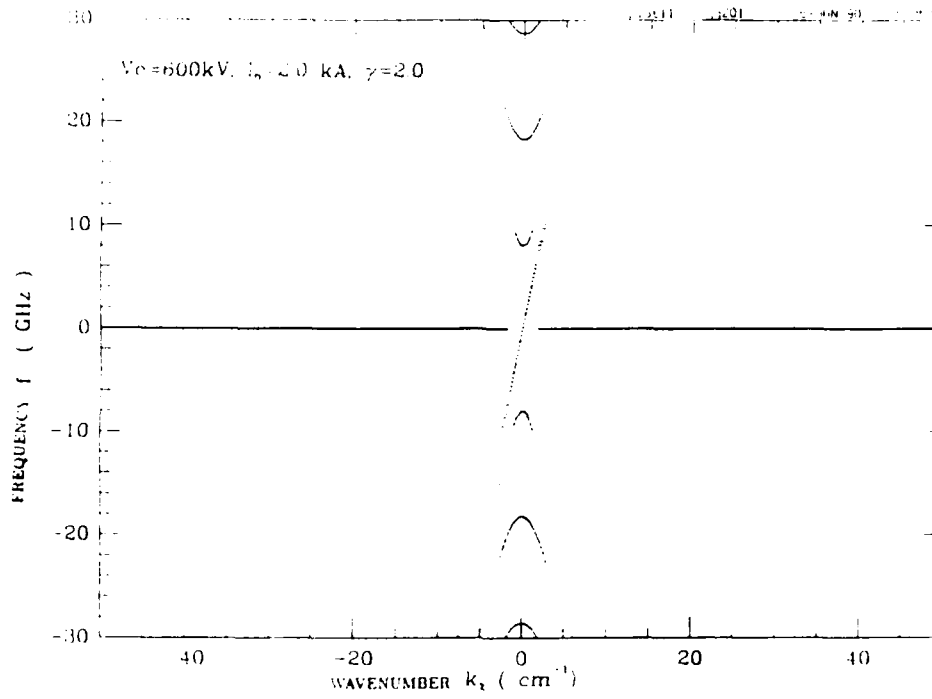
Figure 15: The dispersion relation of the two space charge waves supported by a beam for $\gamma_b > \gamma_c^{1/3}$.
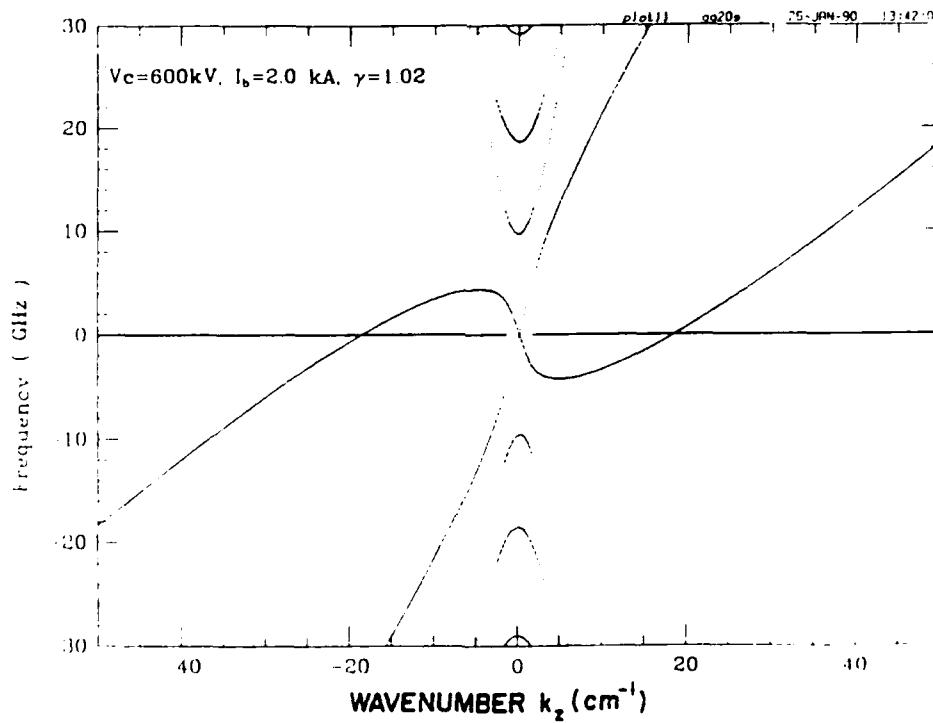
Figure 16: The dispersion relation of the two space charge waves supported by a beam for $\gamma_b < \gamma_c^{1/3}$.

Figure 17: The dispersion relation of the two space charge waves for $\gamma_b = \gamma_c^{1/3}$. (Under this condition the beam current equals the space charge limiting value.)

2.4 Plasma Characterization

In order to understand the physical mechanism of efficiency enhancement in a plasma BWO. i. is important to accurately measure the plasma characteristics. The gun is located in a field free region and the plasma is injected along the axis of a solenoidal magnetic field as shown in Fig. 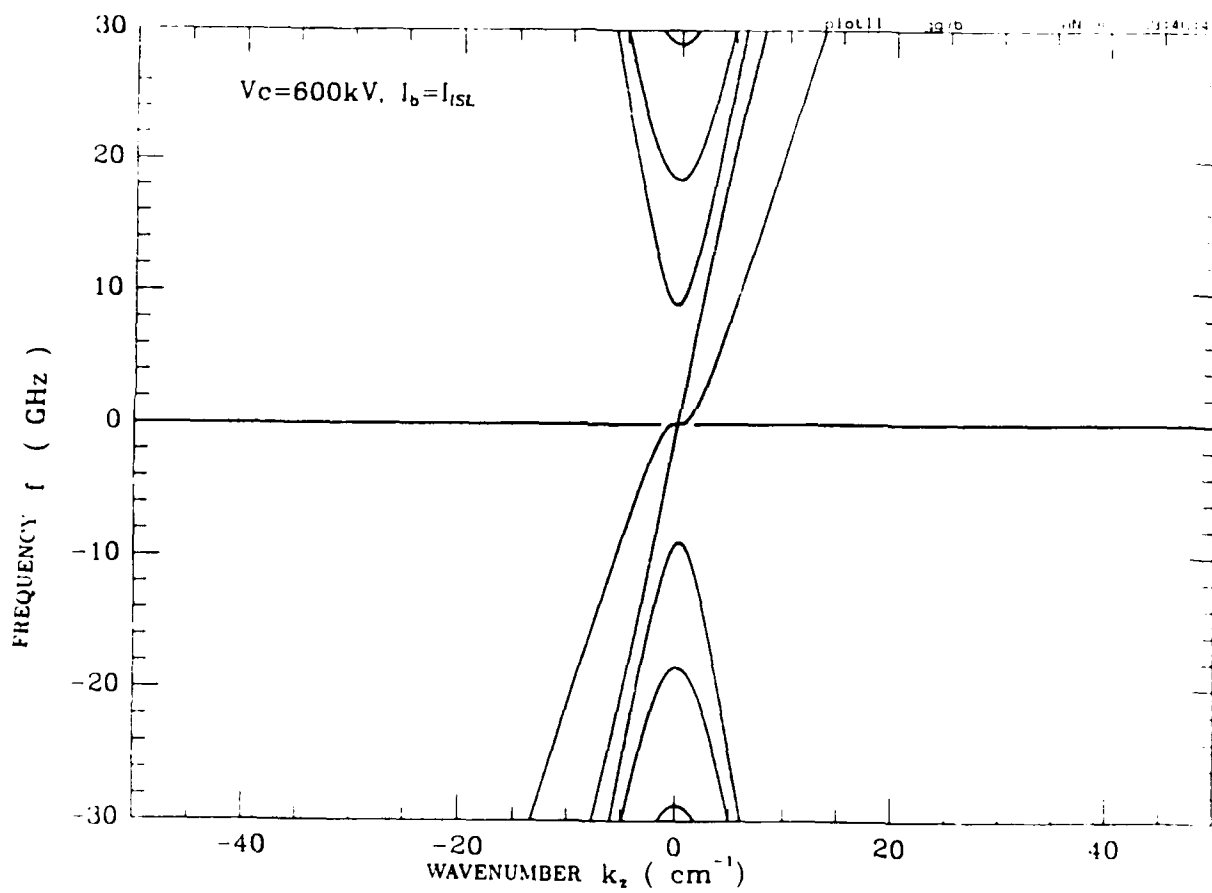18a. Measurements were made of the plasma density, drift velocity and temperature as a function of time, space and magnetic field. We have examined three types of plasma guns (Marshall. Coaxial, and Hydrogen Flashover gun). A sketch of the geometry for two of these two guns is given in Fig. 18b,c. We used both Langmuir probes and microwave interferometers to measure the plasma density with and without magnetic field. The sketch of the interferometer block diagram and Langmuir probe measurement circuit diagram was shown in Fig. 19. The plasma density vs distance is shown in Fig. 20. The plasma temperature, plasma drift velocity and plasma temperature for both guns are tabulated in Table 2 for the case of zero magnetic field. With magnetic field, the Langmuir probe was located about 1 m away from the gun which is about the same position of the interaction region of the BWO experiment. Figure 21 is the typical result of plasma density vs time inside the magnetic field ($B = 12$ kG) for Hydrogen Flashover gun. The hydrogen flashover gun generated a plasma cloud moving at an average velocity of about 5-10 cm/μsec and with a temperature of 5-15 eV. The detailed results are tabulated in Table 3.
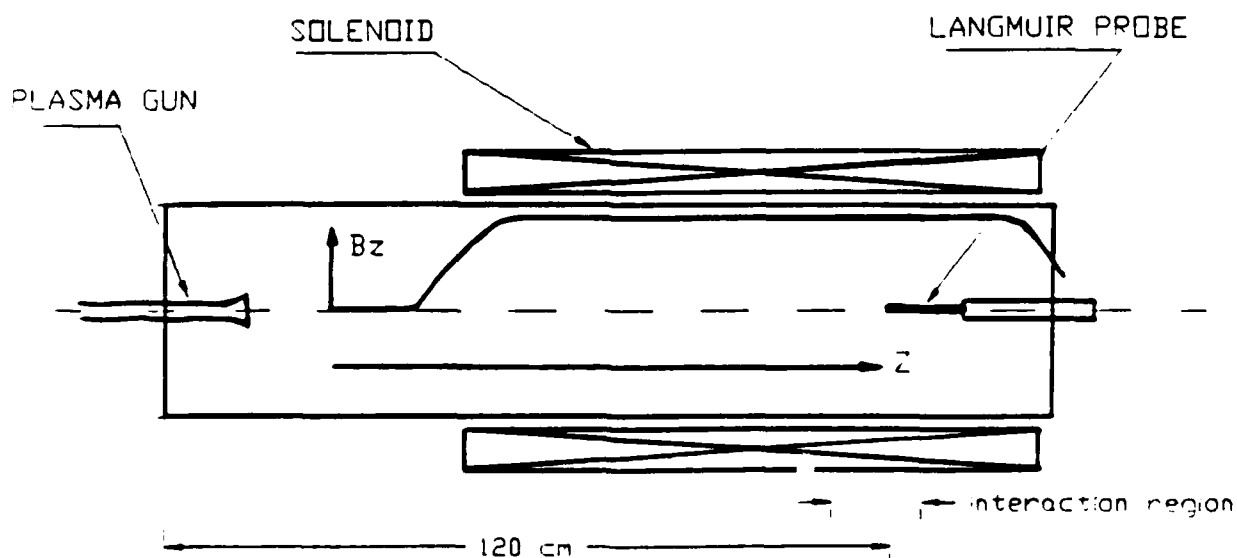
Figure 18a: A schematic diagram of the plasma gun and Langmuir probe position relative to the solenoidal magnetic field (for plasma characterization).

(b) **Marshall Plasma Gun**

(c) **Hydrogen Plasma Gun**

TiH2 in Sodium Silicate Solution

Brass
Solder
Graphite

1/4 Rigid Coax Cable Slide Through a Wilson Seal

Stainless Steel

Unit in inch
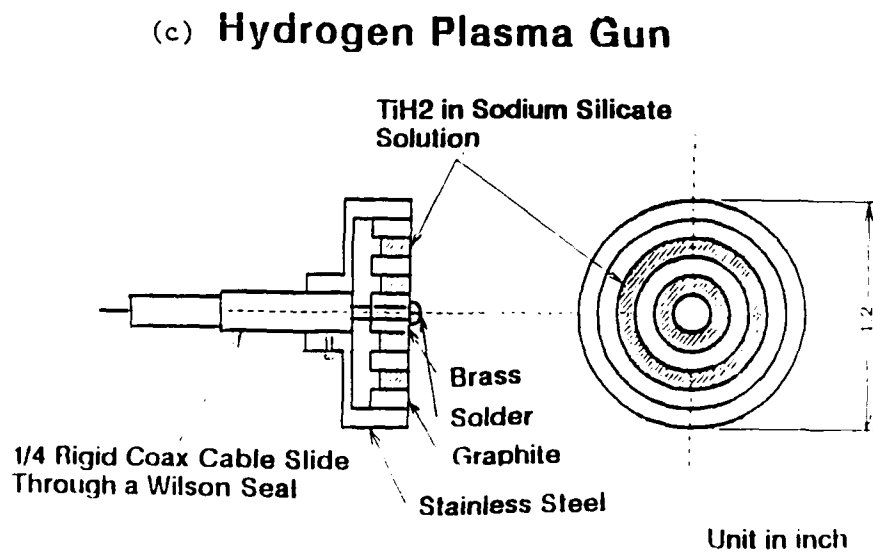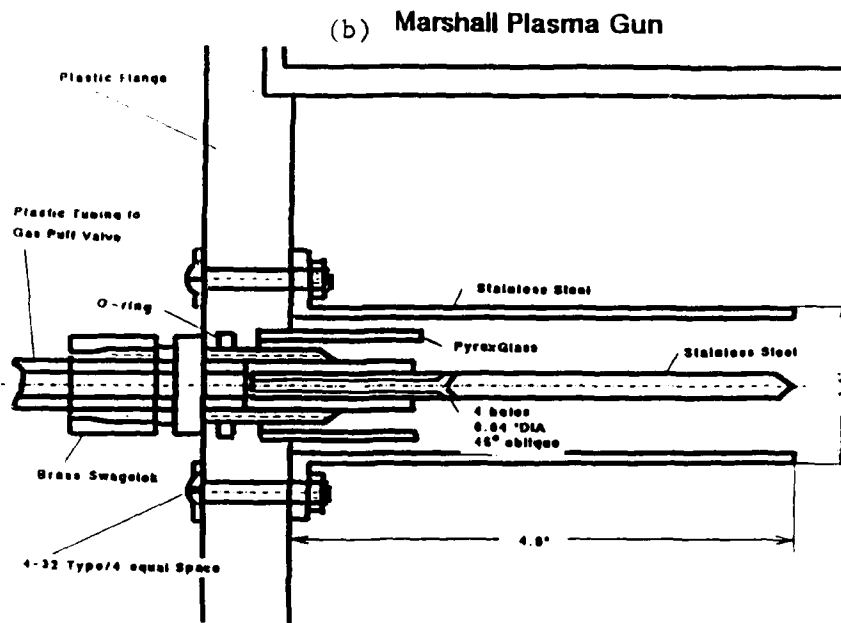
Figure 18: Sketch of geometry for (b) Marshall gun, (c) Hydrogen Flashover gun.
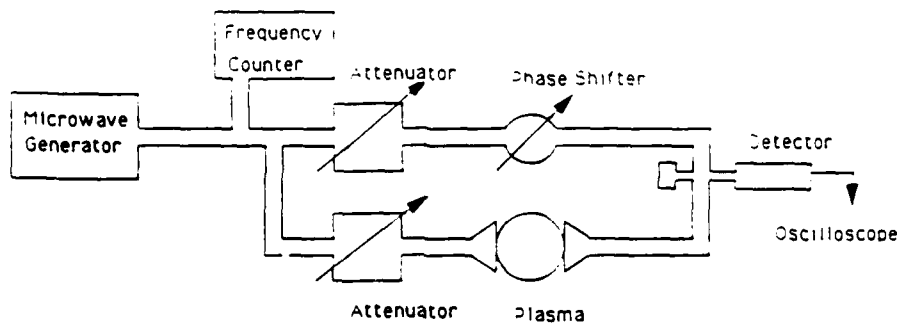
(a) Plasma density measurement using interferometer
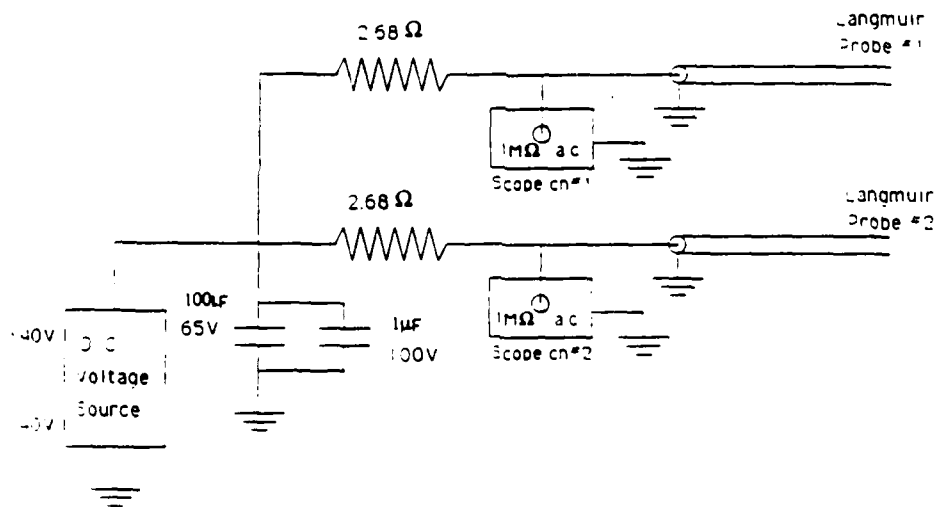
(b) Langmuir Probe Measurement Circuit

Figure 19: (a) Block diagram of Interferometric measurement. (b) Circuit sketch of Langmuir Probe measurement.

Plasma Density Measured from Ion Saturation Current

Hydrogen Flashover Gun

(Irvine Type)

Gun Charging Voltage=10kV

$B_z=0$

$1/r^3$ decay

plasma density ($\times 10^{11}$ cm^{-1})

distance away from the gun (cm)
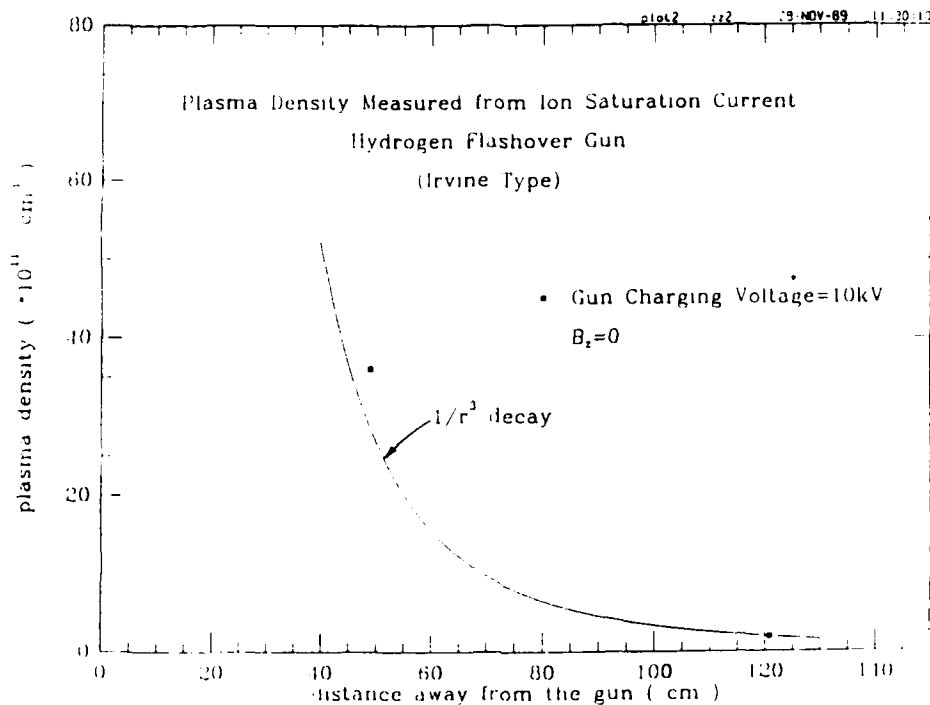
Figure 20: Plasma density vs distance without magnetic field.

$n_{max} = 2.0 \times 10^{11} cm^{-3}$

Plasma Density

Time (50 μs / div)
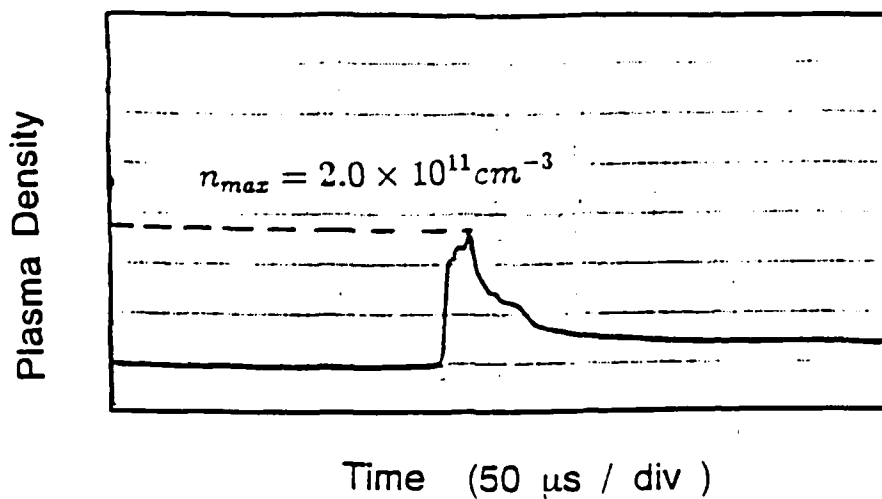
Temperature $T \approx few\ eV$

Plasma drift velocity $\approx 5 - 10 cm/\mu sec$

Figure 21: Typical result of plasma density vs time inside the magnetic field ($B = 12$ kG) for Hydrogen Flashover Gun.

Table 2: Plasma Characteristics Measurement Using Langmuir Probe Technique

Hydrogen Flashover Plasma Gun, $B = 0$
Langmuir Probe located 41 cm from the Gun

Gun Charge Voltage (kV)	Drift Velocity (cm/μs)	Temperature (eV)	Plasma density (cm^{-3})
10	8.7	11.6	3.30×10^{12}
12	10.0	12.2	3.61×10^{12}
15	14.3	13.3	3.46×10^{12}

Langmuir Probe located 119 cm from the Gun

Gun Charge Voltage (kV)	Drift Velocity (cm/μs)	Temperature (eV)	Plasma Density (cm^{-3})
10	7.69	3.33	2.34×10^{10}
12	8.33	3.50	3.74×10^{10}
15	8.50	3.70	5.40×10^{10}

Marshall Type Plasma Gun, $B = 0$
Langmuir Probe located 119 cm from the Gun

Gas Type	Gun Charge Voltage (kV)	Gas Pressure (psi)	Temperature (eV)	Plasma Density (cm^{-3})
Argon	5	8	3.85	3.44×10^{10}
Argon	5	10		3.40×10^{10}
Argon	5	12		2.31×10^{10}
Argon	6	8		1.15×10^{11}
Argon	6	10		1.03×10^{11}
Argon	6	12		0.86×10^{11}
Helium	5	8	3.57	1.43×10^{11}
Helium	5	10		0.95×10^{11}
Helium	5	12		1.07×10^{11}
Nitrogen	5	8	2.0	2.55×10^{11}
Nitrogen	5	10		2.79×10^{11}
Nitrogen	5	12		2.71×10^{11}

Table 3: Plasma Characteristics Measurement Using Langmuir Probe Technique

Hydrogen Flashover Plasma Gun
Langmuir Probe located 119 cm from the Gun

Magnetic Field (kG)	Gun Charge Voltage (kV)	Drift Velocity (cm/μs)	Temperature (eV)	Plasma density (cm^{-3})
9.0	12.0	10.6	9.0	2.70×10^{11}
10.4	12.0	11.2	9.3	2.40×10^{11}
11.3	12.0	12.3	10.2	2.75×10^{11}
12.3	12.0	12.5	10.5	2.69×10^{11}

Marshall Type Plasma Gun
Langmuir Probe located 119 cm from the Gun
Gun Charge Voltage 5 kV

Gas Type	Magnetic Field (kG)	Gas Pressure (psi)	Temperature (eV)	Plasma Density (cm^{-3})
Argon	9.0	8	5.0	4.0×10^{11}
Argon	10.4	8		4.0×10^{11}
Argon	11.3	8		2.2×10^{11}
Argon	12.25	8		5.4×10^{11}
Argon	13.5	8		4.0×10^{11}
Argon	15.5	8		4.0×10^{11}
Helium	9.0	8	7.0	2.3×10^{11}
Helium	10.4	8		3.4×10^{11}
Helium	11.3	8		3.5×10^{11}
Helium	12.25	8		2.5×10^{11}
Nitrogen	9.0	8	8.33	4.3×10^{11}
Nitrogen	10.4	8		3.4×10^{11}
Nitrogen	11.3	8		4.3×10^{11}
Nitrogen	12.25	8		4.3×10^{11}

2.5 Experimental Studies of the Starting Current in a Relativistic Vacuum BWO

The vacuum BWO was studied experimentally over wide range of beam currents, from the threshold (starting current) to 75% of the limiting current and over wide range of voltages and various magnetic fields. Frequency, power and pulse shape were analyzed. Most important, however, are the measurements of the BWO starting current. Usually, it is very difficult to achieve low beam currents with field emission guns which favors high current density ($\sim$10kA/cm^2). Using the novel techniques described in section 2.2, we were able to reduce the total beam current to a value below 100A while still maintaining a good beam uniformity. This enable us for the first time to make four independent measurements of the starting current (two beam diameter, two beam energies). The experimental results are:

1. $r_b = 0.775$ cm

   $I_{start} \leq 114$ A   at 430 kV   double cathode gun   AKI/O = 53/50 mm

   $I_{start} \leq 140$ A   at 600 kV   double cathode gun   AKI/O = 58/55 mm

2. $r_b = 0.26$ cm

   114 A $< I_{start} <$ 335 A   at 430 kV   double cathode gun   AKI/O = 55/55 mm

   132 A $< I_{start} <$ 432 A   at 600 kV   double cathode gun   AKI/O = 35/55 mm

From the experiment, it was found that as the beam current increases above I_{start}, the envelope of the microwave pulse is effected and the envelop is characterized by more structured. At $I \gg I_{start}$ region, we found even more structure and the microwave output pulse is narrower. This may be due to the self-modulation (see section 2.10).

28

2.6 Frequency Pulling in Relativistic Vacuum BWOs

The frequency of interaction in a vacuum BWO is expected to depend on the beam energy. Since the beam's slow space charge wave is drastically modified by space charge close to the limiting current (see section 2.3) the exact relativistic dispersion relation was used to calculate the new interaction frequency. This frequency is defined here as the intersection of the SSCW with the cold TM_{01} dispersion relation in the corrugated waveguide. The difference between the two is called " frequency pulling". Figure 22 shows the cold slow wave structure dispersion relation superimposed on the beam's slow space charge wave as calculated for various beam currents. From this plot, we see that not only the slope of the slow space charge wave is changed by varying the beam current but the line is also displaced. The interaction frequency could be determined by the intersection point of the dispersion curve of the slow space-charge wave and the TM_{01} structure wave. Figure 23 shows the interaction frequency of TM_{01} mode vs the diode voltage for various beam currents. For the calculations presented in this figure the beam radius is 0.75 cm. Figure 24 shows similar calculation for a beam with a smaller radius (0.26 cm). Figure 23 shows that the interaction frequency is a function of the beam current even for a fixed gun voltage, i.e. it is a function of the gun geometry (like anode-cathode gap). By using the measured relation between the gun voltage and current (see section 2.2), we can now transform Fig. 23 to Fig. 25 which show the calculated interaction frequency for seven different experimental gun geometries which were studied separately (see section 2.2). The horizontal dashed lines correspond to the upper and lower cut-off frequencies (band pass) of the TM_{01} mode in the slow wave structure. Figure 26 shows the experimentally measured frequencies for two of the seven gun geometries.

29
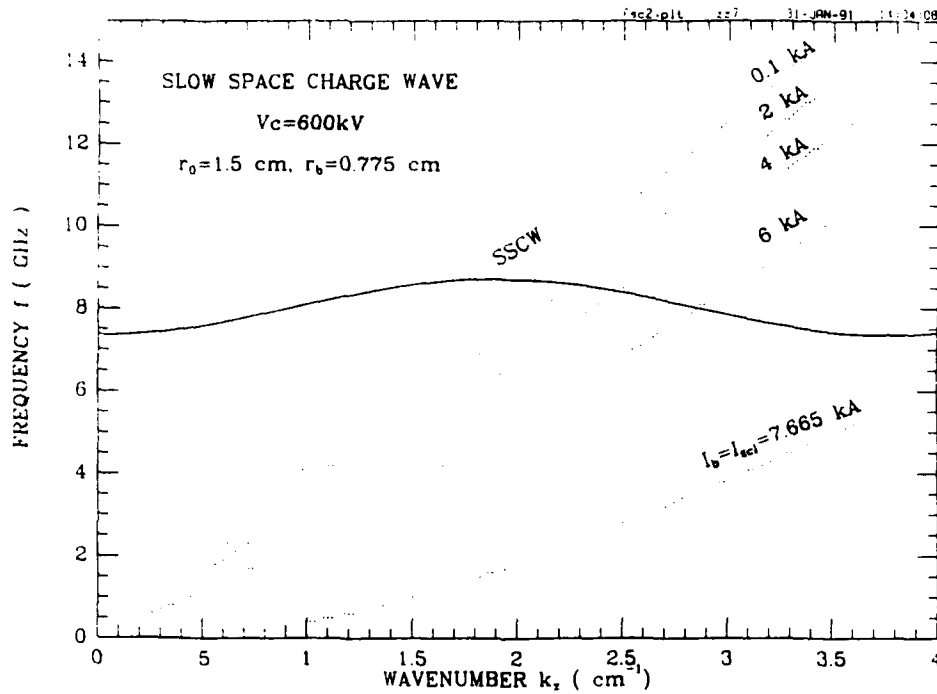
Figure 22: Cold slow wave structure dispersion relation superimposed on the beam's slow space charge wave as calculated for various beam currents.
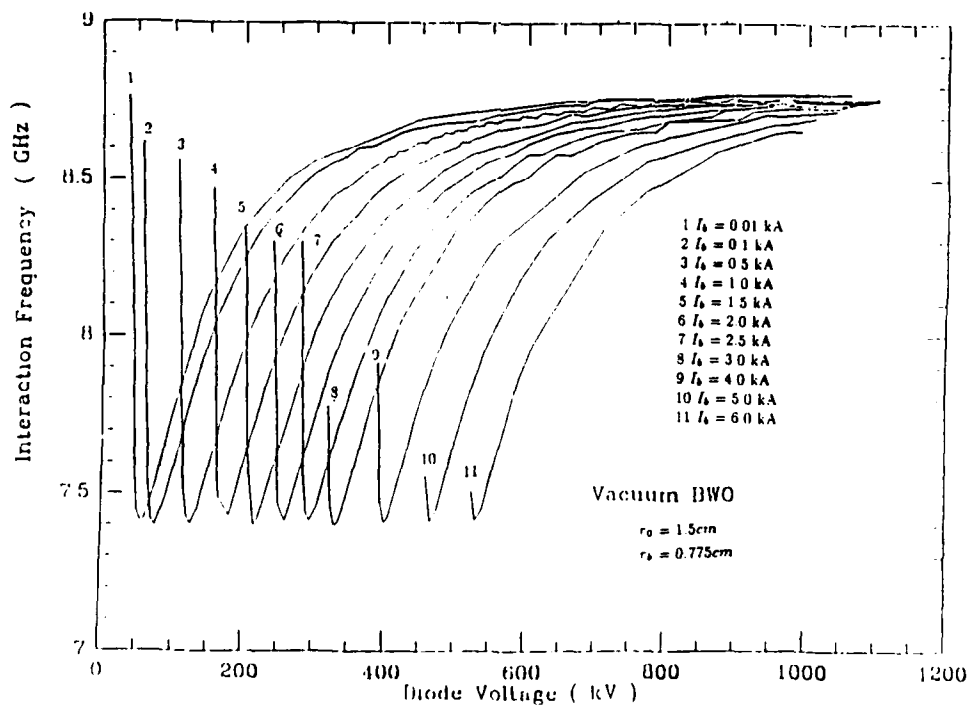
Figure 23: The interaction frequency of TM_{01} mode vs the diode voltage for various beam currents, $r_b = 0.775$ cm.
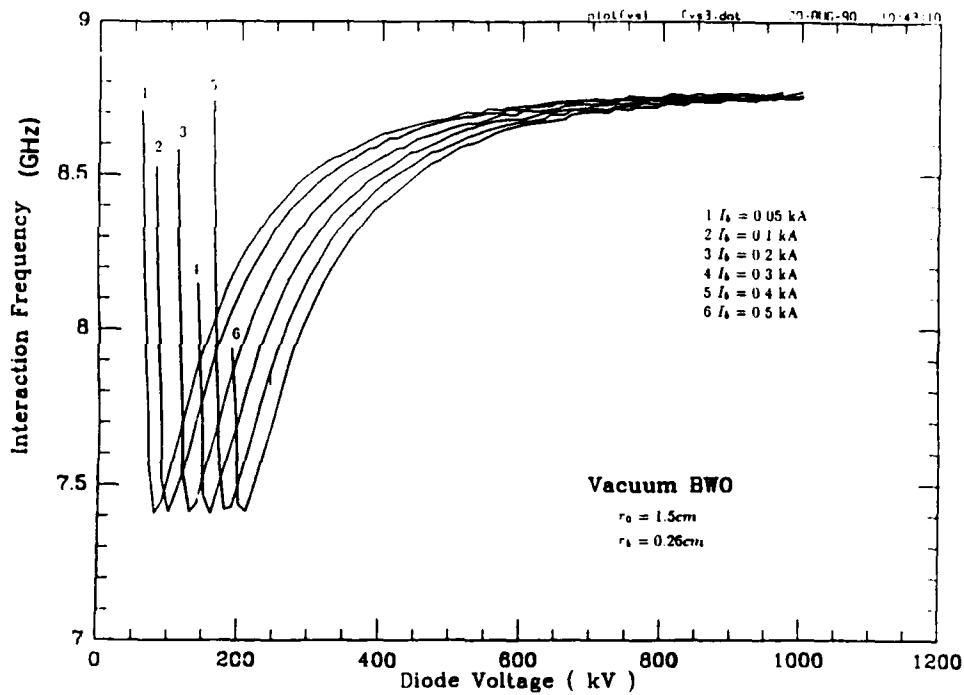
Figure 24: The interaction frequency of TM_{01} mode vs the diode voltage for various beam currents, $r_b = 0.26$ cm.
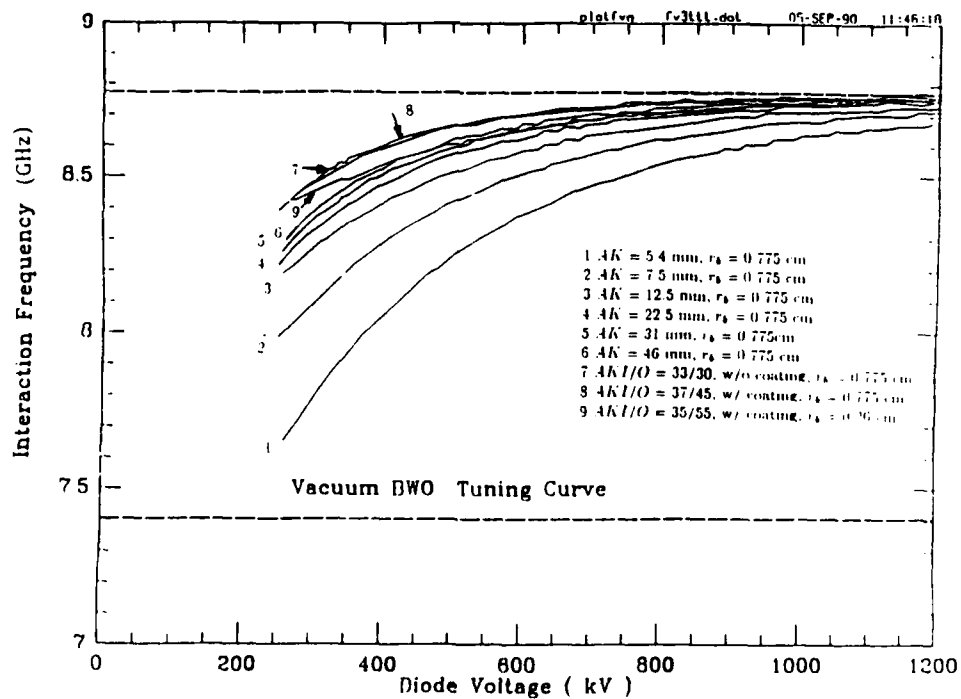
Figure 25: Calculated interaction frequencies for seven different experimental gun geometries.

31

9 5

Resonant Frequency (GHz)

p1●260   ●444   31-JAN-91   14:15:20

9

AKI/O=33/30 mm

AK=12.5 mm

8.5

8

B=15 kG. r_b=0.775 cm

7 5

300   350   400   450   500   550   600   650   700

Diode Voltage (kV)

Figure 26: The experimentally measured frequencies for two of the seven gun geometries.

32

2.7 Experimental Studies of Plasma Loaded BWOs

A plasma filled relativistic BWO was driven by an intense relativistic electron beam with current approaching the vacuum space charge limiting value. The beam propagation in plasma as well as the BWO characteristics like power, frequency and pulse duration were measured. Initial results indicate that the presence of plasma causes only small frequency shifts (compared with the vacuum case) in addition to efficiency enhancement. It also helps to extend the pulse duration. Above a critical plasma density the interaction is quenched.

First we look at the effect of plasma on beam propagation. For anode-cathode gap of 5.4 mm, the measured gun current at 600 kV is about 4.5 kA (beam radius is 0.75 cm, see Fig. 5). Under the same conditions the calculated space charge limiting current in the slow wave structure is about 7.5 kA, and only about 60% of the injected current propagated. As the background plasma density is raised, higher and higher percentage of the injected current propagates. At a background plasma density of about $2 \times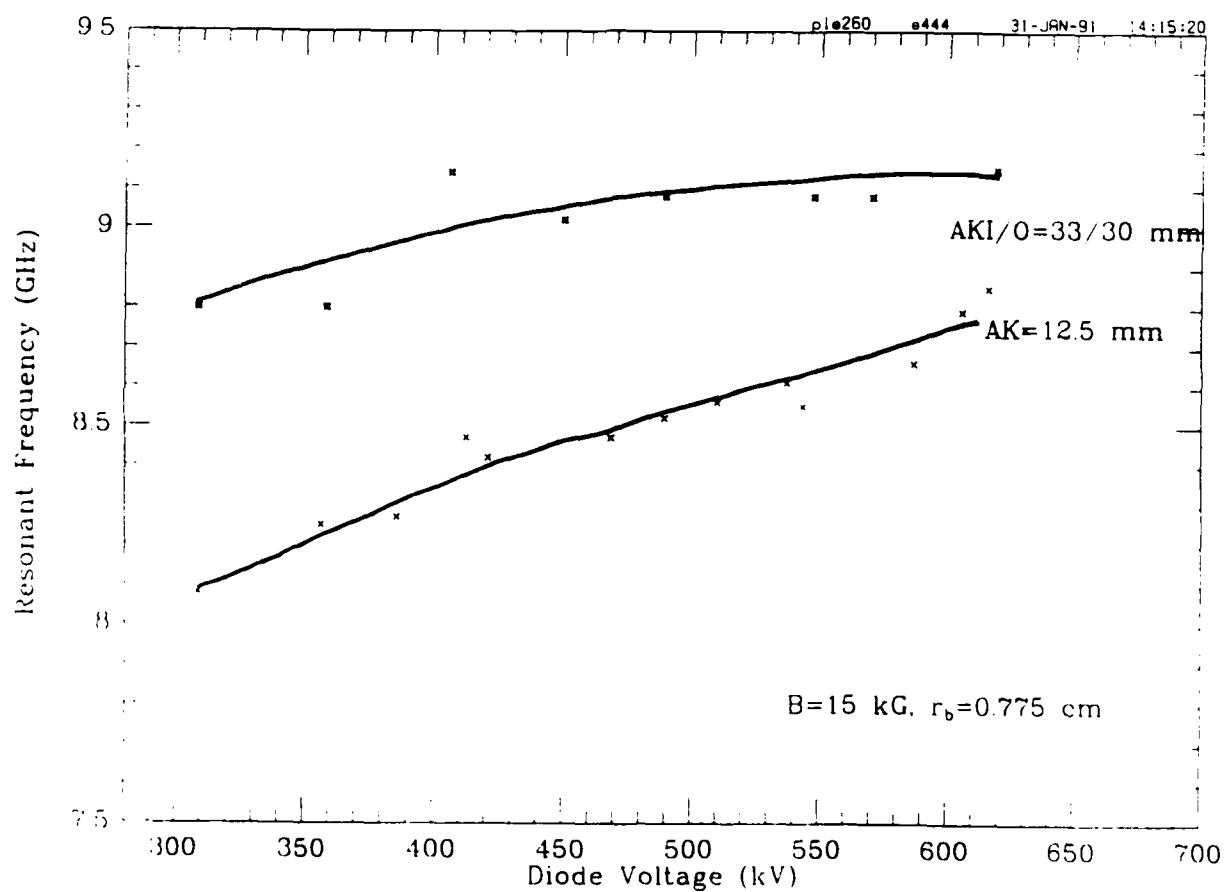 10^{11}$ cm^{-3}, 90% of the beam is transmitted (see Fig. 27). An enhancement of the microwave power generation efficiency was observed over a wide range of injected plasma densities. Variation of the firing delay between the plasma gun and the electron beam allowed a measure of control over the plasma density inside the slow wave structure. The microwave peak power output as a function of this firing delay is shown in Fig. 28. (These results were achieved with the Marshall plasma gun.) Microwave output rises to a peak of almost 600 MW, corresponding to an electron efficiency of about of 40%, compared with about 5% for the vacuum BWO. Under similar conditions this enhanced efficiency is maintained in a plasma loaded BWO even for large beam currents approaching the vacuum space charge limit (a Hydrogen Flashover Gun was used.)

The presence of the plasma caused only a small frequency shift compared to the vacuum case. This frequency shift was measured by heterodyning the BWOs frequency against a preset local oscillator. The beat frequency between the two signals was measured on a high speed recorder (see Fig. 29).

Based on our results, we can draw the following conclusions:

1. A plasma can be generated externally and injected into the BWO interaction area in a reproducible and controlled manner.

2. A plasma filled BWO is characterized by high peak efficiency (about 40%) and small (1 to 5%) frequency upshifts.

3. The plasma allows for the injection of large beam currents. In our experiments, beam currents of up to 75% of the vacuum limit were propagated. Further increases well above the vacuum limit seem feasible.

4. The presence of the plasma increases the microwave pulse duration.

It appears that this enhanced efficiency can be maintained for beam currents approaching and exceeding the vacuum limit. A slightly overmoded (diameter/wavelength = 2 - 3) will be needed for peak power handling capabilities of 5 - 10 GW. Further research may concentrate on investigating such systems.

It is anticipated that plasma injection may also prove beneficial to a variety of high power microwave devices such as gyrotrons and free electron lasers.

33
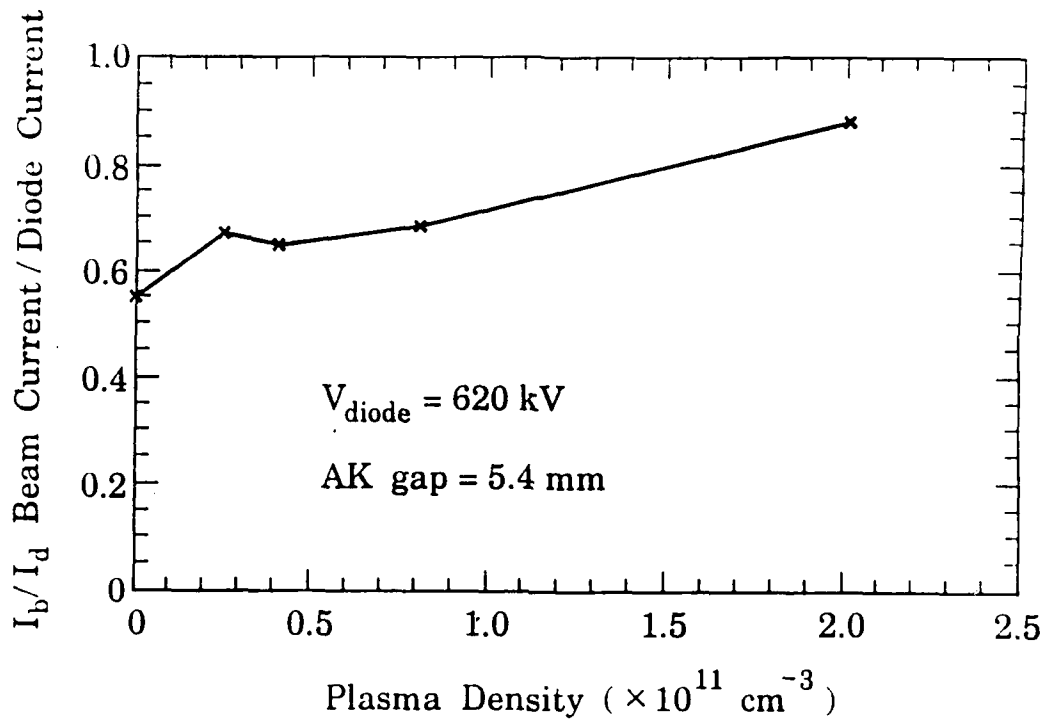
Figure 27: Beam current/diode current vs plasma density (Hydrogen gun).
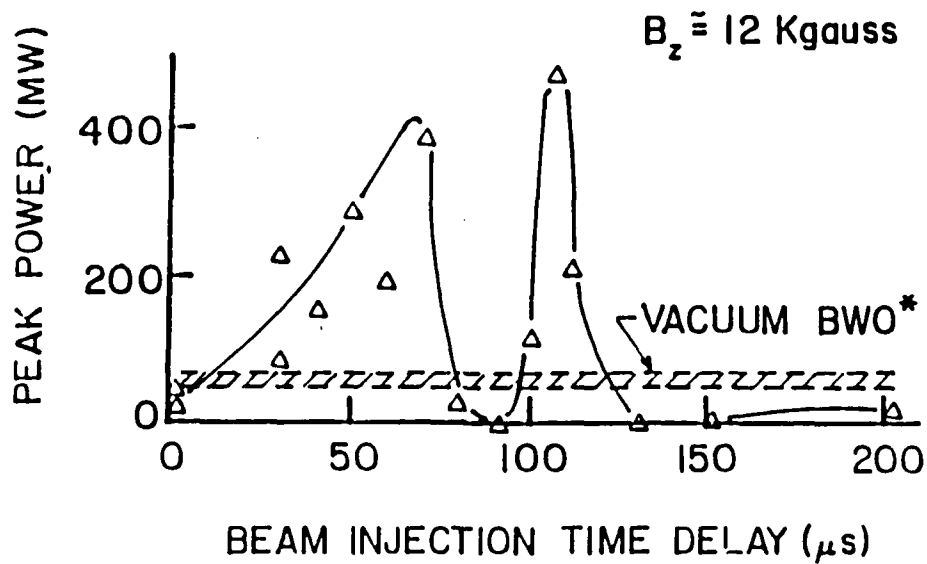
Figure 28: Peak microwave output power vs beam injection time delay (Marshall gun).

Figure 29: Beat frequency signal vs time.

2.8 Finite Length Effects in Slow Wave Structures

When finite length effects are taken into account, the slow wave structure behave like a cavity with discrete resonances. This is especially pronounced when the reflection coefficients at both ends are large. These resonances are due to various axial modes. The number of these resonances is equal to the number of periods in the slow wave structure plus one. We have designed and fabricated a cold test system to measure these resonances as well as the reflection coefficient and the dispersion relation of the TM_{01} mode in the slow wave structure. The cold test system is shown in Fig. 30, and will be excited by a probe (labeled 6 in the figure). The structure is modular and can vary in length from four to six periods. The expected resonances for a four period and six period system are given in Table 4. The results will be compared with the calculation (see Section 2.1).
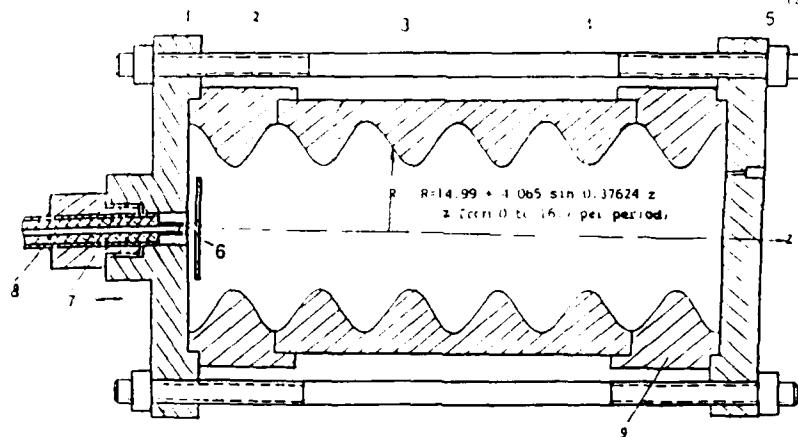
1. Short Plane I. 2&9 Corrugated Waveguide Circuit I & III.5. Short Plane II
3. Corrugated Waveguide Circuit   4. Pole   6. 6a.E Coupler & 6b. H coupler
7. Connector   8. Coaxial Line
* Pay attention to keep three corrugated waveguide identical (preciseness & concentricity)

Figure 30: The schematic drawing of the cold test system.

Table 4: Frequencies Expected from Cold Test of the Slow Wave Structure (GHz)

Sinusoidally Corrugated Waveguide
($R_0 = 1.5$ cm, $L = 1.67$ cm, $h = 0.273$)

Resonance Frequency	4 Period Cavity	6 Period Cavity
$f_0 = f(\beta L = 0)$	7.404	7.404
$f_{\pi/6} = f(\beta L = \pi/6)$	N/A	7.448
$f_{\pi/4} = f(\beta L = \pi/4)$	7.558	N/A
$f_{\pi/3} = f(\beta L = \pi/3)$	N/A	7.702
$f_{\pi/2} = f(\beta L = \pi/2)$	8.046	8.046
$f_{2\pi/3} = f(\beta L = 2\pi/3)$	N/A	8.386
$f_{3\pi/4} = f(\beta L = 3\pi/4)$	8.526	N/A
$f_{5\pi/6} = f(\beta L = 5\pi/6)$	N/A	8.632
$f_\pi = f(\beta L = \pi)$	8.773	8.773

2.9 Linear Theory of Plasma Loaded BWO

A linear theory of plasma loaded BWO was developed (for infinitely strong guiding magnetic field, solid beam). It shows that below some critical background plasma density the instability is absolute (BWO), while above it, it is convective (TWT) in nature. Growth rates were also calculated.

The linear model was derived for the excitation of electromagnetic waves in a plasma-filled corrugated-wall waveguide with an arbitrarily large sinusoidal corrugation. The model neglects the electron plasma waves in the plasma (Trivelpiece–Gould modes) for the time being, and treats only the modified symmetric TM electromagnetic waves. The theory predicts that, when driven by an electron beam, the presence of a plasma in the slow wave structure will cause an increase in the oscillation frequency, because the dispersion relation for the electromagnetic (TM_{01}) wave is raised in frequency (see Fig. 31). As can be seen from Fig. 32, the presence of the plasma effect higher order modes, too. The temporal growth rates of a high frequency mode approach those of the fundamental mode for very high plasma densities (Fig. 33). A simplified analytical model predict enhancement in the spatial growth rate and a switch from absolute to convective instability at a critical plasma density of $N_p \cong 2 \times 10^{12}$ cm^{-3}. The predicted enhancement in the linear growth rate is attributed to a decrease in the grope velocity of the backward wave in the presence of the background plasma.

Even though this simplified model predicts some interesting features like enhancement of the linear growth rate, it occurs at a plasma density which is 100 times large than those used in the experiment. It is clear that the present linear theory will have to be considerably expanded to better explain the experimental results and to be used as a tool with predictive capabilities. The linear theory, of course, can not be used to analyze efficiency enhancement which is a non-linear phenomenon. The presence of the plasma can cause a substantial increase in the spatial growth rate of the aboslute instability (Fig. 34). For high plasma density the absolute instability is suppressed and only the convective instability remains.
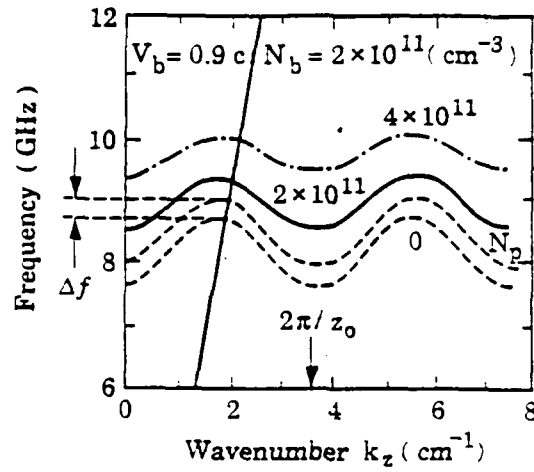
Figure 31: Calculated dispersion relation of the plasma loaded BWO.
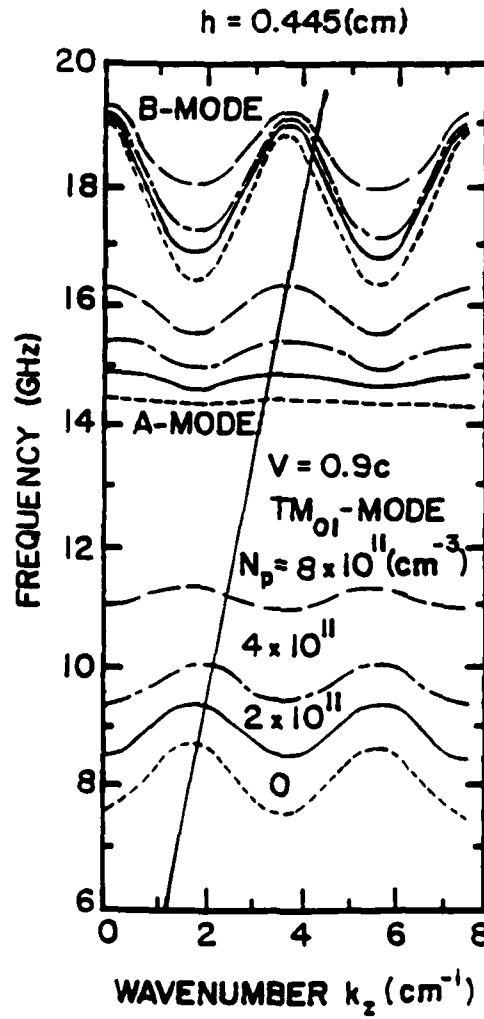
Figure 32: Dispersion curves for three modes for various plasma densities N_p, $N_b = 0$.

39
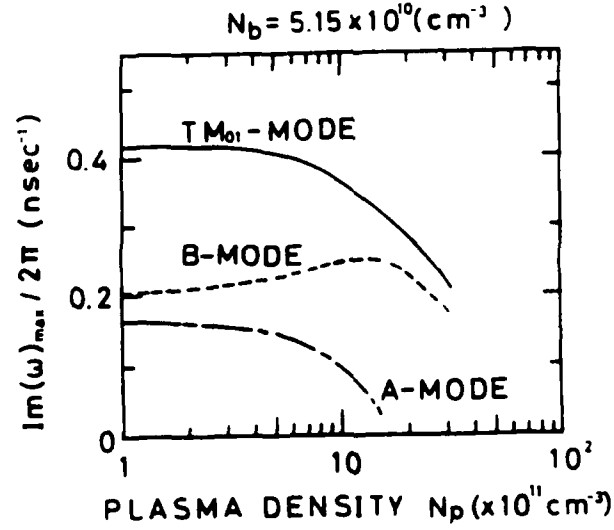
Figure 33: Peak growth rates $Im(\omega)_{max}/2\pi$ vs plasma density.
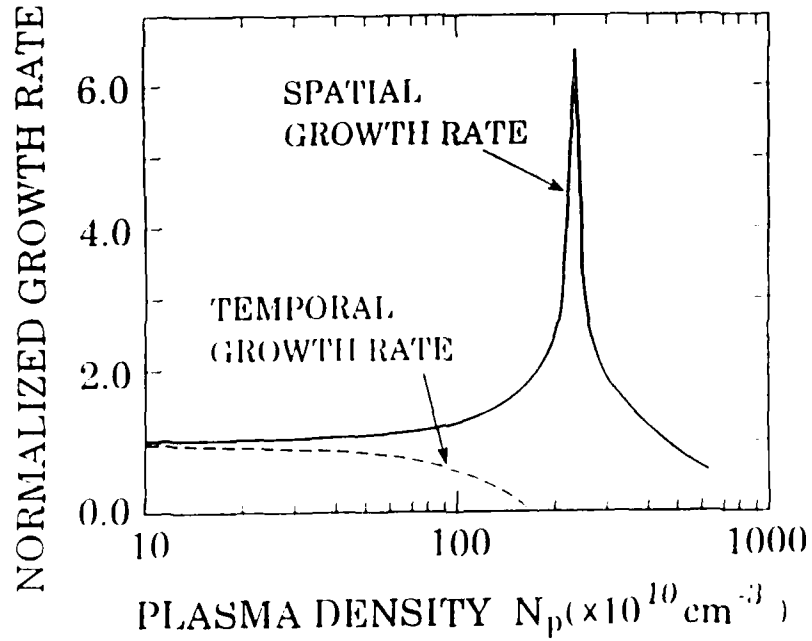
Figure 34: Simplified theoretical result of the maximum spatial growth rate (solid curve) for $Im(\omega) = 0$ normalized to the vacuum case vs plasma density N_p; $N_b = 5.15 \times 10_{1}0$ cm^{-3}. The maximum temporal growth rates for $Im(k) = 0$ normalized to the vacuum case are shown by dashed curve.

2.10 Theory of Relativistic Backward Wave Oscillators

Relativistic backward wave oscillators (BWOs) have proven to be efficient, high power microwave sources in the centimeter and millimeter wave range, capable of radiating hundreds of megawatts of power. One approach to increasing the power generating capabilities of these devices is to introduce plasma into the device.[1]

As a first step in the development of a comprehensive theory of plasma loaded relativistic BWO operation, we have developed a linear and nonlinear theory for a vacuum relativistic BWO of a finite length. To this end we have derived a set of reduced equations self consistently describing the slow evolution of the envelope of the radiation field and the relativistic motion of the particles under the following assumptions: (a) the electron's motion is one dimensional along the z-axis (axis of symmetry) due to a strong applied magnetic field; (b) the beam interacts with only one spatial harmonic of the electromagnetic field. The model takes into account the finite reflectivity of the electromagnetic wave at both boundaries of the interaction region and allows large variation in the longitudinal velocity of the electron beam. The model equations depend on six normalized parameters: the length, $k_0 L$; the initial beam velocity, $\beta_z(0)$ (corrected by taking into account DC beam space charge effects); the value of the radiation group velocity, $|\beta_g|$; the value of the combined reflection coefficient at the boundaries of the RF structure, $|R|$, the current $\hat{I}$ and the beam AC space charge parameter, $\hat{\omega}_{sp}$. This is in contrast to previous models,[2] in which radiation is assumed to leave the interaction region without reflection and variations in the longitudinal velocity are assumed to be small. Note, that in this case, the number of normalized parameters can be reduced to two: current and A.C. space charge parameter.

The normalized length is given by $k_0 L = L \omega_0 / (\beta_z(0)c)$, where c is the speed of light, L is the length of the structure, ω_0 is the frequency determined from the intersection of the dispersion curve of a corrugated wave guide and the beam dispersion curve (see Fig. 35). The normalized current is given by the following expression,

$$\hat{I} = 4\pi \frac{I}{I_A} \left(\frac{L}{d}\right)^2 \frac{1}{\beta_z |\beta_g|} C. \tag{10}$$

where $I_A = (mc^3/q)$ is the Alfven current in Amperes, I is the beam current in Amperes, d is the period of the structure, and C is the coupling coefficient.

The value for C can be obtained from the solution of Maxwell's equations in the corrugated structure[3] without the electron beam using the following expression

$$C = |\int_0^d \frac{dz}{d} E_z(r_{b_1}, z)|^2 / \int_0^d \frac{dz}{d} \int^{r_w(z)} \frac{2\pi r dr}{d^2} \left(|\mathbf{E}(r, z)^2| + |\mathbf{B}(r, z)|^2\right).$$

where $r_w(z)$, (r_b) is the wall radius (beam radius) and $\mathbf{E}$, $\mathbf{B}$ and E_z are the electric, magnetic fields and longitudinal component of the electric field, respectively. The AC space charge parameters, $\hat{\omega}_{sp}$ is the frequency of beam plasma oscillations (including the effect of the beam geometry) normalized to the time of flight, $L/v_z(0)$. The exact expression for $\hat{\omega}_{sp}$ will be given elsewhere.

We calculated the start oscillation current for different values of the parameters $k_0 L$ and R and fixed the values of the other parameters. The normalized start oscillator current is

related to the normalized current (Eq. (10)) as follows

$$\tilde{I}_{start} = \hat{I}(k_0L)/\left(\gamma_0^3\beta_z^2(0)\right) \qquad (11)$$

Figure 36 displays the normalized start oscillation current as a function of the normalized length k_0L for combined amplitude reflection coefficients of 0, 0.3 and 0.7. From the plot, we observe that for the $|R| = 0$ case the start current roughly has a constant value, $\tilde{I} \simeq 7.7$. For $|R| \neq 0$, on average, the same scaling exists in addition to a periodic dependence on k_0L, which is due to the interference between the amplified and reflected waves. The actual value of the start oscillation current can be obtained from Eqs. (10) and (11) and Fig. 36.

$$I_{start} = 1.35 \left(\frac{d}{L}\right)^3 \frac{\gamma_0^3\beta_z^2(0)|\beta_g|}{C(k_0d)} \tilde{I} \qquad (kA) \qquad (12)$$

We observe that by varying the normalized length parameter by $\pi/2$, one can expect a variation in the start oscillation current of a factor of three for the $R = .7$ case. The presence of a low density plasma modifies the dispersion characteristics of the RF structure. Simple estimates show that a change in the parameter k_0L (the operation point) of order $\pi/2$ corresponds to $\omega_p/\omega_0 \simeq 0.3$, where $\omega_p = (4\pi n q^2/m)^{1/2}$ is the plasma frequency and n is the plasma number density. Note, to achieve a similar variation in the k_0L parameter will require about 60% variation in the voltage on the gun. The preceding results are not sensitive to variations in $\beta_z(0)$ and $|\beta_g|$. Figure 37 shows the normalized frequency shift, $\delta\omega$, at start oscillation versus k_0L assuming L fixed. Here $\delta\omega = \omega(k_0L) - \omega(k_0L = 30)$. Variation of $\delta\omega$ with k_0L assuming the structure fixed occurs when beam energy is varied, and the point of intersection of the beam and structure dispersion curves illustrated in Fig. 35 moves. In the case of $|R| = 0$ the operating frequency decreases with increasing k_0 reflecting the continuous changes in the intersection point. When $|R| \neq 0$ the frequency tends to change in discrete steps. This is a manifestation of the tendency of the cavity to have eigenfrequencies as the reflectivity is raised. On the average the operating frequency tracks the intersection frequency; however, with high reflectivity the frequency changes in steps. Figure 38 shows the time history for the electronic efficiency for two examples: the beam current is two and five times larger than the start oscillation current. The normalized length $k_0L = 30$, $\beta_z(0) = .768$, $\beta_g = .24$, $|R| = 0$ and $\bar{\omega}_{sp} = 0$. As it can be seen, for the larger current, the radiated power has large fluctuations (i.e., over-bunch instability) and for currents less than some critical value, $\hat{I}_{cr}$, the radiation power is constant. For very large values of k_0L (~ 100) and $|R| = 0$ the critical value $\hat{I}_{cr} \simeq 3\hat{I}_{start}$, which is consistent with previous results.[2] In the case of $|R| \neq 0$, the $\hat{I}_{cr}$ is a complicated function of k_0L and is shown on Fig. 36 together with the value of $\tilde{I}$ (Eq. (10)) at start oscillation for $|\beta_g| = 0.24$ and $\beta_z(0) = 0.746$. A similar behaviour of $\hat{I}_{cr}$ versus k_0L is anticipated for other values of $|\beta_g|$ and $\beta_z(0)$. Preliminary estimates indicate that Maryland BWO is operating in the overbunch regime. This part of the work was presented at a number of conferences (see Section 2.12) and a manuscript is in preparation.
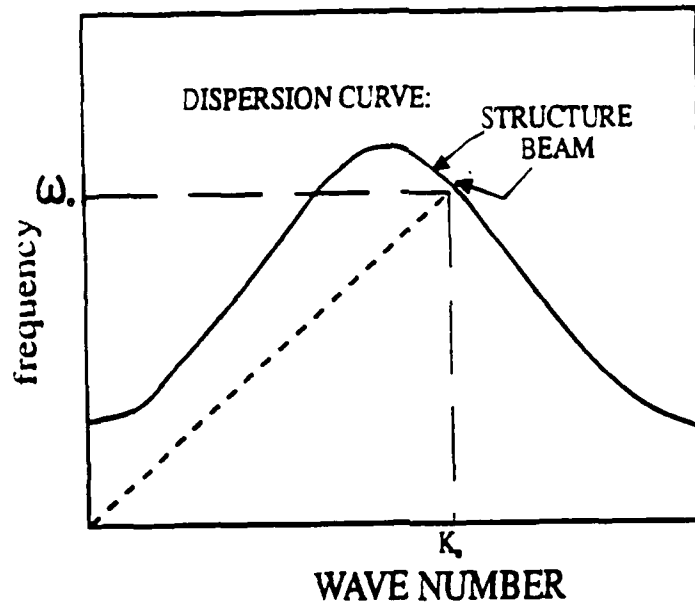
Figure 35: Dispersion diagram of the BWO.
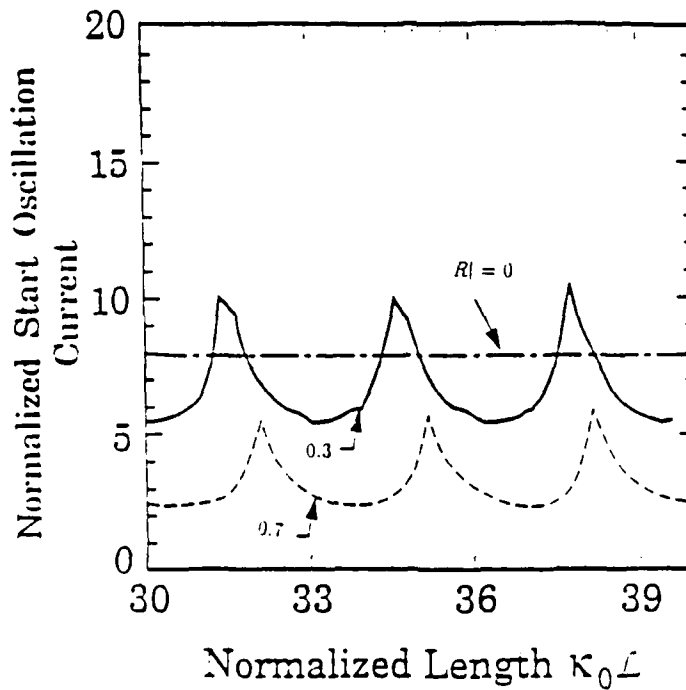
Figure 36: Normalized start oscillation current. I, vs. normalized length. k_0L, for a BWO with $R=0$. .3. and .7 solid line. dashed line. and large dashed line. respectively.
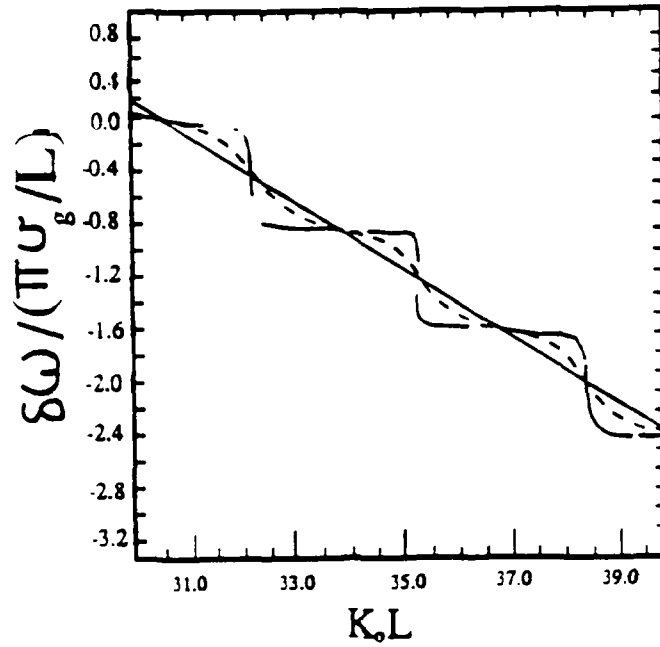
Figure 37: Normalized frequency shift. $\delta\omega$. versus normalized length $k_0 L$ (fixed L) at the start oscillation current for BWO with $R = 0$, .3 and .7 solid line, dashed line, and large dashed line, respectively.
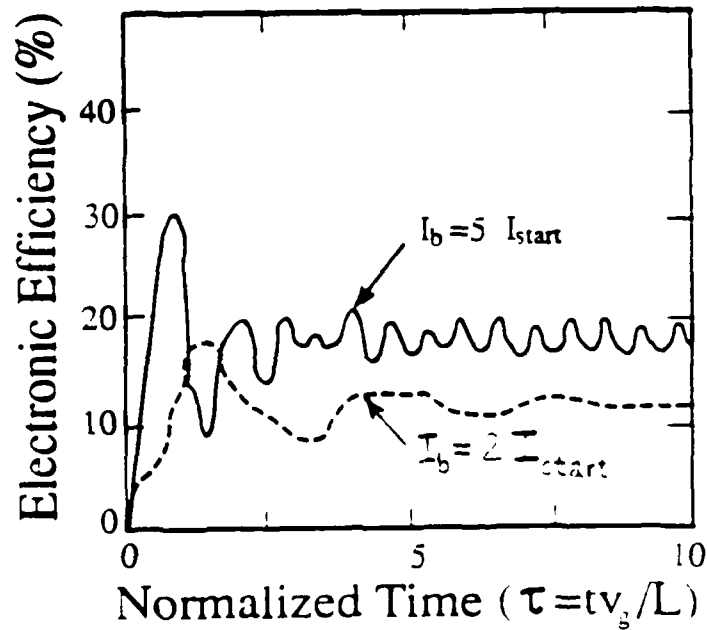
Figure 38: Efficiency of relativistic BWO versus normalized time with $R = 0$ for $I = 5\ I_{start}$ (solid line) and $I = 2\ I_{start}$ dashed line.

2.11 Open Research Topics

We achieved considerable progress on both the experimental and theoretical aspects of high power microwave generation using plasma loaded BWO. The work is not complete, though, and additional research is needed in order to take full benefit of the innovative approach of plasma microwave electronics. Experimentally, the following subjects need to be addressed (partial list):

(a) operation at currents well above the vacuum space charge limiting value

(b) measurement of the starting currents in the presence of plasma

(c) optimization with respect to interaction, efficiency and pulse length

(d) improved diagnostics to probe the plasma processes, and improved plasma generation techniques

(e) investigation of overmoded systems

Theoretically, our work needs to be expanded in order to gain a better understanding of the three-component system (beam/plasma/wave), finite magnetic field and space charge effects, and interaction in overmoded-multiwave systems. It is expected that the combined experimental and theoretical efforts will lead to major achievement in this area and in plasma microwave electronics.

2.12 References

1. Y. Carmel et al, Phys. Rev. Lett. **62**, 20 (1989), p 2389.

2. N.S. Ginzburg, et al, Izv. Vuz. Radifiz. **21** (1978), p1037.

3. A. Bromborsky, et al, IEEE Trans. Micr. Theory and Tech. **MTT-32** (1984), p 600.

2.13 Papers Published

- Invited Talks

  1. B. Levush and T.M. Antonsen, Jr., International Topical Conference on Research Trends in Coherent Radiation Generation and Particle Accelerators, Lajolla, CA, February 1991.

  2. V.L. Granatstein, T.M. Antonsen, Jr., S. Bidwell, J. Booske, Y. Carmel, W.W. Destler, R.A. Kehs, P.E. Latham, B. Levush, W.R. Lou, I.D. Mayergoyz, K. Minami and D.J. Radack, "A Program of High Power Microwave Source Research and Development from 8 GHz to 600 GHz," Invited paper, presented at BEAMS '90, Novosibirsk, USSR, July 2-5, 1990.

  3. Y.Carmel, W.W. Destler, V.L. Granatstein, K. Minami, W.R. Lou, "Demonstration of Efficiency Enhancement in a High Power Backward Wave Oscillator by Plasma Injection," 1989 IEEE International Conference on Plasma Science, Conference Record 89CH2760-7, p. 150.

- Journal Publications

  1. Y. Carmel, H. Guo, W.R. Lou, D. Abe, V.L. Granatstein, and W.W. Destler, "A Novel Method for Determining the Electromagnetic Dispersion Relation of Periodic Slow Wave Structures," *Appl. Phys. Lett.*, vol. 57, no. 13, p. 1 (1990).

  2. M.M. Ali, K. Minami, K. Ogura, T.Hosokawa, H. Kazama, T. Watanabe, Y. Carmel, V.L. Granatstein, W.W. Destler, R.A. Kehs, W.R. Lou, and D. Abe, "Absolute Instability for Enhanced Radiation from a High-Power Plasma Filled Backward Wave Oscillator," *Phys. Rev. Lett.*, vol. 65, no. 7, p. 855 (1990).

  3. Y. Carmel, K. Minami, W.R. Lou, R.A. Kehs, W.W. Destler, V.L. Granatstein, D.K. Abe, and J. Rodgers, "High-Power Microwave Generation by Excitation of a Plasma-Filled Rippled Boundary Resonator," *IEEE Trans. Plasma Sci.*, vol. 18, no. 3, p. 497 (1990).

  4. K. Minami, Y. Carmel, V.L. Granatstein, W.W. Destler, W.R. Lou, D.K. Abe, R.A. Kehs, M.M. Ali, T. Hosokawa, K. Ogura, and T. Watanabe, "Linear Theory of Electromagnetic Wave Generation in a Plasma-Loaded Corrugated-Wall Resonator," *IEEE Trans. Plasma Sci.*, vol. 18, no. 3, p. 537 (1990).

  5. Y. Carmel, K. Minami, R.A. Kehs, W.W. Destler, V.L. Granatstein, D. Abe, W.L. Lou, "Demonstration of Efficiency Enhancement in a High Power Backward Wave Oscillator by Plasma Injection," *Phys. Rev. Lett.*, vol. 62, no. 3, p. 2389 (1989).

- Articles in Conference Proceedings

  1. W.R. Lou, Y. Carmel, B. Levush, T.M. Antonsen, W.W. Destler, V.L. Granatstein, R.A. Kehs and K. Minami, "Studies of High Power Plasma Filled Backward Wave Oscillators" Proceedings of 5th National HPM Conference, West Point, NY (1990).

46

2. B. Levush and T.M. Antonsen. Jr., "Theory of Relativistic Backward Wave Oscillators," Proceedings of the 15th International Infrared and Millimeter Wave Conference, Orlando, FL 1990.

- Conference Publications

  1. American Physical Society, Division of Plasma Physics Meeting (Cincinnati, OH, November, 1990), Bulletin, vol. 35, no. 9, p 1936.

  2. American Physical Society, Division of Plasma Physics Meeting (Cincinnati, OH, November, 1990), Bulletin, vol. 35, no. 9, p 1937.

  3. American Physical Society, Division of Plasma Physics Meeting (Washington, D.C., April, 1990), Bulletin, vol. 35, no. 4, p 1002.

  4. IEEE International Conference on Plasma Science Meeting (Oakland, CA, May, 1990), Conference Record, 90CH2857-1, p 140.

  5. IEEE International Conference on Plasma Science Meeting (Oakland, CA, May, 1990), Conference Record, 90CH2857-1, p 135.

- Seminars

  1. "Plasma Loaded Backward Wave Oscillators," University of Maryland, February 13, 1990

APPENDIX

Copies of Relevant Papers Published During this Period

Absolute Instability for Enhanced Radiation from a High-Power Plasma-Filled Backward-Wave Oscillator

M. M. Ali,[1] K. Minami,[1],[3] K. Ogura,[1],[3] T. Hosokawa,[1] H. Kazama,[1] T. Ozawa,[1] T. Watanabe,[2] Y. Carmel,[3] V. L. Granatstein,[3] W. W. Destler,[3] R. A. Kehs,[3],[4] W. P. Lou,[3] and D. Abe[3]

[1]*Graduate School of Science and Technology, Niigata University, Niigata, 950-21 Japan*
[2]*National Institute for Fusion Science, Nagoya, 464 Japan*
[3]*Laboratory for Plasma Research, University of Maryland, College Park, Maryland 20742*
[4]*Harry Diamond Laboratory, Adelphi, Maryland 20783*
(Received 16 January 1990)

The linear theory of electromagnetic radiation from a backward-wave oscillator with a plasma-filled, sinusoidally corrugated waveguide driven by a relativistic electron beam has been derived and analyzed numerically. The presence of plasma can cause a substantial increase in the spatial growth rate of the absolute instability. For high plasma densities, however, the absolute instability is suppressed and only the convective instability remains. The predicted radiation enhancement can be attributed to a decrease in the group velocity of the backward wave in the presence of a plasma.

PACS numbers: 52.40.-w, 41.80.Ee, 52.25.Sw, 85.10.Jz

In recent years, a dramatic resurgence in research activities on relativistic electronics for high-power microwave sources has been taking place all over the world, driven by the development of new technologies and the requirements of present and future applications.[1] Gyrotrons and free-electron lasers are examples of such new devices. The backward-wave oscillator (BWO) driven by an intense relativistic electron beam is another microwave source on which research has been conducted primarily in the U.S. and U.S.S.R. for the last fifteen years.[2-10] Previously, gas-filled BWOs were observed to yield significant microwave output power at X-band frequencies.[3,9] Recently, however, considerable increases in both the output power and the efficiency of a BWO due to plasma injection from an external plasma gun have been observed.[10] Lin and Chen[11] have recently reported numerical simulations of the experiments, although they assumed an artificial periodic boundary condition in the axial direction which did not correspond to the experiments. They reported that a parametric beam-plasma wave interaction could not be the dominant mechanism for the efficiency enhancement and that the enhancement could be attributed to a decrease in the phase velocity of the most unstable beam mode in the presence of a background plasma. In order to understand analytically the physical reason for the observed enhancement, we have developed a linear theory of the beam-plasma interaction and have analyzed numerically the absolute instability[12] in plasma-filled BWOs.

First, we consider an infinitely long axisymmetric waveguide, i.e., slow-wave structure, whose wall radius varies with the axial coordinate z according to $R(z) = R_0 + h\cos(k_0 z)$, where $k_0 = 2\pi/z_0$. Here R_0, h, and z_0 are, respectively, the average waveguide radius, the amplitude of corrugation, and its period. A uniform, cold,

and collisionless plasma with density N_p is assumed to be present, and a beam with uniform electron density N_b, a longitudinal velocity v, and radius $R_b < R_0 - h$ is present in the slow-wave structure. An infinitely strong external magnetic field which confines electron motion to be strictly along the field lines is applied in the axial direction z. We have obtained the linear dispersion relation $D(k,\omega) = 0$ for the symmetric TM modes with field components E_r, E_z, and B_θ.[13] Here, D is the value of the determinant of a matrix for which the element of the mth column and nth row, D_{mn}, is given by

$$D_{mn} = [1 + (n-m)Q_n](K_n C_{mn}^J + L_n C_{mn}^N), \tag{1}$$

$$C_{mn}^J = \sum_{q=0}^{\infty} \frac{(Y_n a)^{2q+|n-m|} J_0^{(2q+|n-m|)}(Y_n)}{2^{2q+|n-m|} q!(q+|n-m|)!},$$

$$K_n = Y_n J_0(X_n\delta)N_1(Y_n\delta) - X_n J_1(X_n\delta)N_0(Y_n\delta),$$

$$L_n = X_n J_0(Y_n\delta)J_1(X_n\delta) - Y_n J_0(X_n\delta)J_1(Y_n\delta),$$

$$X_n^2 = R_0^2 \left[\frac{\omega^2}{c^2} - k_n^2 \right] \left[1 - \frac{\omega_p^2}{\omega^2} - \frac{\omega_b^2}{\gamma^3(\omega - k_n v)^2} \right], \tag{2}$$

$$Y_n^2 = R_0^2 \left[\frac{\omega^2}{c^2} - k_n^2 \right] \left[1 - \frac{\omega_p^2}{\omega^2} \right],$$

$$Q_n = \frac{k_0 k_n}{w^2/c^2 - k_n^2}, \quad a = \frac{h}{R_0}, \quad \delta = \frac{R_b}{R_0}, \quad k_n = k + nk_0.$$

A similar expression for C_{mn}^N holds, with J_0 replaced by N_0 in C_{mn}^J given by (2). Here, we have assumed a phase factor $\exp[-i(\omega t - k_n z)]$ for time and spatial variations of the rf electric fields, and the other notations are standard. We confine our analysis here to the case of the high-frequency electromagnetic TM$_{01}$ mode with $\omega > \omega_p$. Our dispersion relation (1) tends to previously

obtained results[4,5] in the limit of small a.

The following parameters[9,10] are adopted unless specified otherwise; the relativistic factor $\gamma = 2.23$, $R_0 = 1.445$ cm, $R_b = 0.9$ cm, $h = 0.445$ cm, $z_0 = 1.67$ cm, and $N_b = 2.09 \times 10^{11}$ cm^{-3}. The plasma density N_p is considered to be a variable. For these parameters, we must calculate a 9×9 determinant equation, with the terms up to the order of a^{10} in (2), to obtain 1% numerical accuracy in periodicity for two periods of wave number k_0.[13]

The spatial growth rate is a more practical measure of the strength of instabilities than is the temporal growth rate,[12] as will be discussed later in detail. There can be many roots of $D(k,\omega) = 0$ that have complex $k = k_r + ik_i$ for a real ω. In order to sort out the spatially growing waves of convective and absolute instabilities from other roots of evanescent or stable waves, we deform the path of integration in the inverse Laplace transformation in the complex $\omega = \omega_r + i\omega_i$ plane downward to the real axis. If k_i has different signs when ω_i takes a large positive value and zero, then the wave is convectively unstable; otherwise, it is an evanescent wave. If the deformation of the path of integration towards the real axis is prevented by merging of two roots (saddle point) for some positive ω_i from both sides of the k half planes, then the instability is absolute which corresponds to a BWO. In general, ω and k at the saddle point are both complex[12,14] ($k_s = k_{rs} + ik_{is}$, $\omega_s = \omega_{rs} + i\omega_{is}$), and the absolute instability causes electromagnetic radiation from an infinitely long slow-wave structure even if a feedback mechanism does not exist. The spatial growth rate k_{is} and the real part k_{rs} of the wave number at the saddle point versus N_p are plotted in Fig. 1(a), while the temporal growth rate $\omega_{is}/2\pi$ and the oscillation frequency $\omega_{rs}/2\pi$ are shown in Fig. 1(b). As N_p increases the saddle point goes down, and the spatial growth rate is enhanced. As the point moves into the $\omega_i < 0$ region as shown in Fig. 1(b), the absolute instability disappears suddenly and only the convective instabilities continue to exist for exceedingly large N_p. These convective instabilities [corresponding to a plasma traveling-wave tube (TWT)] cannot give rise to any radiation unless a feedback mechanism exists in the slow-wave structure. The maximum spatial growth rates k_{im} for $\omega_i = 0$ are a measure of the amplification in the plasma BWO and are shown in Fig. 1(a). The group velocity,[15] approximately given by ω_{is}/k_{is}, and the phase velocity ω_{rs}/k_{rs} vs N_p are shown in Fig. 2 for an infinitely long ($L = \infty$) plasma-loaded, slow-wave structure. The absolute value of the group velocity decreases with N_p while the phase velocity slightly increases with N_p. The group velocity, however, changes direction and becomes positive for plasma density $N_p > 1.6 \times 10^{12}$ cm^{-3} as shown in Fig. 2 (solid circles), in which case the system works as a plasma TWT ($\omega_i < 0$), because the wave is still growing spatially.

In our linear theory, the output radiation is proportional to $\exp(2\omega_{is}t)$, where t is the interaction time be-
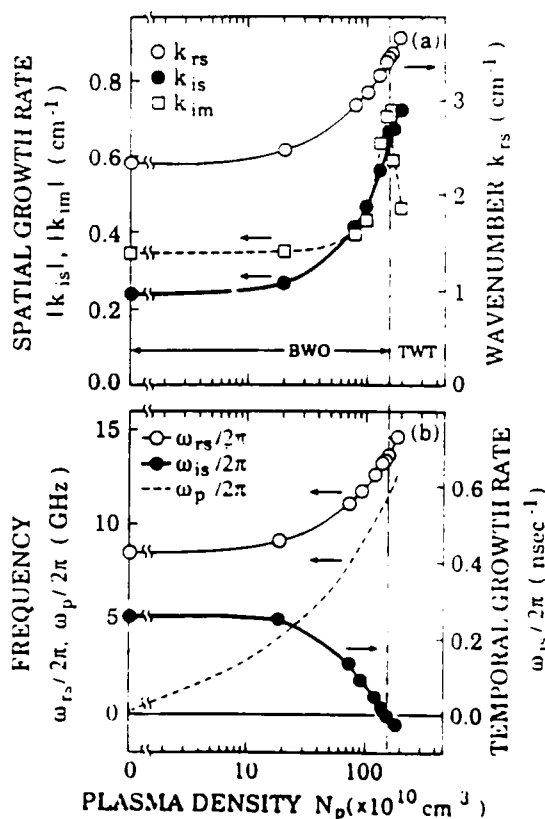

FIG. 1. (a) The spatial growth rate k_{is}, the real part k_{rs}, at the saddle point, and the maximum spatial growth rate for $\mathrm{Im}(\omega) = 0$, k_{im}, vs plasma density N_p. (b) Temporal growth rate $\omega_{is}/2\pi$, oscillation frequency $\omega_{rs}/2\pi$, at the saddle point, and plasma frequency $\omega_p/2\pi$ vs N_p.

tween the beam and the backward wave. In real experiments, the interaction time $t \gg 1$ nsec is given by the ratio of a finite L and the group velocity. Then, $\exp(2\omega_{is}t) = \exp(2k_{is}L) \gg 1$. The increase in k_{is} with N_p as shown in Fig. 1(a) may thus enhance the radiation. This is the reason why the spatial growth rate k_{is} is a more practical and critical measure of the instabilities than the temporal growth rate $\omega_{is}/2\pi$ for a slow-wave structure with finite axial length. The predicted enhancement can be attributed to an increase in the interaction time, i.e., a decrease in the group velocity of the backward wave. As shown in Fig. 1(a), our result predicts linear enhancement for values of N_p 1 order greater than that observed in Ref. 11.

In order to elucidate the physical meaning of the radiation enhancement, the maximum spatial growth rate k_{im} of the plasma BWO in the limit of small a has been analyzed in a qualitative way. The procedure used here is not very different from that in Ref. 11. A 2×2 determinant equation $D(k,\omega) = 0$, with $-1 \leq m,n \leq 0$, is used, and only the terms up to order a are taken into account in (2). We assume that the beam term in X_n [see Eq. (2)] is small, and the spatial growth rate ($\omega_i = 0$) at the intersection of the beam space-charge wave $\omega = kv$
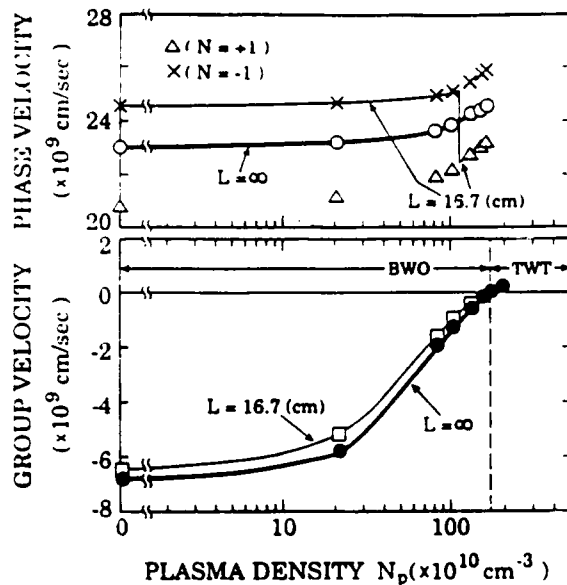
FIG. 2. Phase and group velocities of the plasma-loaded slow-wave structure in the case of $L = \infty$ vs N_p, shown, respectively, by solid and open circles. Those for a slow-wave structure with finite axial length $L = 16.7$ cm are shown by thin lines.

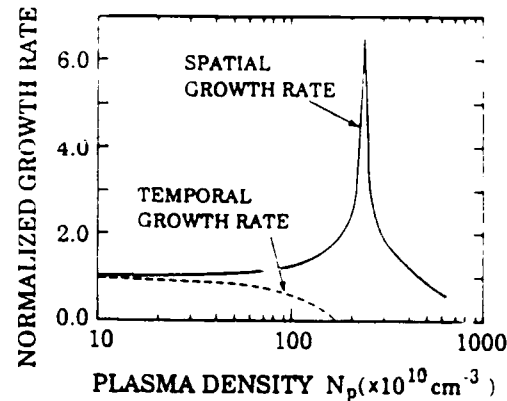FIG. 3. Simplified theoretical result of the maximum spatial growth rate (solid curve) for $Im(\omega) = 0$ normalized to the vacuum case vs plasma density N_p; $N_b = 5.15 \times 10^{10}$ cm^{-3}, $a = 0.1$ and other parameters are the same as those in Figs. 1 and 2. The maximum temporal growth rates for $Im(k) = 0$ normalized to the vacuum case are also shown by the dashed curve.

and the backward wave $Y_1 = 2.405$ is calculated. The final dispersion relation results in a quartic equation. It must be emphasized here that the previous analytical result[5] for $\gamma \gg 1$ gives no enhanced growth rates for the parameters in the experiments[9,10] with $\gamma = 2.23$. The spatial growth rate versus N_p calculated from the quartic equation is shown in Fig. 3. A resonant increase in the spatial growth rates is found and the result is qualitatively similar to k_{im} in Fig. 1(a). If one ignores the fourth-order term in the quartic equation assuming that it is small, the peak in Fig. 3 goes to infinity at $k_r = k_0$ and at the cutoff frequency, where the group velocity of the backward wave is zero. The decrease in the group velocity enhances the interaction between the backward wave and the beam. This is the physical reason for the enhanced radiation from the plasma BWO predicted in the present analysis. The temporal growth rate $(k_i = 0)$ which corresponds to $\omega_{is}/2\pi$ in Fig. 1(b) has also been calculated in the same 2×2 determinant equation, and the result is shown by a dashed line in Fig. 3. It should be noted that the temporal growth rate is zero for $N_p > 1.7 \times 10^{12}$ cm^{-3}.

So far we have treated an infinitely long slow-wave structure. For a finite-length device, different modes may be linked. In our analysis we considered four modes—two structure modes (forward and backward TM_{01}) and two beam space-charge modes (four roots in the dispersion relation). The oscillation is affected by the reflection coefficients R_1 and R_2 at both ends.[14] The oscillation does not occur at the k_r of the saddle point, but at a growing root k_+ near k_r, where k_+ is found

from the following simultaneous equations:

$$D(k_+, \omega) = 0, \quad D(k_+ + \epsilon, \omega) = 0,$$

$$\epsilon = k_- - k_+ = -2\pi N/L - i\ln(R)/L,$$

$$R = |R_1 R_2|, \quad \text{and} \quad N = \pm 1, \pm 2, \ldots$$

Here, k_- is the evanescent root propagating in the opposite direction to k_+ in order to feed back the oscillation energy to the original position. In this work, we neglect mode conversion at both ends and consider only the growing wave with highest growth rate k_+ and the evanescent wave with smallest damping rate k_- because the main contribution comes from these two waves. Note that, to have oscillation, in addition to $\omega_i > 0$, the spatial growth rate $Im(k_+)$ must surpass the spatial damping rate $Im(k_-)$, because $R \le 1.0$. This imposes an additional restriction to backward-wave oscillation. We do not find k_+ in the case of convective instabilities. The phase and group velocities for $L = 16.7$ cm and $R = 1.0$ are shown in Fig. 2. The thin line for phase velocity denotes the physical solutions which change from $N = -1$ to $N = 1$ as N_p increases. The plasma BWOs will not operate $(\omega_i < 0)$ for L and R less than the critical values[13] for given N_p and N_b.

In conclusion, we present a small-signal-gain calculation for a plasma-loaded slow-wave structure immersed in an infinitely large axial magnetic field for frequencies $\omega > \omega_p$. It was found that the presence of the plasma modifies both the dispersion relation and the nature of the vacuum linear instability. For low plasma densities, the instability is absolute. For large plasma densities, the group velocity changes sign, in which case the instability became convective. The present analysis predicts a considerable increase both in the spatial growth rate and in the oscillation frequency with increased N_p [Fig. 1(b)]. The saturated levels and efficiencies[11] of plasma

BWOs are beyond the scope of the present linear analysis. Nonlinear calculations are underway.

[1]B. Levush and A. T. Drobot, in *High Power Microwave Sources*, edited by V. L. Granatstein and I. Alexeff (Artech House, Boston, 1987) p. 3.

[2]Y. Carmel et al., r. ys. Rev. Lett. 33, 1278 (1974).

[3]Yu. V. Tkach et al., Fiz. Plazmy 1, 81 (1975) [Sov. J. Plasma Phys. 1, 43 (1975)].

[4]L. S. Bogdankevich, M. V. Kuzelev, and A. A. Rukhadze, Zh. Tekh. Fiz. 50, 233 (1980) [Sov. Phys. Tech. Phys. 15, 143

(1980)].

[5]V. I. Kurilko, V. I. Kucherov, and A. O. Ostrovskii, Zh. Tekh. Fiz. 51, 1415 (198.) [Sov. Phys. Tech. Phys. 26, 812 (1981)]; V. I. Kurilko, Yu. V. Tkach, and V. A. Shendrik, ibid. 44, 956 (1974) [ibid. 19, 607 (1974)].

[6]A. Bromborsky and B. Ruth, IEEE Trans. Microwave Theory Tech. 32, 600 (1984).

[7]R. A. Kehs et al., IEEE Trans. Plasma Sci. 13, 559 (1985).

[8]J. A. Swegle, J. W. Poukey, and G. T. Leifeste, Phys. Fluids 28, 2882 (1985).

[9]K. Minami et al., Appl. Phys. Lett '3, 559 (1988).

[10]Y. Carmel et al., Phys. Rev. Lett. 62, 2389 (1989).

[11]A. T. Lin and L. Chen, Phys. Rev. Lett. 63, 2808 (1989).

[12]R. J. Briggs, *Electron Stream Interaction with Plasma* (MIT Press, Cambridge, MA, 1964), Chap. 2.

[13]Details of our analysis will be published elsewhere.

[14]E. M. Lifshitz and L. P. Pitaevskii, *Physical Kinetics* (Pergamon, New York, 1981), Chap. 6.

[15]A. F. Alexandrov, L. S. Bogdankevich, and A. A. Rukhadze, *Principle of Plasma Electrodynamics* (Springer-Verlag, New York, 1984), p. 34.

High-Power Microwave Generation by Excitation of a Plasma-Filled Rippled Bondary Resonator

Yuval Carmel

K. Minami

Weiran Lou

R. Alan Kehs

William W. Destler

Victor L. Granatsten

D. K. Abe

J. Rodgers

High-Power Microwave Generation by Excitation of a Plasma-Filled Rippled Boundary Resonator

YUVAL CARMEL, MEMBER, IEEE, K. MINAMI, WEIRAN LOU,
R. ALAN KEHS, SENIOR MEMBER, IEEE, WILLIAM W. DESTLER, MEMBER, IEEE,
VICTOR L. GRANATSTEIN, SENIOR MEMBER, IEEE, D. K. ABE, AND J. RODGERS

Abstract—An experimental demonstration of a strong enhancement of the interaction efficiency in a high-power relativistic backward-wave oscillator when plasma is injected is presented. Controlled plasma injection enhances the interaction efficiency over the vacuum case by a factor of up to 8 to a value of about 40%. A linear theory of electromagnetic wave generation in plasma-loaded corrugated wall resonators is reviewed. A number of physical mechanisms are considered to account for the enhanced interaction, including two variations of a three-wave interaction involving the electron-beam slow space-charge wave, the slow electromagnetic waves in the structure, and the quasi-electrostatic waves in the plasma.

I. INTRODUCTION

THE FIELD of plasma electronics dates back to 1949 when several authors [1] discussed the excitation of electromagnetic waves in a plasma by an electron beam by virtue of stimulated Čerenkov radiation. Since 1949 this field of research has expanded to include beam heating of plasmas, collective acceleration of charged particles by plasma fields, and the excitation and amplification of electromagnetic waves. This last area has been referred to in the literature as "plasma microwave electronics" [2].

The introduction of plasma into vacuum microwave devices can have several beneficial effects. It is expected that plasma microwave devices could be tuned in frequency by exercising control over the plasma density up to the millimeter wave regime. Finally, extremely high-power microwave devices may be realized by using beam currents well above the space-charge-limiting current in vacuum. These currents may be realized by using a plasma to neutralize the beam space charge.

The practical realization of plasma microwave devices involves serious difficulties which have yet to be fully overcome. These difficulties include the generation of uniform, steady-state, highly ionized plasmas, high noise

levels which may have an adverse effect on the operation of microwave amplifiers depending on the application envisioned, the lack of a fully developed linear and nonlinear theory of plasma devices, and the problem of coupling the electromagnetic radiation both into and out of the plasma.

In particular, the problem of coupling the electromagnetic radiation to plasma waves has proved to be quite complicated and must be resolved before truly effective plasma microwave devices may be realized. The difficulty lies with the slow longitudinal oscillations which are excited in the plasma. For nonrelativistic beams, these oscillations have very slow phase velocities ($v_{phase} \ll c$) and behave like quasi-electrostatic oscillations. As a consequence, they are mostly trapped in the plasma. Recent efforts have sought to reduce the losses during the extraction of energy from a plasma by using relativistic electron beams. Under these conditions the wave excited in the plasma may have a phase velocity $v_{phase} \sim c$, allowing it to be more easily extracted from the plasma.

The purpose of this work is to study the feasibility of generating very high-power microwave radiation by using relativistic electron beams in plasma-loaded microwave devices. Over the years a wide variety of high-power microwave (HPM) vacuum devices have been studied, including the well-known magnetron, klystron, and backward wave oscillator, as well as newer devices such as the gyrotron, the free-electron laser, and the virtual cathode oscillator [3]. All of these sources have one thing in common—they are driven by an intense unneutralized electron beam which interacts unstably in high vacuum with an electromagnetic wave, leading to the conversion of the kinetic energy of the beam into electromagnetic radiation. The power levels available from such devices have grown by an order of magnitude every decade since 1940. For example, advanced, large diameter, overmoded backward wave oscillators (like the multiwave Čerenkov and multiwave diffraction generator) have recently achieved efficient operation at power levels of about 15 GW [4] at a wavelength of 3 cm and 4.5 GW [5] at a wavelength of 6.5 mm, and operation at a wavelength of 2 mm has been demonstrated [6]. The thrust of this work is to evaluate efficiency enhancement in a small diameter, relativistic backward-wave oscillator using a different approach—that of plasma loading.

Backward-wave oscillators (BWO's) are ideal candidates for the evaluation of plasma effects on microwave generation because they are relatively simple devices, providing fairly effective conversion of electron-beam energy into radiation, and can be easily filled with plasma. Initial studies [7], [8] have utilized background plasmas produced by the electron-beam impact ionization of a low-pressure neutral gas background and have demonstrated enhanced microwave output power. In recent experiments high-power microwave radiation was observed in a relativistic backward-wave oscillator which was externally filled with a highly ionized plasma [9]. Controlled plasma injection enhanced the interaction efficiency relative to the vacuum case by as much as a factor of 8, resulting in an efficiency of about 40%.

Section II of this paper reviews wave propagation in a plasma-filled smooth-walled waveguide; Section III contains a discussion of the space-charge-limiting current in plasma-loaded waveguides. A linear theory of plasma-filled corrugated structures is reviewed in Section IV. Section V summarizes the results from an experimental, plasma-loaded, high-power BWO that demonstrated a strong enhancement in the interaction efficiency, and Section VI contains a discussion of the results, including such questions as possible coupling mechanisms, mode stability, and future trends in plasma microwave electronics.

II. REVIEW OF WAVE PROPAGATION IN PLASMA-FILLED, SMOOTH-WALLED, CYLINDRICAL WAVEGUIDES

Plasma effects in conventional microwave-generating devices can usually be neglected since the plasma frequency of the background gas is much smaller than the plasma frequency of the electron beam. Typically, $\omega_p/\omega_b < 10^{-2}$, where $\omega_p = (eN_p/m_e\epsilon_0)^{1/2}$ is the background plasma frequency, and $\omega_b = (eN_b/m_e\epsilon_0)^{1/2}$ is the beam-plasma frequency. Recent theoretical studies, however, have predicted that the presence of a plasma in high-power microwave devices may lead to enhanced performance, attracting renewed scientific interest [2], [10]–[16].

One of the characteristics of a fully ionized plasma is its ability to support electric fields of almost arbitrarily large amplitude. A small local deviation from neutrality in an otherwise neutral plasma can give rise to very large local fields. As an example, consider a uniform plasma with an average density of 10^{14} cm^{-3}. A 1% fluctuation in the local electron density over a distance of 1 mm produces a local electric field of $\sim 10^6$ V/cm. This capability of sustaining very high electric fields makes plasma attractive for use in high-power density microwave generators.

The presence of a plasma in a waveguide changes the characteristics of the guide and adds new slow modes of propagation. For the purpose of this discussion, the term "plasma" will be used to describe a fully ionized gas which, in the absence of external disturbances, is electrically neutral. It is further assumed that the ions in the plasma are stationary, and that the electrons have no thermal or random velocities and undergo no collisions. In other words, we will consider an ideal electron plasma. The term "plasmaguide mode" will be used to denote ny of the additional waveguide modes that exist due to the presence of the plasma inside of the guide. These are the slow-wave modes on a nondrifting, ion-neutralized plasma column [17].

In order to generate microwave radiation, we are interested in waves that can cause bunching in an axially streaming relativistic electron beam. Therefore only waves with axial components E_z will be considered. There are two such families of waves: The first is the familiar TM$_{lv}$ family of electromagnetic modes which will be somewhat modified by the presence of the plasma, and the second is a family of plasmaguide modes.

As was demonstrated by Trivelpiece and Gould (T–G) [17], the dispersion relation for a plasma-loaded, smooth-walled, cylindrical waveguide immersed in an infinitely large axial magnetic field is given by:

$$\frac{\omega^2}{c^2} = k_z^2 + \frac{(p_{lv}/R_0)^2}{1 - \omega_p^2/\omega^2} \tag{1}$$

where ω is the angular frequency; k_z is the axial wave number; c is the speed of light in vacuum; R_0 is the waveguide radius; and p_{lv} is the vth root of the lth order Bessel function of the first kind.

If the operating frequency of the device is greater than the plasma frequency ($\omega > \omega_p$), the electromagnetic waves in the plasma-loaded waveguide are very similar to the TM waves in a smooth-walled empty waveguide, as can be seen from (1). The only difference is that the cutoff frequency for the plasma-filled guide is increased relative to the empty waveguide by:

$$\omega_{co}^2 = \left(\frac{p_{lv}}{R_0}\right)^2 + \omega_p^2. \tag{2}$$

This shift in the cutoff frequency can be seen in Fig. 1(b), where the dispersion curve for the lowest-order symmetric electromagnetic mode (labeled "TM$_{01}$") is displayed. In addition, the presence of the plasma in the waveguide allows k_z^2 to take on positive real values for $\omega < \omega_p$, thus giving rise to a propagating wave. Fig. 1(b) also displays plots of several plasma-guide (T–G) modes. The geometry of the problem is shown in Fig. 1(a).

Thus the lower branches in Fig. 1(b) represent a family of plasma-guide modes having a high-frequency cutoff at ω_p and no low-frequency cutoff. One of the interesting features of the plasma-guide modes is that the high-frequency cutoff is independent of the geometry and depends only on the plasma frequency. This is in contrast with the electromagnetic waveguide modes whose cutoff frequencies depend intimately on the geometry. Another difference between the plasma-guide and electromagnetic modes is the fact that for operating frequencies within the plasma-guide mode band ($0 < \omega < \omega_p$), all of the plasma-guide modes ($l \geq 0$, $v \geq 1$) will propagate simultaneously if excited. In contrast, at frequencies above the plasma frequency the number of electromagnetic wave-
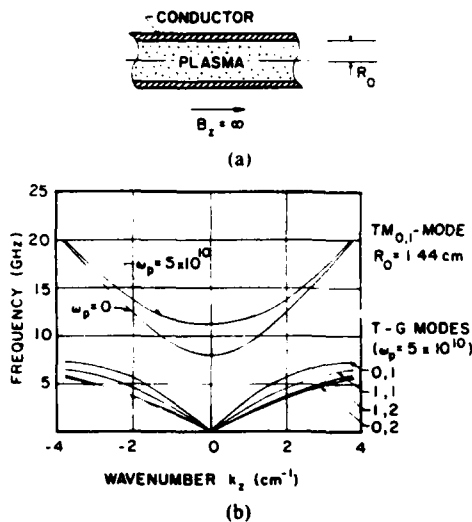
Fig. 1. (a) A smooth-wall plasma-loaded waveguide immersed in an infinitely large guiding magnetic field (model of Section II). (b) The dispersion relation for a plasma-loaded smooth-wall waveguide having a radius of $R_0 = 1.44$ cm. A single TM_{01} mode with and without a plasma, as well as several plasma-guide (T–G) modes, are shown.

guide modes that can propagate at any given frequency is finite, though increasing with frequency. The principal feature of plasma-guide propagation is that a plasma column can support modes of wave propagation below the plasma frequency, even in the absence of electron drift motion.

As was pointed out earlier, the plasma-guide modes are electromechanical in nature. The wave propagation results from the interchange between the kinetic energy of the electrons and the stored energy in the electric field. In contrast, for the case of electromagnetic waves in an evacuated waveguide, the wave propagation results from the interchange of the electric and magnetic stored energy. Nevertheless, there are some similarities between the two families of waves in terms of the field components, mode structure, and power-carrying capabilities. Table I compares the field components and power carried by the two classes of waves for the case of azimuthal symmetry ($l = 0$).

The two families of modes propagate in two different frequency ranges. While the T–G (plasma-guide) modes propogate below the plasma frequency, the electromagnetic modes can only propagate at frequencies above:

$$\omega > \left[\omega_p^2 + \left(\frac{p_{0\nu}}{R_0}\right)^2 \right]^{1/2}. \tag{3}$$

Using Table I, a number of informative plots for the T–G modes may be generated. For example, Fig. 2 shows the electric field configuration for the two lowest-order T–G modes (T–$G_{(0,1)}$ and T–$G_{(0,2)}$). The power carried by these same modes as a function of frequency is plotted in Fig. 3, where a plasma frequency of 4 GHz and a maximum electric field amplitude of 100 kV/cm has been assumed. From this figure it is clear that the presence of the plasma inside the waveguide does not lower the power-handling capabilities of the system. As the wave fre-

TABLE I
FIELD COMPONENTS AND AXIAL POWER FLOW FOR AZIMUTHALLY SYMMETRIC ELECTROMAGNETIC ($TM_{0\nu}$) AND PLASMA-GUIDE (T–G) MODES

	Symmetric $TM_{0\nu}$ Mode in Empty Cylindrical Waveguide	Symmetric Plasmaguide (T–G) Mode in Cylindrical Waveguide
E_r	$A J_0(k_c r)$	$A J_0(k_c r)$
E_z	$-j A \frac{k}{k_c} J_0'(k_c r)$	$-j A \frac{k}{k_c}(1 - \frac{\omega_p^2}{\omega^2}) J_0'(k_c r)$
H_ϕ	$-j A \frac{\omega \epsilon}{k_c} J_0'(k_c r)$	$-j A \frac{\omega \epsilon}{k_c}(1 - \frac{\omega_p^2}{\omega^2}) J_0'(k_c r)$
Axial power flow P	$\frac{1}{2}\pi R_0^2 |A|^2 \frac{k \omega \epsilon}{k_c^2} J_1^2(k_c r)$	$\frac{1}{2}\pi R_0^2 |A|^2 \frac{k \omega \epsilon}{k_c^2}(1 - \frac{\omega_p^2}{\omega^2}) J_1^2(k_c r)$

$k_c = p_{0\nu}/R_0$: Cut-off wavenumber for the specific mode of interest. $A = E_z(r = 0)$: Electric field amplitudes on axis.
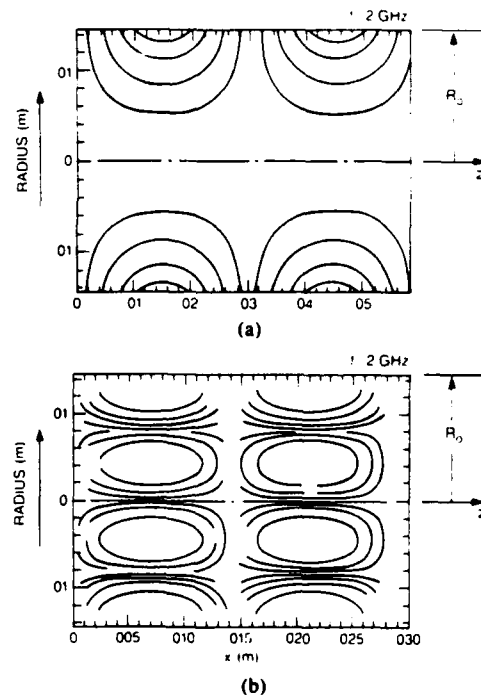
Fig. 2. Electric field configuration for the two lowest-order, symmetric-plasmaguide modes. (a) T–$G_{(0,1)}$. (b) T–$G_{(0,2)}$. Both were calculated for $\omega_p = 2\pi \cdot 4$ GHz, $R_0 = 1.44$ cm at a frequency of 2 GHz.

quency of the T–G mode approaches the plasma frequency, the wave becomes increasingly electrostatic in nature, its power-carrying capability diminishes, and its group velocity $\partial\omega/\partial k$ decreases to zero. Fig. 4 shows the radial distribution of the three field components E_z, E_r, and H_θ for the lowest order ($l = 0$, $\nu = 1$) symmetric plasma-guide mode for various frequencies. As before, as ω approaches $\omega_p = 4$ GHz (in this example), both H_θ and E_r decrease to zero. Only the electrostatic component E_z remains unchanged.

III. SPACE-CHARGE-LIMITING CURRENT IN PLASMA-LOADED WAVEGUIDES

In essence, a backward-wave oscillator consists of an electron beam confined radially by a strong longitudinal

Fig. 3. Calculated power-carrying capabilities of the two lowest-order symmetric plasma-guide modes versus frequency ($\omega_p = 2\pi \cdot 4$ GHz).

Fig. 4. Calculated radial dependence of E_z, E_r, and H_θ for the lowest-order, symmetric plasma-guide mode at few frequencies ($\omega_p = 2\pi \cdot 4$ GHz, $R_0 = 1.44$ cm).

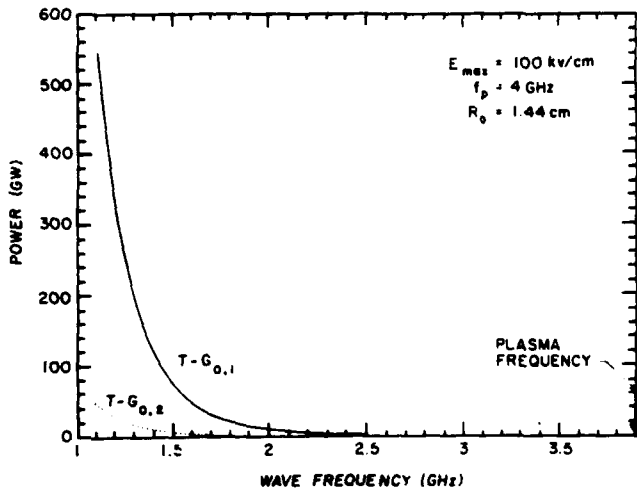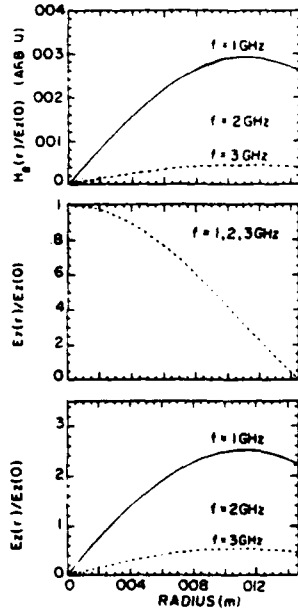magnetic field and propagating axially through a slow-wave structure. The slow-wave structure consists of a cylindrical waveguide with a periodically varying wall radius $R(z)$ sinusoidally rippled about the mean radius R_0, such that:

$$R(z) = R_0 + h \cos k_0 z \qquad (4)$$

as shown in Fig. 5, where h is the ripple amplitude, z_0 is the ripple period, and $k_0 = 2\pi/z_0$.

The slow-wave structure supports a set of electromagnetic modes in the waveguide which has phase velocities parallel to the beam velocity and propagate at less than the speed of light. These slow electromagnetic waves interact resonantly with the negative energy slow space-charge wave supported by the beam, which leads to an instability that transfers kinetic energy from the beam to
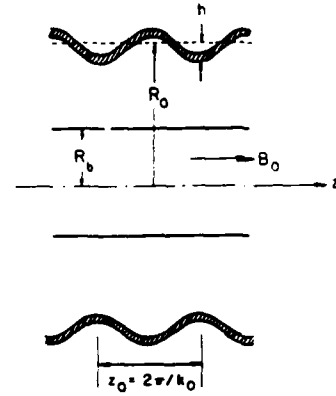

Fig. 5. The slow wave structure and beam model of Section III.

the electromagnetic field of the struct ... The backward-wave oscillator is so named because, at the point of beam and electromagnetic structure-mode resonance, the structure mode has a negative group velocity, resulting in the propagation of electromagne: c energy backward along the beam—i.e., the Poynting vector points antiparallel to the beam velocity.

As indicated in Section I, recent theoretical studies have predicted that the introduction of a plasma into vacuum HPM devices may lead to greatly enhanced performance [2], [10]-[16]. For the purposes of the discussion of the space-charge-limiting current, we will approximate the corrugated-wall waveguide with a smooth-walled waveguide having the same average radius. In the presence of a background plasma, the space-charge-limiting current in a smooth-walled cylindrical waveguide can be increased by a factor of $(1 - f)^{-1}$, where $f = n_i/n_e$ represents the amount of charge neutralization provided by the ions in the background plasma. The increased space-charge-limiting current may allow microwave-generating devices to transport more intense electron beams, leading to the possibility of generating enhanced power levels.

The space-charge-limiting current in the presence of the plasma for a thin hollow beam with a mean radius R_b and a thickness $\Delta \ll R_b$ is given by [18]:

$$I_l = \frac{17[\gamma^{2/3} - 1]^{3/2}}{[2 \ln (R_0/R_b)][1 - f]} \text{ [kA]} \qquad (5)$$

where $\gamma = (1 - v^2/c^2)^{-1/2}$ is the relativistic mass factor for the beam electrons. By increasing the beam current through introduction of a background plasma, a new limitation is encountered which is imposed by the $\quad$ et of beam-plasma instability. This instability will occur at current levels that are larger than the vacuum-limiting current by the factor [2]:

$$\left[\frac{\gamma(1 - \gamma^{-2})}{(1 - \gamma^{-2/3})}\right]^{3/2}. \qquad (6)$$

For mildly relativistic electron beams having $\gamma = 3$, the actual current carried by the beam in the presence of

plasma may be as much as seven times larger than the vacuum case. The increased injected current level may simply allow operation at higher beam power and result in enhanced microwave power output without affecting the interaction efficiency or the physical interaction mechanism.

IV. Linear Theory of Plasma-Loaded Corrugated Waveguides

In addition to affecting the space-charge-limiting current, the presence of plasma in the slow-wave structure may completely alter the nature of the beam–wave interaction, leading to greatly enhanced device power-generation efficiency. The studies reported here are the first that clearly belong to this latter category.

The linear theory of thin annular beams in an evacuated corrugated wall structure has been treated both analytically and numerically by researchers in the U.S. [19] and the Soviet Union [20]. The introduction of plasma into the slow-wave structure, however, necessitates the development of an extension to the vacuum theory. Previous treatment of the linear theory of plasma-loaded structures [21], [22] used the approximation of small corrugation amplitudes ($h/R_0 \ll 1$). Recently, a linear theory allowing for the treatment of arbitrarily large corrugation amplitudes has been developed. A complete description of the theory can be found in [23]. The main results of this linear theory describing the excitation of electromagnetic waves in a plasma-filled BWO by a relativistic electron beam are presented below, where the dispersion relation and growth rates of plasma-filled periodic structures have been calculated.

In developing the linear theory the following assumptions were made: (i) The magnitude of the axial-guiding magnetic field is taken to be infinite, confining the electron motion in the beam to one dimension; (ii) the beam is monoenergetic, with an axial streaming velocity v_b; (iii) the beam is of uniform density N_b and completely fills the waveguide; (iv) the waveguide is infinite in length and the waveguide wall is perfectly conducting; (v) only the symmetric (TM_{0r}) electromagnetic modes are considered; and (vi) the plasma-guide modes are neglected.

In general, the linearized normal electromagnetic modes of a periodic corrugated wall structure are the transverse electric (TE) modes, with electric and magnetic field components E_θ, B_r, and B_z, and the transverse magnetic (TM) modes, with field components E_r, E_z, and B_θ. In our idealized one-dimensional system the TE waves do not perturb the axial electron motion and will not be considered further, since they cannot cause beam instabilities. The TM waves, on the other hand, are capable of perturbing the axial beam velocity and beam density and assumption (v) above is justified.

The periodicity of the slow-wave structure permits the field components and beam perturbation to be expanded in an infinite Floquet sum. Assuming azimuthal symmetry, the axial and radial components of the TM_{0r} electric

field can be expressed as [23]:

$$E_z = \sum_{n=-\infty}^{\infty} A_n J_0\left(\frac{x_n}{R_0}r\right)\exp\left[i(k_n z - \omega t)\right] \qquad (7)$$

$$E_r = \sum_{n=-\infty}^{\infty} A_n \left[-\frac{ik_n x_n}{R_0\left(\frac{\omega^2}{c^2} - k_n^2\right)}\right] J_1\left(\frac{x_n}{R_0}r\right)$$
$$\cdot \exp\left[i(k_n z - \omega t)\right] \qquad (8)$$

where ω_b is the beam-plasma frequency, and

$$k_n = k_z + nk_0$$

$$x_n^2 = R_0^2\left(\frac{\omega^2}{c^2} - k_n^2\right)\left[1 - \frac{\omega_p^2}{\omega^2} - \frac{\omega_b^2\gamma^{-3}}{(\omega - k_n v)^2}\right].$$

Assumption (iv) requires that the tangential electric field vanishes at the waveguide wall. Using the axial and radial electric-field components of (7) and (8), we express this boundary condition in matrix form as:

$$D \cdot A = \sum_{m,n=-\infty}^{\infty} A_n D_{m,n} = 0 \qquad (9)$$

where A is a column vector with elements A_n, and D is a matrix with elements $D_{m,n}$. A dispersion relation results when a nontrivial solution to (9) is found by solving the determinant equation det $|D| = 0$.

In order to numerically analyze experimental systems, the infinite matrix of (9) must be truncated to a finite size. For example, to analyze an experimental system with a corrugation amplitude ratio $h/R_0 = 0.3$, a truncated matrix with a rank of nine was found to be sufficient.

Fig. 6 displays the calculated TM_{01} mode dispersion curves in a plasma-filled corrugated waveguide for a variety of plasma densities. The beam space-charge line, assuming infinitesimal beam density ($\omega_b = 0$), is superimposed on this dispersion curve and has been plotted for the case which corresponds to the experimental parameters to be described in the next section. As can be seen in Fig. 6, the presence of the plasma tends to raise the TM_{01} mode cutoff frequency relative to the vacuum cutoff frequency while also causing a decrease in the group velocity everywhere, resulting in a "flattening" of the dispersion relation.

When the beam density is neglected ($\omega_b = 0$), the radiation frequency ω is real for real values of the axial wave number k_z and no instabilities are expected. To obtain the TM_{01} growth rates, a nonzero value of ω_b must be used and the dispersion equation must be solved for complex values of ω for real values of k_z. Fig. 7 displays the growth rate Im($\omega/2\pi$) calculated for the experimental parameters. The results are similar to those found in [15], with the exception that in this case the peak growth rate is a function of the plasma density as shown in Fig. 8. The calculations predict, therefore, a considerable decrease in the linear growth rate for plasma densities of $N_p \geq 10^{12}$ cm^{-3}.
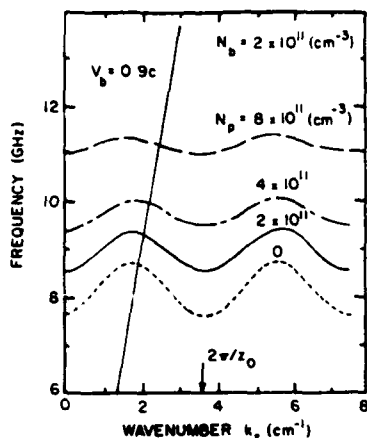
Fig. 6. The calculated effect of varying the plasma density on the corrugated waveguide dispersion ($R_0 = 1.445$ cm, $h = 0.445$ cm, $z_0 = 1.67$ cm).
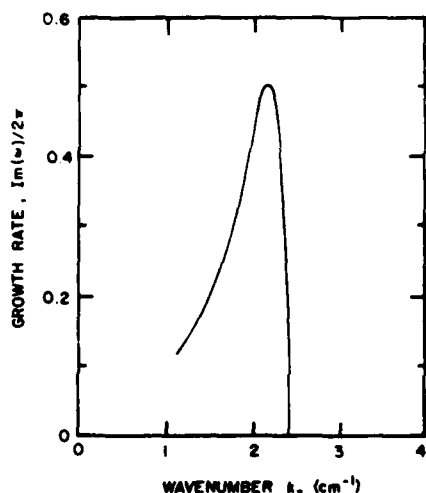

Fig. 7. Calculated linear growth rate for the TM_{01} mode versus wavenumber k_z for the case where $N_p = 2 \cdot 10^{11}$ cm^{-3}, $N_b = 6.3 \cdot 10^{10}$ cm^{-3} (solid beam).
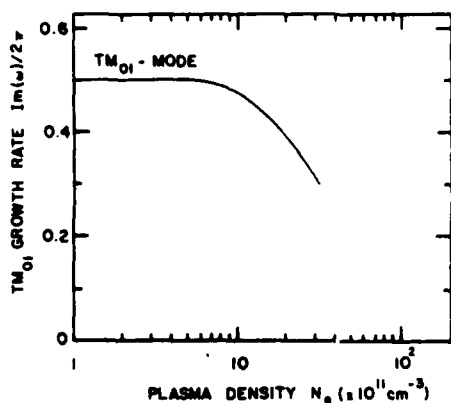

Fig. 8. Calculated peak growth rate $I_m(\omega)/2\pi$ versus the plasma density for the TM_{01} mode (solid beam of density $N_b = 6.3 \cdot 10^{10}$ cm^{-3}).

V. Measurement of Efficiency in a Plasma-Loaded BWO

Early experiments testing the effect of plasma on the operation of vacuum BWO's utilized background plasmas produced by electron-beam impact ionization of a low-pressure neutral background gas to demonstrate enhanced
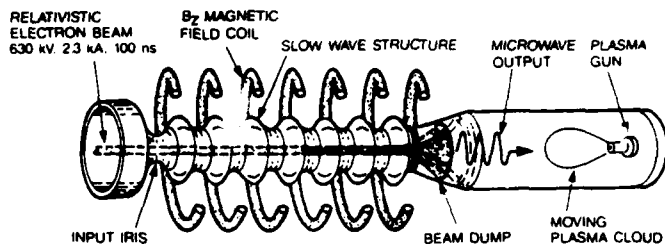

Fig. 9. Schematic diagram of the plasma-loaded BWO experiment. The electron beam is injected from the left and the radiation is extracted at right, where the plasma is injected.

microwave output power [7], [8]. In recent experiments [9] an independently controllable Argon plasma source was used to inject plasma directly into the BWO slow-wave structure, as shown in Fig. 9.

A hollow relativistic electron beam with an injection energy of 630 keV, a beam current of 2.3 kA, and a pulse duration of 100 ns (Fig. 10) was propagated in a sinusoidally rippled slow-wave structure immersed in a uniform axial magnetic field of ~12 kG. The slow-wave structure had an average radius $R_0 = 1.445$ cm, a corrugation amplitude $h = 0.44$ cm, a corrugation period of $z_0 = 1.67$ cm, and a structure length of 8 periods. The electron beam had an average radius of 0.8 cm, a thickness of 0.2 cm, and an electron density of ~5×10^{11} cm^{-3}.

A coaxial plasma gun [24] was located approximately 100-cm downstream of the slow-wave structure in a field free region and generated an Argon plasmoid which crossed the magnetic field lines at an average velocity of about 1.2 cm/μs on its way towards the interaction region. The system was pre-evacuated to a pressure of <4 $\times 10^{-5}$ T.

In separate experiments the plasma column density was measured with both a 35- and 70-GHz microwave interferometer and its velocity, density, and temperature was measured with Langmuir probes. Preliminary results indicate that the average plasma density could be varied by changing the plasma gun voltage and gas pressure. Realizable plasma densities in the slow-wave structure ranged from 0 up to a maximum value estimated at ~10^{12} cm^{-3}.

There were three principal overlapping time scales in the BWO experiments: The longest time scale was on the order of 10 ms, corresponding to the quarter-cycle time of the pulsed axial-guiding magnetic field. The second longest time scale was on the order of 100 μs, corresponding to the plasma generation and propagation time from the plasma gun to the slow-wave structure. Finally, as noted above, the beam pulse duration was 100 ns. The three time scales were all synchronized such that the beam and plasma interacted in the slow-wave structure during the time that the applied magnetic field was nearly constant and at its peak value.

The plasma density in the slow-wave structure was intentionally varied from shot-to-shot in order to determine its effect on the operational efficiency of the BWO. The plasma density was varied in the slow-wave structure by delaying the time of beam injection into the slow-wave
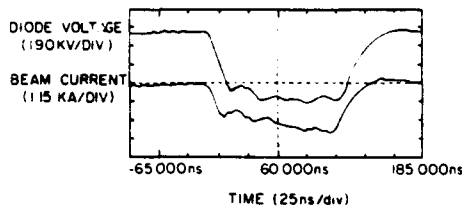
Fig. 10. Diode voltage (top trace) and BWO beam-current waveforms used in the experiment. An annular beam with an average radius of 0.8 cm and a thickness of 0.2 cm was used.

Fig. 11. Peak microwave power (at 8.4 GHz) versus the beam-injection time delay. By adjusting this delay we can set the desired plasma density in the BWO before the injection of the electron beam.

structure relative to the time of initial plasma generation. By changing the relative delay times from shot-to-shot, a greater or lesser density plasma was allowed to diffuse into the slow wave structure at the instant of beam injection.

An enhancement of the microwave power-generation efficiency was observed over a wide range of injected plasma densities, $0 < N_p < N_{p(cr)}$, where $N_{p(cr)}$ is a critical plasma density. This critical plasma density, to be discussed in Section VII, occurred at a delay time $\Delta t \sim 90$ μs relative to the initial generation of the plasma. The efficiency enhancement factor over vacuum BWO operation was found to be dependent on the plasma density and reached a maximum value of eight when the electron beam was injected into an optimized plasma density.

The points of maximum BWO efficiency enhancement were found to occur for two different time delays—once for a short time delay $\Delta t \sim 60$ μs, which occurred during the plasma buildup in the slow-wave structure, and then again for a longer delay $\Delta t \sim 100$ μs, which occurred during the plasma decay. Fig. 11 is a plot of the peak radiated power (at 8.4 GHz) as a function of the beam-injection time delay Δt gathered over a number of shots. At the points of maximum enhancement, indicated by the two relative maxima of Fig. 11, the interaction efficiency increased to almost 40%, compared with approximately 5% for a vacuum BWO under the same operating conditions. The output power was measured using a side coupler calibrated for the TM_{01} mode over the relevant bandwidth.

The plasma density in the slow-wave structure reached its highest values for beam-injection time delays in the range 60 μs $< \Delta t < 100$ μs. In this range the BWO radiation at 8.4 GHz from the fundamental TM_{01} mode was quenched and higher frequency emission in the 12–18-GHz range was observed. At these higher plasma densities the BWO was considered to be overdriven and switched from the fundamental TM_{01} mode to TM_{02} and possibly higher order modes, as indicated in Fig. 12.

An example of the change in frequency spectra that accompanies mode switching is shown in Fig. 13, which plots the single-shot experimental spectrum for an efficiency-enhanced BWO, shown in Fig. 13(a), and an overdriven BWO, as shown in Fig. 13(b). These experimental curves were obtained using a dispersive line technique, where different frequency components are resolved by their different propagation velocities in a dispersive wave-
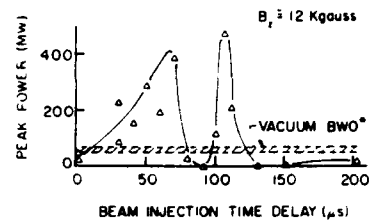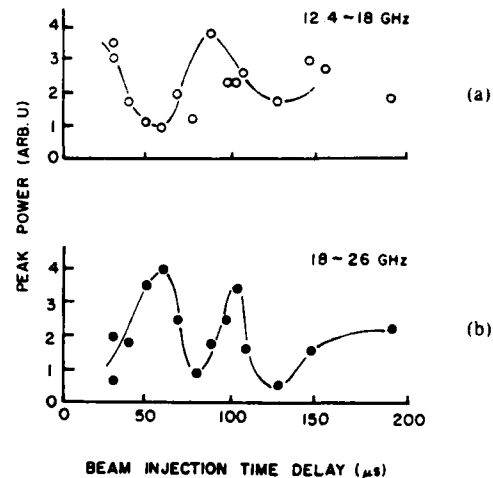
Fig. 12. Microwave radiation detected from the plasma-loaded BWO in the frequency bands: (a) 12–18 GHz (corresponding to emission at high-order mode); and (b) 18–26 GHz (which may correspond to emission due to an electromagnetically pumped FEL; see discussion).
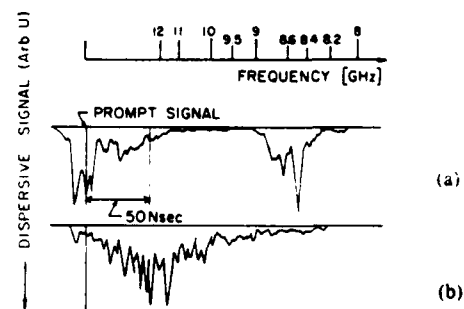
Fig. 13. Spectral results from plasma-enhanced backward-wave oscillator. (a) Maximum enhancement; and (b) overdriven device. The "prompt signal" is a timing reference.

guide. Fig. 13(a) plots the power spectrum emitted by the BWO under the condition of strong plasma enhancement, where the dominant frequency component is centered near 8.4 GHz. A timing-reference microwave signal (labeled prompt) is superimposed on the dispersed signal. Fig. 13(b) represents the spectrum for an overdriven device in which mode switching has clearly occurred and frequency components in the range of 12–18 Gz are present, corresponding to TM_{02} or higher order modes as well as plasma oscillation. At even higher plasma densities microwave breakdown within the device will occur.

Strong microwave emission was also detected in the 18–26 GHz band, proportional in amplitude to the fun-

damental TM_{01} backward-wave oscillations. These high frequencies are believed to be produced by a free-electron laser interaction driven by an electromagnetic pump, as previously reported [25], [26].

In our experiments the introduction of plasma into the device had no adverse effects on the diode voltage and current. The beam current entering the slow-wave structure was unaffected by the presence of the plasma and no effect on the diode shorting time was observed.

VI. DISCUSSION OF RESULTS, COUPLING MECHANISMS, AND FUTURE TRENDS IN PLASMA MICROWAVE ELECTRONICS

As the experiments described in the previous section demonstrate, the presence of a controlled plasma in the BWO slow-wave structure strongly enhances the interaction efficiency over a very wide range of plasma densities. In addition to efficiency enhancement, two other interesting features of the experimental results are: BWO plasma-saturation effects, and mode switching.

It was anticipated that overdriving the device with plasma above a critical density $N_{p(cr)}$ would lead to a quenching of the BWO interaction. As discussed in Section IV, the presence of plasma in the slow-wave structure tends to raise the lower cutoff frequency while simultaneously causing a flattening of the overall dispersion curves. If the device is overdriven to a point where the lower and upper cutoff frequencies are similar, the electromagnetic-mode group velocity is drastically reduced and no backward wave interaction is possible.

The linear theory of electromagnetic waves in plasma-loaded BWO's, presented in Section III, predicts that BWO TM_{01} quenching by plasma saturation might be observed for critical densities,

$$N_{p(cr)} \cong 10^{12} [\text{cm}^{-3}]. \tag{10}$$

If the plasma density is above this critical value, the linear growth rate will begin to decrease as shown in Fig. 8. Linear theory also predicts that mode switching may occur at about the same critical density [23]. Indeed, both BWO plasma saturation, as seen in Fig. 11, and mode switching, as seen in Figs. 12 and 13, were observed when the device was overdriven. This occurred when the beam-injection delay time was adjusted to $\Delta t \sim 90\ \mu s$, corresponding to an estimated plasma density of $N_p < 2 \times 10^{11}$ cm^{-3}, which is far below the value predicted by the linear theory.

The linear theory for a plasma-loaded fundamental TM_{01} mode in a BW predicts that the interaction frequency of the BWO ill increase with increased plasma density, as may be seen in Fig. 6. This predicted increase has not yet been observed experimentally. Recent data indicates that the radiation frequency remains fixed (within the measurement resolution) despite changes in the plasma density. The growth rate predicted by the theory is only slightly larger in the presence of the plasma as compared to the vacuum BWO case.

Thus while the linear theory is successful at predicting some experimentally observed trends such as reduction of the growth rate (plasma saturation) and mode switching due to the presence of the plasma, it does not produce numerical results that are reasonably close to the experimental data. This leads us to the conclusion that the present linear theory must be extended to account for the observed experimental results.

One physical mechanism which may explain the enhanced efficiency is a three-wave interaction involving the beam, electromagnetic, and T–G plasma waves in the periodic slow-wave structure. In a nonperiodic structure, the normal T–G modes will not interact with a relativistic electron beam, as their phase velocities are small compared to the phase velocity of the beam space-charge wave. In a periodic structure, however, the T–G modes are also expected to exhibit periodicity in k-space, as required by the Floquet theorem. The dispersion curve for a periodic plasma is quite different from that shown in Fig. 1(b) for a plasma in a smooth-walled waveguide. Most significantly, there exist some periodic T–G modes that have phase velocities that are equal to that of the relativistic electron beam and are capable of supporting backward waves.

As an example, Fig. 14 plots the uncoupled. shifted dispersion curves for the $T-G_{(0.2)}$ modes (labeled as "plasma waves"), and also the approximate coupled dispersion relation for this mode. The dispersion curve for the lowest-order electromagnetic mode (labeled "TM_{01}") can also be seen. Azimuthal symmetry has been assumed, and, for clarity, only the first five periods in k have been plotted.

For the range of values of the plasma density and beam energy relevant to the experiments reported in this paper, the beam is simultaneously in synchronism with the backward branch of the electromagnetic structure wave and several backward branches of the periodic plasma waves. The slow space-charge wave and the lowest order TM_{01} electromagnetic wave have the same phase velocity ω/k as do one or more of the periodic T–G waves. In addition, the three waves all share a strong common component of the axial electric field E_z. It is possible that the enhanced efficiency observed in the experiment results from this three-wave synchronism; namely, induced scattering of the electromagnetic radiation of electrons in an electrostatic field produced by the background plasma in the presence of a periodic, perfectly conducting wall.

An efficient three-wave interaction also implies a very broad gain curve with respect to the electron-beam energy. This implication is consistent with the foregoing proposed mechanism, since the beam electrons tend to stay in synchronism with both of the backward branches, even as the beam is losing energy. A change of 40% in the beam kinetic energy corresponds to a change of less than 5% in the streaming velocity for our experimental conditions.

A second mechanism which may explain the enhanced emission in the presence of the plasma is a stimulated Raman scattering process which may be described using a
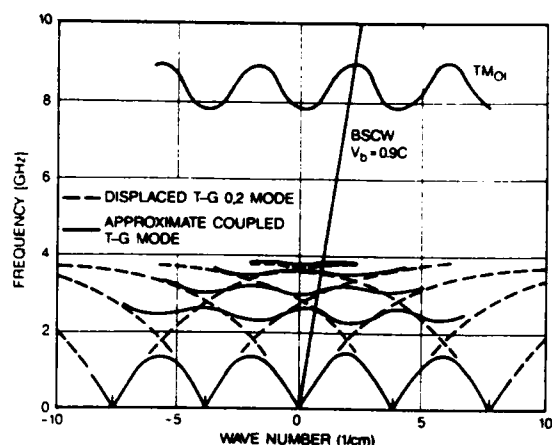
Fig. 14. Schematic sketch of the dispersion diagram for the electromagnetic TM_{01} mode, the plasma-guide T-$G_{(0.2)}$ mode, and a space-charge wave on a low-density beam traveling at $v_b = 0.9c$ (see discussion).
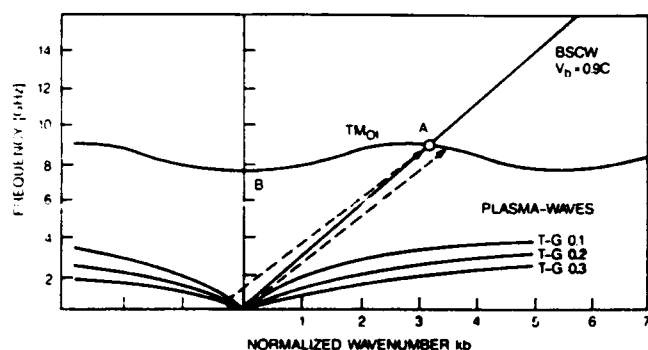

Fig. 15. Schematic sketch of Stokes diagram for three-wave interaction, which involves a backward branch of the plasma-guide (T-G) mode, and two TM_{01} waves of somewhat different frequencies.

Stokes diagram, as shown in Fig. 15. In this figure, the electromagnetic wave (point A) decays into a backward plasma-guide (T-G) wave and an electromagnetic wave which is slightly shifted in frequency. Thus this mechanism proposes a multiwave interaction as the explanation for enhanced efficiency.

It should be noted that for the experiments described in this work, the electron-beam current was always below that of the vacuum limit for the device geometry. As a result, we have not yet studied the radiation generation mechanism at beam currents above this limit. As discussed in Section III, the introduction of plasma into the slow-wave structure may have the effect of neutralizing the RF space charge in the beam (allowing a greater degree of axial bunching) and also may allow the propagation of beam currents above the vacuum space-charge limit. This phenomenon is of great interest to the field of relativistic microwave electronics and may be the subject of future experimental work.

It is anticipated that plasma injection may also prove beneficial to a variety of high-power microwave devices [12]–[16], [21]. Gyrotrons, for example, may achieve a greater degree of tunability and yield higher output power by overcoming the space-charge limit [14].

It was predicted theoretically [12] that larger gain can

be realized in plasma-loaded free-electron lasers that are expected to exhibit greater tunability and performance enhancement by changing the refractive index n in the cavity [13].

REFERENCES

[1] D. Bohm and E. Gross, "Plasma oscillations as a cause of acceleration of cosmic ray particles," Phys. Rev., vol. 74, no. 5, p. 624, Sept. 1948.
    I. Akhiezer and Ya. B. Fainberg, Dokl. Akad. Nauk. SSSR, vol. 65, p. 555, 1949.
[2] M. V. Kuzelev et al., "Relativistic high-current plasma microwave electronics: Advantages, progress and outlook," Sov. J. Plasma Phys., vol. 13, no. 11, pp. 793-800, Nov. 1987.
[3] Special issues on high-power microwave generation, IEEE Trans. Plasma Sci., vol. 13, Dec. 1985, and IEEE Trans. Plasma Sci., vol. 16, Apr. 1988.
[4] S. P. Bugaev et al., "Atmospheric microwave discharge and study of the coherence of radiation from a multiwave Čerenkov generator," Sov. Phys.—Dokl., vol. 32, no. 1, pp. 78-79, Jan. 1988.
[5] S. P. Bugaev et al., "Investigation of a millimeter wavelength range gigawatt power level multiwave Čerenkov generator," in Proc. 7th Int. Conf. High-Power Electron Beams (Karlsruhe, FDR), July 1988, vol. 1, pp. 454-460.
    S. P. Bugaev et al., "Investigation of a millimeter wavelength range relativistic diffraction generator," IEEE Trans. Plasma Sci., this issue, pp. 518-524.
[6] V. I. Bratman et al., "Relativistic Čerenkov source for the millimeter range," Sov. Tech. Phys. Lett., vol. 9, no. 5, pp. 266-267, May 1983.
[7] Yu. V. Tkach et al., "Emission by a relativistic beam at a magneto-Čerenkov resonance in a periodic waveguide," Sov. J. Plasma Phys., vol. 5, no. 5, pp. 568-570, Sept.-Oct. 1979.
[8] K. Minami et al., "Observation of resonant enhancement of microwave radiation from a gas-filled backward wave oscillator," Appl. Phys. Lett., vol. 53, no. 7, pp. 559-561, Aug. 1988.
[9] Y. Carmel et al., "Demonstration of efficiency enhancement in a high power backward wave oscillator by plasma injection," Phys. Rev. Lett., vol. 62, no. 20, pp. 2389-2392, May 1989.
[10] L. S. Bogdankevich et al., "Theory of excitation of plasma filled rippled boundary resonators by relativistic electron beams," Sov. Phys.—Tech. Phys., vol. 25, no. 2, pp. 143-147, Feb. 1980.
[11] V. I. Kurilko et al., "Effect of plasma on the amplification of regular waves by a relativistic beam in a corrugated waveguide," Sov. Phys.—Tech. Phys., vol. 26, no. 7, pp. 812-815, July 1981.
[12] W. B. Pei and Y. S. Chen, "The effect of background plasma in the undulator on free electron lasers," Int. J. Electron., vol. 65, no. 3, pp. 551-564, 1988.
[13] M. B. Reid et al., "Novel approaches to FEL operation: The gas-loaded FEL and a high efficiency FEL design," Int. J. Electron., vol. 65, no. 3, pp. 533-550, 1988.
[14] W. M. Manheimer et al., "Experimental investigation of plasma neutralized operation of a gyrotron," Bull. Amer. Phys. Soc., vol. 33, no. 9, p. 1956, Oct. 1988.
[15] J. S. DeGroot et al., "High power and superpower plasma Čerenkov masers," in Microwave and Particle Beam Sources and Directed Energy Concepts (SPIE vol. 1061). SPIE, Jan. 1989.
[16] R. W. Schumacher et al., "Millimeter wave generation via plasma three wave mixing," Hughes Res. Lab., Malibu, CA, Rep. No. F49620-85-C-0059.
[17] A. W. Trivelpiece and R. W. Gould, "Space charge waves in cylindrical columns," J. Appl. Phys., vol. 30, no. 11, pp. 1784-1793, Nov. 1959.
[18] R. B. Miller, Intense Charged Particle Beams. New York: Plenum, 1982, p. 85.
[19] J. A. Swegle et al., "Backward wave oscillators with rippled wall

resonators: Analytic theory and numerical simulation," *Phys. Fluids*. vol. 28, no. 9, pp. 2882-2894, Sept. 1985.

[20] V. I. Kurilko *et al.*, "Stability of a relativistic electron beam in a periodic cylindrical waveguide," *Sov. Phys.—Tech. Phys.*, vol. 24, no. 12, pp. 1451-1454, Dec. 1979.

[21] L. S. Bogdankevich *et al.*, "Theory of excitation of plasma filled rippled boundary resonators by relativistic electron beams," *Sov. Phys.—Tech. Phys.*, vol. 25, no. 2, pp. 143-147, Feb. 1980.

[22] V. I. Kurilko *et al.*, "Effect of a plasma on the amplification of regular waves by a relativistic electron in a corrugated waveguide," *Sov. Phys.—Tech. Phys.*, vol. 26, no. 7, pp. 812-815, v 1981.

[23] K. Minami *et al.*, "Linear theory of electromagnetic ave generation in a plasma-loaded rrugated wall resonator," *IEEE Trans. Plasma Sci.*, this issue, pp. 37-545.

[24] J. Marshall *et al.*, in *Proc. 2nd Int. Conf. Plasma Phys. Controlled Nucl. Fusion Res.* (Culham, UK), 1965. Vienna: I A. 1966. vol. 2, p. 449.

[25] P. G. Zhukov *et al.*, in *Proc. 3rd Int. Topical Conf. High Power Electron and Ion Beam Res. Tech.*, A. N. Skrinsky, Ed. Novosibirsk, USSR: Inst. Nucl. Phys., 1979. vol. 1, p. 705.
G. G. Denisov *et al.*, *Int. J. Infrared Millimeter Waves*. vol. 5, p. 1389, 1984.

[26] R. A. Kehs *et al.*, "Experimental demonstration of an electromagnetically pumped free electron laser with a cyclotron monic idler." *Phys. Rev. Lett.*, vol. 60, no. 4, pp. 279-281, Jan s8.
R. A. Kehs *et al.*, "Free electron laser pumped by a powerful traveling electromagnetic wave." *IEEE Trans. Plasma Sci.*, this issue, pp. 437-446.

*

Yuval Carmel (S'66-M'74) was born in Israel in 1942. He received the B.Sc.(EE) and M.Sc.(EE) degrees from the Technion, Israel Institute of Technology, in 1966 and 1971, respectively, and Ph.D.(EE) degree from Cornell University, Ithaca, NY, in 1974.

He was with the Government of Israel, the Naval Research Laboratory, and is currently with the University of Maryland, College Park His research interests include electromagnetic radiation from intense electron beams, free electron lasers. advanced concepts in millimeter-wave tubes, gyrotrons, and backward wave oscillators.

*

K. Minami, photograph and biography not available at the time of publication.

*

Weiran Lou was born in Hangzhou. China, on July 2, 1963 He received the B.S. (electrical engineering, 3) and M.S. (optical engineering, 1986) degr from Zhejiang University, Hangzhou, China. He is currently a Ph.D. degree candidate in the Electrical Engineering Department, University of Maryland, College Park. His research interests include high-power microwave generations and microwave-plasma interaction.

R. Alan Kehs (S'68-M ?S-SM'88) received the B.S. and M.S. degrees ir ectrical engineering, and the M.S. and Ph.D. degrees in physics from the University of Maryland. College Park, in 1970, 1973, 1984, and 1987, respectively.

He has been employed by the Harry Diamond Laboratories, Adelphi, MD, since 1975, where his esearch interests have centered on the generat n and use of intense relativistic electron beams— with emphasis on the production of high-power microwave radiation.

Dr. is a member of Eta Kappa Nu, Sigma Xi, and the nerican Physical Society.

*

William . Destler (M'84), photograph and biography not available at the time of publication.

*

Victor L. Granatstein (S'59-M'64-SM'86) received the Ph.D. degree in 1963 from Columbia University, New York City, in electrical engineering and plasma physics.

After a year of postdoctoral work at Columbia University, he was a member of the Technical Staff of Bell Telephone Laboratories from 1964-1972. During 1969-1970 he was a Visiting S r Lecturer at the Hebrew University of Jerusalem. In 1972 he joined the Naval Research Laboratory as a Research Physicist and from 1978-1983 served as Head of the High-Power Electromagnetic Radiation Branch. In August 1983 he became a Professor in the Electrical Engineering Department at University of Maryland, College Park, and also serves as a Consultant to the Naval Research Laboratory, the Science Applications International Corporation, the Jet Propulsion Laboratory, and the State of Maryland (Department of Natural Resources). He is presently leading experimental and theoretical studies of electromagnetic radiation from relativistic electron beams, advanced concepts in millimeter-wave tubes, free electron lasers, and gyrotron amplifiers. He is Associate Editor of the *International Journal of Electronics* and has been a Guest Editor of the IEEE TRANSACTIONS ON MICROWAVE THEORY AND TECHNIQUES and the IEEE JOURNAL OF QUANTUM ELECTRONICS. He has been a reviewer for the NSF, AFOSR, DOE DNA, ONR, and ARO. He has co-authored more than 100 research papers in regular journals, and holds a number of patents on active and passive microwave devices. Since 1988 he has been Director of the Laboratory for Plasma Research at the University of Maryland.

Professor Granatstein is a Fellow of the American Physical Society.

*

D. K. Abe, photograph and biography not available at the time of publication.

*

J. Rodgers, photograph and biography not available at the time of publication.

Linear Theory of Electromagnetic Wave Generation in a Plasma-Loaded Corrugated-Wall Resonator

K. Minami

Yuval Carmel

Victor L. Granatstein

William W. Destler

Weiran Lou

D. K. Abe

T. Hosokawa

K. Ogura

t. Watanabe

Linear Theory of Electromagnetic Wave Generation in a Plasma-Loaded Corrugated-Wall Resonator

K. MINAMI. YUVAL CARMEL. MEMBER. IEEE. VICTOR L. GRANATSTEIN. SENIOR MEMBER. IEEE.
WILLIAM W. DESTLER. MEMBER. IEEE. WEIRAN LOU. D. K. ABE.
R. ALAN KEHS. SENIOR MEMBER. IEEE. M. M. ALI.
T. HOSOKAWA. K. OGURA. AND T. WATANABE

Abstract—A linear theory of the excitation of electromagnetic waves in a plasma-filled corrugated-wall waveguide with an arbitrarily large sinusoidal corrugation has been derived and analyzed numerically. The theory predicts that, when driven by an electron beam. the presence of a plasma in the slow wave structure will cause an increase in the oscillation frequency, and that the temporal growth rates of a high-frequency mode approach those of fundamental mode for high plasma densities. The latter result may account for the high-frequency modes observed in our plasma-filled backward-wave oscillator.

I. INTRODUCTION

THE ELECTRON beam excitation of slow wave structures has been an active research area for more than half a century [1]. With recent progress in intense relativistic electron beam (IREB) technology, a new generation of high-power microwave sources is being developed. The backward-wave oscillator (BWO) is one of the most prominent IREB-driven high-power microwave sources [2]-[5]. Peak powers in excess of 3 GW in a single-stage device. 15 GW in a two-stage device. long pulse lengths of several microseconds. high efficiencies (>50%). and a pulse repetition rate of 400 Hz have been reached in a variety of experiments [6]. More commonly, power levels of hundreds of megawatts at frequencies ranging from 8 to 35 GHz have been reported. although frequencies as high as 150 GHz have been demonstrated.

Recent experiments at the University of Maryland have demonstrated high-efficiency high-power operation through the introduction of a background plasma into an X-band BWO structure [7], [8].

As a first step toward understanding this phenomenon. a linear dispersion relation for a plasma-loaded BWO has been derived and analyzed numerically. with special emphasis placed on using system parameters consistent with experiments performed at the University of Maryland [7], [8]. The development of the dispersion relation may lead to a discussion of a three-wave interaction (beam/plasma/ slow electromagnetic wave) as a possible physical mechanism to explain experimental observations.

Section II of this paper contains the derivation of a dispersion relation for waves in an infinitely long plasma-loaded corrugated-wall waveguide excited by an electron beam. Section III presents the numerical analyses of the interaction, and a discussion of this work. along with conclusions. is presented in Section IV.

II. DISPERSION RELATION FOR A PLASMA-LOADED CORRUGATED-WALL WAVEGUIDE

The analyses presented here are based on the slow-wave structure shown in Fig. 1. The slow-wave structure consists of an axially symmetric. cylindrical waveguide whose wall radius. $R(z)$. varies sinusoidally according to the relation

$$R(z) = R_0 + h \cos (k_0 z) \qquad (1)$$

where h is the corrugation amplitude. $k_0 = 2\pi/z_0$ is the corrugation wavenumber, and z_0 is the length of the corrugation period.

A solid uniform electron beam of density N_b and radius $R_b < R_0 - h$ goes through the waveguide. which is loaded completely with a cold. uniform. collisionless plasma of density N_p. The entire system is immersed in a strong. longitudinal magnetic field. which magnetizes both the beam and the plasma. There is no restriction on the relationship between the beam density and the plasma density. but the plasma frequency and the beam plasma frequency. $\omega_p = (e^2 N_p/m_e \epsilon_0)^{1/2}$ and $\omega_b = (e^2 N_b/m_e \epsilon_0)^{1/2}$. respectively, are assumed to be much smaller than the electron cyclotron frequency.

We further assume that i) the beam current is taken to be much less than the space-charge-limiting current for a smooth-walled waveguide with the same average radius: ii) the beam is monoenergetic with all electrons having identical longitudinal velocity v: and iii) the beam has an
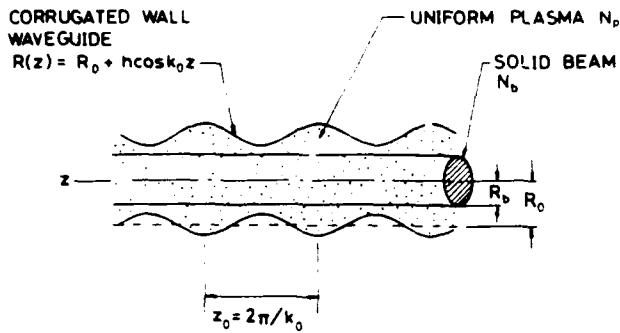
CORRUGATED WALL
WAVEGUIDE
$R(z) = R_0 + h\cos k_0 z$

UNIFORM PLASMA N_p

SOLID BEAM N_b

$z_0 = 2\pi/k_0$

Fig 1. Slow wave structure and beam model of sections II–IV for solid electron beam of radius R_h, within perfectly conducting plasma-loaded corrugated-wall waveguide.

equilibrium position, and is free from instabilities which cause macroscopic deformations.

The dispersion relation for a plasma-filled BWO was previously derived for the case of a slow-wave structure with a small corrugation amplitude [9], [10] and only included terms up to the order of $(h/R_0)^2$. In our experiments, however, the corrugation amplitude was not small ($h/R_0 = 0.308$), necessitating the derivation of a dispersion relation for arbitrarily large values of $h/R_0 < 1$.

The assumption of an infinitely large guiding magnetic field implies that the only nonvanishing terms in the relative dielectric tensor are along the major diagonal. For the beam–plasma case in a linearized scheme of treatment, the relative dielectric tensor, in cylindrical coordinates, may be given by

$$[\epsilon] = \begin{bmatrix} 1 & 0 & 0 \\ 0 & 1 & 0 \\ 0 & 0 & \epsilon_{zz} \end{bmatrix} \qquad (2)$$

and by [10]

$$\epsilon_{zz} = 1 - \left(\frac{\omega_p}{\omega}\right)^2 - \frac{\omega_b^2}{\gamma^3(\omega - k_n v)^2} \qquad (3)$$

where γ is the relativistic factor, and k_n is the wavenumber (to be defined later).

The periodicity of the corrugated structure permits the field components and the beam perturbation to include an infinite number of components in the wavenumber space according to the Floquet theorem [11]. Only TM waves perturb the axial velocity and the density of the beam. Accordingly, we will focus our attention on the dispersion relations for the axisymmetric case of these modes alone. From Maxwell's equations and (2) and (3), one can obtain the following expressions for the axial and radial RF electric fields E_z and E_r for the axisymmetric TM electromagnetic modes:

$$E_z(r, z) = \sum_{n=-\infty}^{\infty} E_{zn} \exp\left[i(k_n z - \omega t)\right] \qquad (4)$$

$$E_r(r, z) = \sum_{n=-\infty}^{\infty} \frac{ik_n}{\frac{\omega^2}{c^2} - k_n^2} \exp\left[i(k_n z - \omega t)\right] \frac{dE_{zn}}{dr} \qquad (5)$$

where k_z is the axial wavenumber, and

$$k_n = k_z + nk_0$$

$$E_{zn} = A_n J_0\left(\frac{x_n}{R_0} r\right) \qquad 0 \leq r \leq R_h$$

$$= B_n J_0\left(\frac{y_n}{R_0} r\right) + C_n N_0\left(\frac{y_n}{R_0} r\right), \qquad (6)$$

$$R_h \leq r \leq R(z)$$

$$x_n^2 = R_0^2 \left(\frac{\omega^2}{c^2} - k_n^2\right)\left[1 - \frac{\omega_p^2}{\omega^2} - \frac{\omega_b^2}{\gamma^3(\omega - k_n v)^2}\right] \qquad (7)$$

$$y_n^2 = R_0^2 \left(\frac{\omega^2}{c^2} - k_n^2\right)\left(1 - \frac{\omega_p^2}{\omega^2}\right). \qquad (8)$$

The constants B_n and C_n in (6) can be expressed in terms of the constant A_n from the conditions for the continuity of E_r and E_z at $r = R_h$ as

$$B_n = -\frac{\pi\delta}{2} K_n A_n, \qquad C_n = -\frac{\pi\delta}{2} L_n A_n$$

$$K_n = y_n J_0(x_n\delta)N_1(y_n\delta) - x_n J_1(x_n\delta)N_0(y_n\delta)$$

$$L_n = x_n J_0(y_n\delta)J_1(x_n\delta) - y_n J_0(x_n\delta) J_1(y_n\delta) \qquad (9)$$

$$\delta = R_h/R_0.$$

The RF electric fields E_z and E_r must satisfy the boundary condition that, at the perfectly conducting corrugated waveguide surface, the tangential electric field E_t must be zero; i.e.,

$$E_t(r = R(z))$$

$$\propto E_z(r = R(z)) + E_r(r = R(z)) \frac{dR(z)}{dz} = 0. \qquad (10)$$

Substituting (4)–(9) into (10), the dispersion relation which describes the dependence of the angular oscillation frequency ω on the axial wavenumber k_z is derived from the requirement for the existence of a nontrivial set of solutions of amplitudes A_n.

Equation (10) is a dispersion relation which gives a relationship between ω and k_z; however, (10) is only of limited use in itself, because it is dependent on the coordinate z and involves as yet unknown coefficients A_n. To eliminate these quantities, we proceed as in [9] and [10], multiplying (10) by $\exp(-imk_0 z)$ and integrating from $z = -\pi/k_0$ to $z = \pi/k_0$. The important difference from previous works [9], [10] is that this work uses an arbitrary corrugation amplitude h, and all the higher order terms

TABLE I
NUMERICAL FACTORS $H(|n - m|, s)$ AS DEFINED BY EQUATION (15) IN TEXT[a]

s \ $|n-m|$	0	1	2	3	4	5	6	7	8	9	10
0	1		4		64		2304		147456		14745600
1		2		16		384		18432		1474560	
2			8		96		3072		184320		17694720
3				48		768		30720		2211840	
4					384		7680		368640		30965760
5						3840		92160		5160960	
6							46080		1290240		82575360
7								645120		20643840	
8									10321920		371589120

[a] Blank boxes indicate that $1/H(|n - m|, s) = 0$. Factors 3×3, 5×5, and 9×9 determinant calculations are shown by thick lines. Here s is given by $s = 2q + |n - m|$ as in equation (15). Adjacent diagonal numbers are related to each other by a factor enclosed by a circle.

are included in the analysis. The resulting dispersion relation is found to be

$$\sum_{n = -\infty}^{\infty} A_n \int_{-\pi/k_0}^{\pi/k_0} \exp\left[i(n - m)k_0 z\right]$$

$$\cdot \left(1 + \frac{ik_n}{\frac{\omega^2}{c^2} - k_n^2}\frac{d}{dz}\right)$$

$$\times \left[K_n J_0\left(\frac{y_n}{R_0} R(z)\right) + L_n N_0\left(\frac{y_n}{R_0} R(z)\right)\right] dz = 0.$$

$$(11)$$

To solve (11), $J_0(y_n R(z)/R_0)$ and $N_0(y_n R(z)/R_0)$ are Taylor expanded about $R(z) = R_0$. The following relations are useful formulas which facilitate the calculation:

$$\cos^{2s} u = \frac{1}{2^{2s-1}}\left[\sum_{j=0}^{s-1}\binom{2s}{j}\cos 2(s - j)u + \frac{1}{2}\binom{2s}{s}\right]$$

$$\cos^{2s+1} u = \frac{1}{2^{2s}}\sum_{j=0}^{s}\binom{2s + 1}{j}\cos\left[2(s - j) + 1\right]u$$

$$\int_{-\pi}^{\pi} \cos mu \cos nu\, du = \begin{cases} 0 & (m \neq n) \\ \pi & (m = n \neq 0) \end{cases}$$

$$\int_{-\pi}^{\pi} \sin mu \cos nu\, du = 0.$$

Equation (11) may be expressed in matrix notation:

$$D \cdot A = \sum_{m \cdot n = -\infty}^{\infty} D_{mn} A_n = 0 \qquad (12)$$

where A is a column vector with elements A_n, and D is a matrix with elements D_{mn} obtained from the integral in (11).

$$D_{mn} = \left[1 + (n - m)Q_n\right](K_n C_{mn}^J + L_n C_{mn}^N) \qquad (13)$$

where

$$C_{mn}^J = \sum_{q=0}^{\infty} \frac{(y_n \alpha)^{2q + |n - m|} J_0^{(2q + |n - m|)}(y_n)}{2^{2q + |n - m|} q!(q + |n - m|)!}$$

$$Q_n = \frac{k_0 k_n}{\frac{\omega^2}{c^2} - k_n^2}, \qquad \alpha = \frac{h}{R_0} \qquad (14)$$

and C_{mn}^N is obtained by replacing J_0 in C_{mn}^J by N_0.

Equation (12) represents an infinite set of linear equations in unknown A_n's. Each term C_{mn}^J in (14) is of the form:

$$C_{mn}^J = \frac{(y_n \alpha)^s J_0^{(s)}(y_n)}{H(|n - m|, s)} \qquad (15)$$

where $s = 2q + |n - m| = 1, 2, \cdots$ is an integer, $J_0^{(s)}(y_n)$ is the sth derivative of the Bessel function $J_0(y_n)$. The numerical factor $H(|n - m|, s)$ has been calculated and tabulated in Table I. For the diagonal terms, $H(|n - m|, s)$ in the matrix D are found by using $(n - m) = 0$ in the table. Similarly, for the first off-diagonal terms, $(n - m = \pm 1)$ is used, and so on.

The dispersion relation for the plasma-filled BWO is expressed by the determinant equation $D = \det[D] = 0$. In the limit of infinitesimally small h, the dispersion relation given by (13) agrees with previous calculations [9], [10]. Beam and plasma effects are included in (13) through the terms x_n and y_n given by (7) and (8), which are the functions of ω_p and ω_h. For the case without plasma ($\omega_p = 0$), the calculated dispersion curves coincide with those previously calculated for the vacuum BWO's [12]-[15].

When no beam is present ($\omega_h = 0$), $\text{Im}(\omega)$ becomes zero for real values of k_z, as there can be no instability, and the numerical computation of (13) is simplified. In this case, $\text{Re}(\omega)$, at the intersection of the dispersion relation of the slow-wave structure and the beam space-charge wave (BSCW), is considered to be the eigenfrequency of the plasma-filled BWO.

As is well known. waves with frequencies less than the plasma frequency ω_p, can be propagated in a smooth-walled cylindrical plasma waveguide [16]. This wave is called the Trivelpiece–Gould mode. In the following numerical analyses of our dispersion relation, we confine ourselves to electromagnetic modes with angular frequencies greater than the plasma frequency ω_p.

III. NUMERICAL RESULTS

A. Dispersion Relation for Infinitesimal Beam Densities

First. we present numerical computations for the case of infinitesimally small beam densities ($\omega_b = 0$) where the oscillation frequency $\omega/2\pi$ is real for a real-valued wavenumber k_z. In this case, $y_n = x_n$ from (7) and (8), and hence, $K_n = -2/\pi\delta$ and $L_n = 0$ in (9). The terms including L_n are necessary to take into account when the beam density is high. The following parameters. corresponding to experimental conditions. were used in the computations: relativistic factor $\gamma = 2.23$ (i.e.. $v/c = 0.9$): average waveguide radius $R_0 = 1.445$ cm: and axial corrugation period $z_0 = 1.67$ cm. The corrugation amplitude was varied over a wide range. and included the experimental value. $h = 0.445$ cm. The plasma density N_p was treated as a variable.

In Fig. 2. the dispersion curves calculated using a $3 \times 3(-1 \le [m, n] \le 1)$, $5 \times 5(-2 \le [m, n] \le 2)$. and $9 \times 9(-4 \le [m, n] \le 4)$ determinant. as defined by (13), are plotted over a range of wave numbers. $k_z = 0$ to $k_z = 7.5248$ cm^{-1}. which corresponds to two full wavenumber periods of the slow-wave structure. The plasma density was $N_p = 2 \times 10^{11}$ cm^{-3} and the corrugation amplitude was $h = 0.445$ cm.

For each of the three cases (3×3, 5×5. and 9×9 matrices) shown. respectively. by dashed. dot-dashed. and solid lines, the terms with constant factors used in C^J_{mns} in (15) of the determinant equation are highlighted by the thick lines in Table I. The three lowest curves in Fig. 2 are labeled the "TM$_{01}$ mode" because they are related to their well-known lowest-order counterpart in the smooth-walled plasma-filled waveguide. On the other hand, the next higher frequency mode to the TM$_{01}$ mode is labeled the "A" mode which seems to be composed by displaced TM$_{01}$ modes in a smooth-walled waveguide. The third high-frequency mode is named the "B" mode in the present paper. Other high-frequency modes were not calculated for presentation in this paper.

The beam space-charge wave (BSCW) $v/c = 0.9$ is superimposed on the electromagnetic modes in Fig. 2 and is indicated by a straight line. The intersections of the BSCW with the TM$_{01}$, A and B electromagnetic modes are considered to be the eigenfrequencies of the plasma-loaded corrugated waveguide.

In the case of the 3×3 determinant equation. only the terms $-1 \le [m, n] \le 1$ were used in (13). In other words, three displaced periodic modes were superposed and the terms up to the order of $\alpha^2 = (h/R_0)^2$ were included. It should be noted that in the case of the 3×3
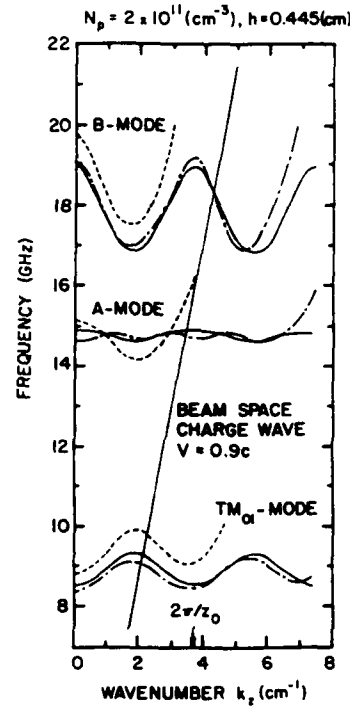

Fig. 2. Dispersion curves calculated using 3×3. 5×5. and 9×9 determinant equations shown. respectively. by dashed. dot-dashed. and solid lines for three electromagnetic modes. $N_p = 2 \times 10^{11}$ cm^{-3}. $h = 0.445$ cm. Straight line is the beam space charge wave for $v/c = 0.9$.

determinant. the required periodicity (from the application of the Floquet theorem) cannot be satisfied even for a single wavenumber period. $0 \le k_z \le 3.7624$ cm^{-1}. as shown in Fig. 2. This indicates that the previously derived dispersion relation [9]. [10] may not be used to accurately describe BWO's with large corrugation amplitudes ($\alpha \sim 1$). Even using a 5×5 determinant equation, the required periodicity in the dispersion curve is not obtained for the range of wavenumbers $0 \le k_z \le 7.5248$ cm^{-1}.

To get satisfactory periodicity in this wavenumber range, it has been found that a 9×9 determinant equation, including terms up to $(y_n\alpha)^{10}J_0^{(10)}(y_n)$ in (14), must be used. The rest of the numerical results described in this paper were calculated using such a 9×9 determinant.

The dispersion relation for extremely small corrugation (h) values is shown in Fig. 3 for the case . $N_p = 2 \times 10^{11}$ cm^{-3}. The dashed and the solid lines correspond to $h = 0.01$ and $h = 0.1$ cm, respectively. It can be seen that the TM$_{01}$ and A-modes are closely approximated by the superposition of the displaced TM$_{01}$ mode in a smooth-walled waveguide. whereas the B-mode consists of displaced TM$_{01}$ and TM$_{02}$ modes in a smooth-walled waveguide. The three modes are increasingly separated in frequency as h increases.

In Fig. 4. the dispersion relation of the three modes for a various plasma densities N_p, as well as the vacuum case, are shown for $h = 0.445$ cm, which corresponds to our experimental parameters [7]. [8]. The empty waveguide results (dotted line in Fig. 4) coincide with those in pre-
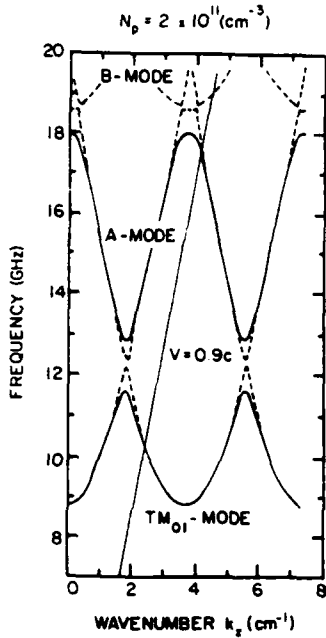
The eigenfrequencies of three modes versus plasma density are plotted in Fig. 5. The eigenfrequencies increase almost linearly with the plasma density. The dashed line is the background plasma frequency, and it is estimated to be approaching gradually to the eigenfrequency of the TM_{01} mode for high densities, when the resonant enhancement of the Raman scattering process was predicted [10].

Once the dispersion relation $D = 0$ is solved numerically (as in (13)), one can determine the relative magnitudes between the eigenvectors A_n, where $n = 0, \pm 1, \pm 2, \cdots$. In other words, the relative amplitudes, $|A_n/A_0|$, of the shifted periodic modes can be calculated for practical parameters. Since we have solved a 9×9 determinant equation to get the dispersion relation, inhomogeneous simultaneous equations of eight unknown variables A_n/A_0 with $n = \pm 1, \cdots, \pm 4$ can be solved numerically.

An example of a solved set of $|A_n/A_0|$'s is shown in Fig. 6 for the case of $N_p = 2 \times 10^{11}$ cm^{-3}. From Floquet's theorem, A_n must be a periodic function of the wavenumber $k_0 = 2\pi/z_0$. For $|n| \gg 1$, $|A_n/A_0|$ becomes quite small, as shown in the figure. A small value of A_n does not necessarily mean that the far shifted periodic modes are not important. This is because the y_n^2 terms in (8) get large negative values for $|n| \gg 1$, $\omega > \omega_p$ and $\omega/k_z < c$. Under this condition of imaginary arguments, the Bessel functions J_0 are replaced by the modified Bessel functions, I_0. This fact results in large value of $I_0(|y_n|)$ in (15) when we superpose electric fields of orthogonal modes at the boundary of the slow wave structure. In other words, $D_{mn}A_n$ decrease very slowly as $|n|$ increases, because $|y_n\alpha|$ is not smaller than unity.

For example, given $k_z = 4.01$ cm^{-1} and $N_p = 2 \times 10^{11}$ cm^{-3}, one obtains:

$$(D_{-4,-4})(A_{-4}) = (1.5 \times 10^6) \times (8.0 \times 10^{-5}) = 120$$

$$(D_{0,0})(A_0) = (27) \times (1.00) = 27$$

$$(D_{4,4})(A_4) = (5.7 \times 10^{11}) \times (1.3 \times 10^{-10}) = 75$$

$$(D_{-4,4})(A_4) = (-3.2 \times 10^9) \times (1.3 \times 10^{-10})$$
$$= -0.42$$

$$(D_{4,-4})(A_{-4}) = (-2.7 \times 10^3) \times (8.0 \times 10^{-5})$$
$$= -0.21.$$

This means that the relative magnitude of the off-diagonal terms of $D_{mn}A_n$ are not negligibly small in comparison to the major diagonal terms. The right-hand side of $D = 0$ is of the order of 10^{-2} in practical computations. In conclusion, we must superpose many displaced modes to satisfy the boundary condition (10) when $\alpha \sim 1$.

B. Dispersion Relation for a Solid Beam with Finite Density

So far, the numerical calculations were made under the assumption that $N_b = 0$ and the growth rate $\text{Im}(\omega) = 0$.

Fig. 3. Dispersion curves for $N_b = 2 \times 10^{11}$ cm^{-3}, $N_b = 0$ for cases of $h = 0.01$ cm (dashed line), and $h = 0.1$ cm (solid line).
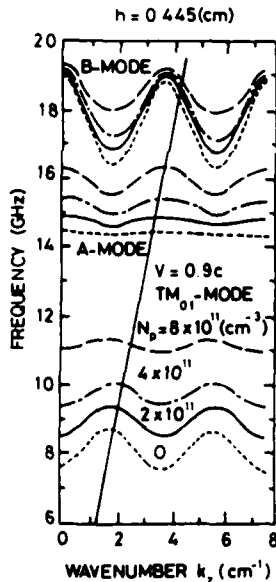

Fig. 4. Dispersion curves for three modes for various plasma densities N_p. In all cases, $N_b = 0$ and $h = 0.445$ cm.

vious calculations [12], [15]. It is clear from the figure that the plasma presence in the waveguide shifts the dispersion curve of the TM_{01} mode up in frequency also tends to "flatten" it; i.e., reduces the overall group velocity of the curve.

For the A-mode, the dispersion curve is very flat originally ($N_p = 0$) and tends to change with frequency as N_p increases. In the same figure, the beam space-charge line corresponding to $v/c = 0.9$ is shown. The intersections of this beam line with the electromagnetic modes are the expected eigenfrequencies of the plasma BWO interaction for infinitesimal electron beam densities.

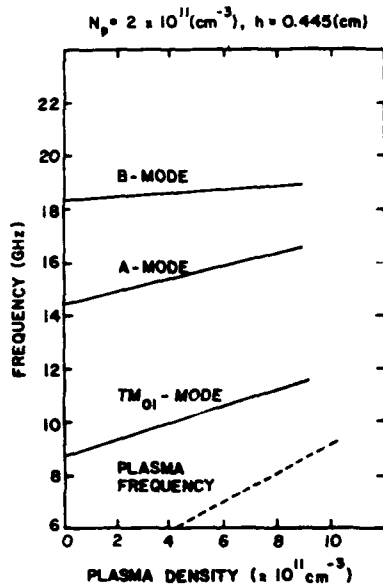$N_p = 2 \times 10^{11}(cm^{-3})$, $h = 0.445(cm)$

Fig. 5. Eigenfrequencies for three modes versus plasma density for beam $v/c = 0.9$.

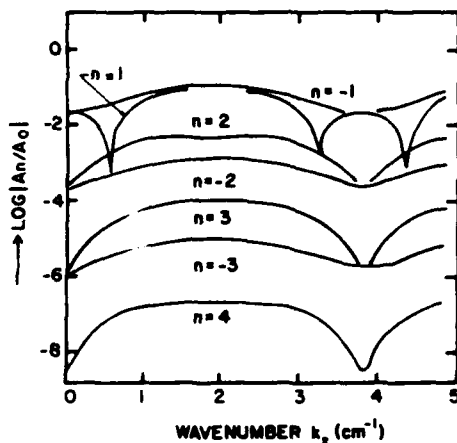
Fig. 6. Relative magnitudes of orthogonal modes. $|A_n/A_0|$ versus wavenumber k, for $N_p = 2 \times 10^{11}$ cm^{-3}.

To obtain the growth rates in the presence of the beam, nonzero values of ω_b must be included—we are now looking for complex roots of ω for real values of the wavenumber, k_z, assuming practical values of the beam density N_b. In the following calculations, a solid beam with the radius $R_b = 0.9$ cm and a density of $N_b = 5.15 \times 10^{10}$ cm^{-3} was assumed.

The calculation was performed as follows: we plot a mapping of absolute values $|D|$ of the 9 × 9 determinant D, on the complex plane for given parameters. Because

$$D(\omega, k_z) \cong D(\omega_0, k_z) + (\omega - \omega_0)\frac{dD}{d\omega} = K \quad (16)$$

and $D(\omega_0, k_z) = 0$, the solution can be found at the center of the contour circle lines of $|D|$. This is because (16) is an equation of circles with radius $|K|$ in the complex ω plane.

An example of the contour mapping is shown in Fig. 7. where $N_p = 2 \times 10^{11}$ cm^{-3}, $N_b = 5.15 \times 10^{10}$ cm^{-3}, $v/c = 0.9$, and $k_z = 2.0$ cm^{-1} have been assumed. In this figure, the horizontal and vertical axes are Re$(\omega)/2\pi$ and Im$(\omega)/2\pi$, respectively. Three real roots and a pair of complex conjugate roots are observed at the centers of circles. The heart-shaped white part near in the middle of the figure is where the values of the determinant are extremely large (for example, on the order of 10^{40}). The dispersion relation for complex ω versus real k_z for $N_p = 2 \times 10^{11}$ cm^{-3}, $N_b = 5.15 \times 10^{10}$ and $v/c = 0.9$ is shown in Fig. 8. The thick solid lines are the real part of the complex frequency $\omega/2\pi$, and the thin solid lines are for the real root. The result is not very different from those in [13] and [14] for vacuum BWO's, except that the growth rates are a function of plasma density in this case. The two thin lines close to $v/c = 0.9$ are the slow (SBSCW) and fast (FBSCW) beam space-charge waves, as was shown in [14].

The dispersion relation for relatively large plasma density, $N_p = 2 \times 10^{12}$ cm^{-3}, and $N_b = 5.15 \times 10^{10}$ cm^{-3} is shown in Fig. 9. Interactions between BSCW and the A or B modes are depicted in detail. There are again the SBSCW and the FBSCW near the $v/c = 0.9$ line. The peak growth rate Im$(\omega)_{max}$ can be found near the point where the complex conjugate roots and two real roots merge.

The imaginary part Im$(\omega)/2\pi$ versus k_z is plotted for various conditions in Fig. 10. The solid, chained, and dashed lines correspond to the intersections of the BSCW with the TM$_{01}$, A, and B modes respectively. The cases I, II, and III are for $N_p = 2 \times 10^{11}$, 2×10^{12}, and 3.2×10^{12} cm^{-3}, respectively. For relatively small values of N_p of the case I, the dominant mode of oscillation is the TM$_{01}$ mode, whereas for large values of N_p, i.e., cases II and III, the growth rates for B-mode approach to those for TM$_{01}$ mode, resulting in a possibility of higher frequency mode to oscillate.

In Fig. 11 the peak growth rate, Im$(\omega)_{max}/2\pi$ is plotted versus the plasma density N_p in the slow wave structure. The growth rates do not change appreciably up to densities of $N_p = 6 \times 10^{10}$ cm^{-3}. In such cases, the maximum growth rate for the TM$_{01}$ mode is considerably greater than those of the A and B modes. Around $N_p = 10^{12}$ cm^{-3}, the peak growth rate for the B mode approaches those for the TM$_{01}$ mode. In other words, other high-frequency oscillations may arise when N_p is high, in addition to TM$_{01}$ mode with an increased oscillation frequency. This is the main result obtained in the present linear analysis.

IV. Discussion and Conclusion

We have numerically analyzed the linear dispersion relation of a plasma-loaded corrugated-wall slow wave structure immersed in an infinitely large axial magnetic field. It is found that the terms including L_n in (13) affect only Im(ω); Re(ω) is unchanged even if the L_n term is neglected.
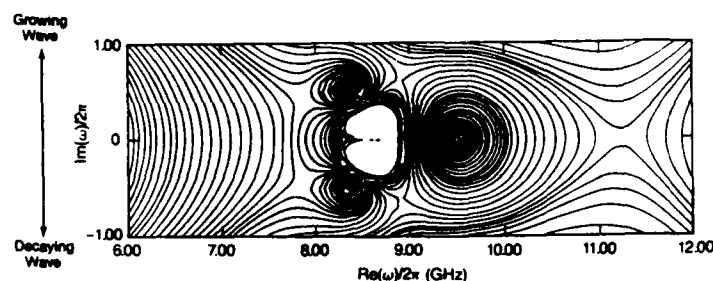
Fig. 7. Contour map of absolute value of 9×9 determinant $|D|$ on complex $\omega/2\pi$ plane for $N_p = 2 \times 10^{11}$ cm^{-1}. $N_b = 5.15 \times 10^{10}$ cm^{-1}. $h = 0.445$ cm. $z_0 = 1.67$ cm, and $k_z = 2.0$ cm^{-1}. Three real roots and pair of complex conjugate roots are shown.
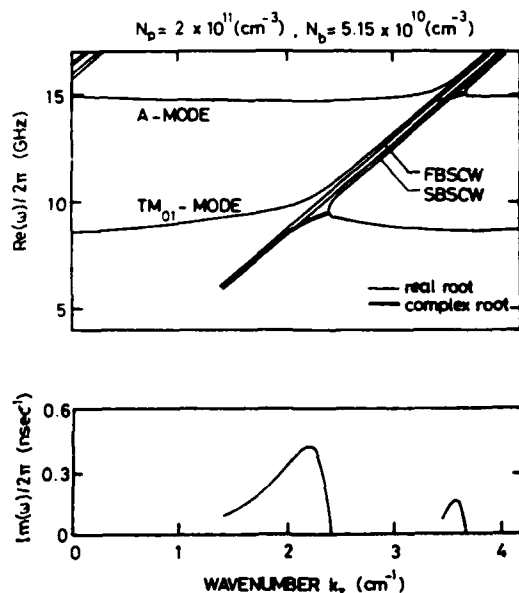

Fig. 8. Dispersion curves and linear growth rates for $N_p = 2 \times 10^{11}$ cm^{-1}. $N_b = 5.15 \times 10^{10}$ cm^{-3}.
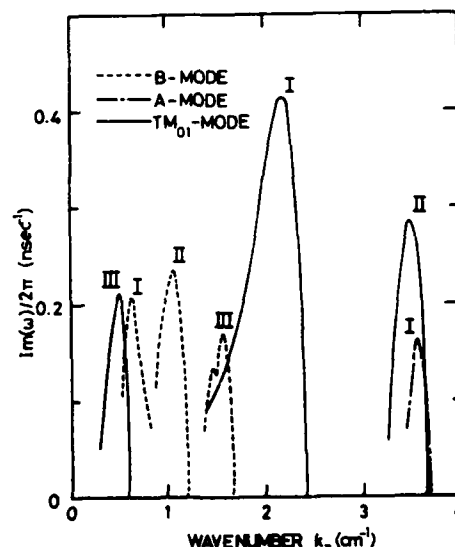
Fig. 10. Growth rate. $\text{Im}(\omega)/2\pi$, versus wavenumber k_z. Case I: $N_p = 2 \times 10^{11}$ cm^{-1}: Case II: $N_p = 2 \times 10^{12}$ cm^{-1}: Case III: $N_p = 3.2 \times 10^{12}$ cm^{-1}. In all cases, $N_b = 5.15 \times 10^{10}$ cm^{-1}.
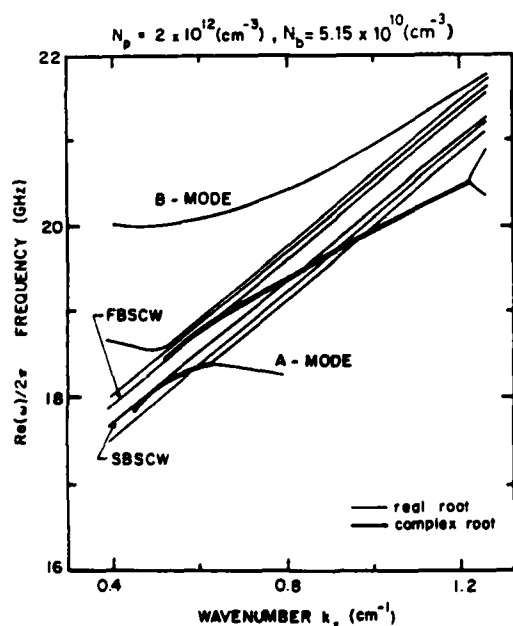
Fig. 9. Dispersion curves for $N_p = 2 \times 10^{12}$ cm^{-1}. $N_b = 5.15 \times 10^{10}$ cm^{-1}. Only real parts are shown in detail.
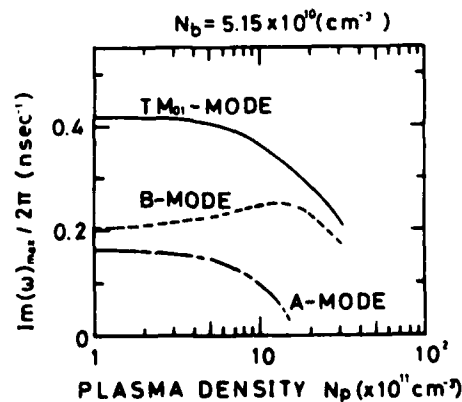
Fig. 11. Peak growth rates $\text{Im}(\omega)_{max}/2\pi$ versus plasma density.

It was found that for deep corrugation ($\alpha = 0.308$), corresponding to our practical BWO devices, nine displaced periodic modes must be superposed, and that terms up to the order of $(y_n\alpha)^{10}$ in (14) must be calculated to have numerical results within an accuracy of 1%.

According to the linear theory, the primary effect of the presence of plasma in the slow wave structure is an in-

crease in the oscillation frequency of the TM_{01} mode. The second effect is an appearance of higher modes. For plasma densities greater than 10^{12} cm^{-3}, an oscillation of B mode can be predicted, as shown in Fig. 11. A mode-switching observed in our experiment [8] may be related to the result of the present linear theory.

The enhancements of the oscillation observed in our experiments may be beyond the scope of the linear theory derived in this paper. The experimental observations indicate a strong enhancement at the TM_{01} interaction. It is possible that a nonlinear process is responsible for the observed enhancement. Further analyses to understand the observed enhancement are under way.

ACKNOWLEDGMENT

The authors are indebted to Drs. T. M. Antonsen, Jr. and B. Levush of the University of Maryland and to Dr. J. A. Swegle of the Lawrence Livermore National Laboratory for their invaluable advice and discussion.

REFERENCES

[1] J. R. Pierce, *Traveling Wave Tubes*. New York: Van Nostrand, 1950.
[2] V. L. Granatstein and I. Alexeff, *High-Power Microwave Sources*. Boston: Artech, 1987.
[3] N. F. Kovalev et al., "Generation of powerful electromagnetic radiation pulses by a beam of relativistic electrons," *Pis'ma Zh. Eksp. Teor. Fiz.*, vol. 18, no. 4, pp. 232-235, Aug. 1973.
[4] Y. Carmel et al., "Intense coherent Cherenkov radiation due to the interaction of a relativistic electron beam with a slow-wave structure," *Phys. Rev. Lett.*, vol. 33, no. 21, pp. 1278-1282, Nov. 1974.
[5] S. P. Bugaev et al., "Atmospheric microwave discharge and study of the coherence of radiation from a multiwave Cerenkov generator," *Sov. Phys.—Dokl.*, vol. 32, no. 1, pp. 78-79, Jan. 1988.
[6] M. V. Kuzelev et al., "Relativistic high current plasma microwave electronics: Advantages, progress and outlook," *Sov. J. Plasma Phys.*, vol. 13, no. 11, pp. 793-800, 1987.
[7] K. Minami et al., "Observation of resonant enhancement of microwave radiation from a gas-filled backward wave oscillator," *Appl. Phys. Lett.*, vol. 53, no. 7, pp. 559-561, Aug. 1989.
[8] Y. Carmel et al., "Demonstration of efficiency enhancement in a high-power backward-wave oscillator by plasma injection," *Phys. Rev. Lett.*, vol. 62, no. 20, pp. 2389-2392, May 1989.
[9] L. S. Bogdankevich et al., "Theory of excitation of plasma-filled rippled-boundary resonators by relativistic electron beams," *Sov. Phys.—Tech. Phys.*, vol. 25, no. 2, pp. 143-147, Feb. 1980.
[10] V. I. Kurilko et al., "Effect of a plasma on the amplification of regular waves by a relativistic beam in a corrugated waveguide," *Sov. Phys.—Tech. Phys.*, vol. 26, no. 7, pp. 812-815, July 1981.
[11] C. C. Johnson, *Field and Wave Electrodynamics*. New York: Mc-Graw-Hill, 1965.
[12] A. Bromborsky and B. Ruth, "Calculation of TM_{0n} dispersion relations in a corrugated cylindrical waveguide," *IEEE Trans. Microwave Theory Tech.*, vol. MTT-32, pp. 600-605, June 1984.
[13] J. A. Swegle et al., "Backward wave oscillators with rippled wall resonators: Analytic theory and numerical simulation," *Phys. Fluids*, vol. 28, no. 9, pp. 2882-2894, Sept. 1985.
[14] J. A. Swegle, "Approximate treatment near resonance of backward and traveling wave tubes in the Compton regime," *Phys. Fluids*, vol. 28, no. 12, pp. 3696-3702, Dec. 1985.
[15] R. A. Kehs et al., "A high power backward-wave oscillator driven by a relativistic electron beam," *IEEE Trans. Plasma Sci.*, vol. PS-13, pp. 559-562, Dec. 1985.
[16] A. W. Trivelpiece and R. W. Gould, "Space charge waves in cylindrical plasma columns," *J. Appl. Phys.*, vol. 30, no. 11, pp. 1784-1793, Nov. 1959.

K. Minami was born in Japan in 1938. He received the B. S. (EE) degree at Nagoya Institute of Technology in 1962, the M. S. (EE) degree at the Tokyo Institute of Technology in 1964, and the Ph.D. (EE) degree at Nagoya University in 1969.

Since 1986 he has been a Professor in the Electrical Engineering Department of Niigata University (Japan). His research interests include the generation of high-power microwave radiation, interaction between powerful microwaves and plasmas, and RF characteristics of high critical temperature superconductors.

*

Yuval Carmel (S'66-M'74) was born in Israel in 1942. He received the B.Sc.(EE) and M.Sc.(EE) degrees from the Technion, Israel Institute of Technology, in 1966 and 1971, respectively, and the Ph.D.(EE) degree from Cornell University, Ithaca, NY, in 1974.

He was with the Government of Israel, the Naval Research Laboratory, and is currently with the University of Maryland, College Park. His research interests include electromagnetic radiation from intense electron beams, free electron lasers, advanced concepts in millimeter-wave tubes, gyrotrons, and backward wave oscillators.

*

Victor L. Granatstein (S'59-M'64-SM'86) received the Ph.D. degree in 1963 from Columbia University, New York, in electrical engineering and plasma physics.

After a year of postdoctoral work at Columbia University, he was a member of the Technical Staff of Bell Telephone Laboratories from 1964-1972. During 1969-1970 he was a Visiting Senior Lecturer at the Hebrew University of Jerusalem. In 1972 he joined the Naval Research Laboratory as a Research Physicist and from 1978-1983 served as Head of the High-Power Electromagnetic Radiation Branch. In August 1983 he became a Professor in the Electrical Engineering Department at the University of Maryland, College Park, and also serves as a Consultant to the Naval Research Laboratory, the Science Applications International Corporation, the Jet Propulsion Laboratory, and the State of Maryland (Department of Natural Resources). He is presently leading experimental and theoretical studies of electromagnetic radiation from relativistic electron beams, advanced concepts in millimeter-wave tubes, free electron lasers, and gyrotron amplifiers. He is Associate Editor of the *International Journal of Electronics* and has been a Guest Editor of the IEEE TRANSACTIONS ON MICROWAVE THEORY AND TECHNIQUES and the IEEE JOURNAL OF QUANTUM ELECTRONICS. He has been a reviewer for the NSF, AFOSR, DOE DNA, ONR, and ARO. He has co-authored more than 100 research papers in regular journals, and holds a number of patents on active and passive microwave devices. Since 1988 he has been Director of the Laboratory for Plasma Research at the University of Maryland.

Professor Granatstein is a Fellow of the American Physical Society.

*

William W. Destler (M'84), photograph and biography not available at the time of publication.

Weiran Lou was born in Hangzhou, China, on July 2, 1963. He received the B.S. (electrical engineering, 1983) and M.S. (optical engineering, 1986) degrees from Zhejiang University, Hangzhou, China. He is currently a Ph.D. degree candidate in the Electrical Engineering Department, University of Maryland, College Park. His research interests include high-power microwave generations and microwave-plasma interaction.

*

D. K. Abe, photograph and biography not available at the time of publication.

*

R. Alan Kehs (S'68-M'75-SM'88) received the B.S. and M.S. degrees in electrical engineering, and the M.S. and Ph.D. degrees in physics from the University of Maryland, College Park, in 1970, 1973, 1984, and 1987, respectively.
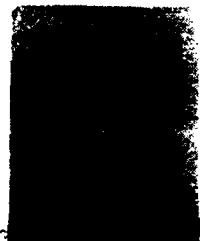
He has been employed by the Harry Diamond Laboratories, Adelphi, MD, since 1975, where his research interests have centered on the generation and use of intense relativistic electron beams—with emphasis on the production of high-power microwave radiation.

Dr. Kehs is a member of Eta Kappa Nu, Sigma Xi, and the American Physical Society.

*

M. M. Ali was born in Bangladesh in 1957. He received the B.Sc. Eng. degree in electrical and electronic engineering from Rajshahi University, Bangladesh, in 1982, and the M.S. (EE) degree from Niigata University (Japan) in 1989. He is presently a Ph.D. degree candidate at the Graduate School of Science and Technology, Niigata University. His research interests include high-power microwave generators, and the application of triggered vacuum gap switches to the generation of chopped wave impulse voltage.

T. Hosokawa was born in Japan in 1966. He received the B.S. (EE) degree from Niigata University in 1989, where he is presently an M.S. degree candidate. His research interests include the generation of high-power microwave radiation and the interaction between powerful microwaves and plasmas.

*

K. Ogura was born in Japan in 1957. He received the B.Sc. degree in physics from Okayama University in 1981, and the M.Sc. and D.Sc. degrees in physics from Kyoto University in 1983 and 1989, respectively.

He is presently on the research staff at the Graduate School of Science and Technology of Niigata University. His research interests include high-power microwave oscillators and their applications to the current drive on tokamak devices.

*

T. Watanabe was born in Japan in 1941. He received the B.S. degree in physics from the Tokyo Institute of Technology in 1964, and the M.S. and Ph.D. degrees from Nagoya University in 1966 and 1969, respectively.

He is currently with the National Institute for Fusion Science, Nagoya. His research interests include nonlinear plasma dynamics, and a generalized scheme to solve numerically a variety of systems of nonlinear equations.

Novel method for determining the electromagnetic dispersion relation of periodic slow wave structures

Y. Carmel, H. Guo, W. R. Lou, D. Abe, V. L. Granatstein, and W. W. Destler

Laboratory for Plasma Research, University of Maryland, College Park, Maryland 20742

A novel method for calculating the dispersion relation of electromagnetic modes in an arbitrary periodic slow wave structure is reported. In this method it is sufficient to know the frequencies corresponding to three special wave number values, with other points calculated using an approximate analytical expression. This technique was successfully applied to determine the dispersion relation of the TM_{01} mode in a sinusoidally corrugated slow wave structure. This structure is commonly used in relativistic high-power backward wave oscillators and traveling-wave tubes, and is expected to have many additional applications.

When an electron beam is injected into a periodic slow wave structure, the beam structure resonance often leads to either an absolute or a convective instability. The beam space-charge waves couple to the slow wave structure normal modes to produce microwave and millimeter wave radiation. The group and phase velocity of the slow wave structure modes, as well as the electron beam characteristics, determine the nature and frequency of the beam-wave interaction.

There are many families of microwave and millimeter wave generating devices whose operation depends on this type of interaction. As an example, Fig. 1 shows schematically the regions of operation of some of these devices in the frequency-wave number domain, as well as some typical slow wave structures. Relativistic traveling-wave tubes[1] (RTWTs) operate below the point where the wave number (normalized to the structure period) is equal to π radians. In this case, both the phase and the group velocities are positive. At $\beta L = \pi$, the upper cutoff frequency, the electromagnetic wave undergoes a phase shift of π radians per period of the slow wave structure. At this point, the phase velocity is positive and the group velocity is zero. Backward wave oscillators (BWOs) as well as carcinotrons operate in the region $\pi < \beta L < 2\pi$, where the phase velocity (ω/β) is positive and the group velocity $(\partial\omega/\partial\beta)$ is negative (ω is the angular frequency and β is the wave number). Extended interaction oscillators (EIO) operate very close to the $\beta L = 2\pi$ point.

Relativistic backward wave oscillators[2] and related devices which typically operate close to the $\beta L = \pi$ point, prove to be efficient and powerful microwave and millimeter wave sources with reported record power levels reaching 15 GW at wavelength of 3 cm[3] and 5 GW at 3 mm,[4] with efficiencies of up to 50%. In these devices, a smoothly corrugated waveguide has been found to be advantageous over alternative periodic structures due to its high-power handling capabilities. Many other devices (to be discussed later) also employ corrugated waveguide slow wave structures operating in both TM and TE modes. It is important, therefore, to know the dispersion relation of such slow wave structures in order to synchronize the phase velocity of the wave with the electron beam to produce efficient

interaction. In this letter we present a novel, accurate, and simple method for calculating the dispersion curve of an infinitely long slow wave structure of arbitrary geometry. This method was successfully applied to determine the dispersion curve of the TM_{01} mode in a sinusoidally corrugated waveguide. The results are then compared with those achieved by using other techniques.

Any periodic slow wave structure with n periods, when shorted at both ends, will exhibit $(n + 1)$ resonant frequencies with a phase shift per period equally spaced between 0 and π. Outside of the region $0 < \beta L < \pi$, the dispersion relation is periodic in β space (Floquet's theorem). This dispersion relation can be either be calculated using computational methods or measured experimentally (cold test).
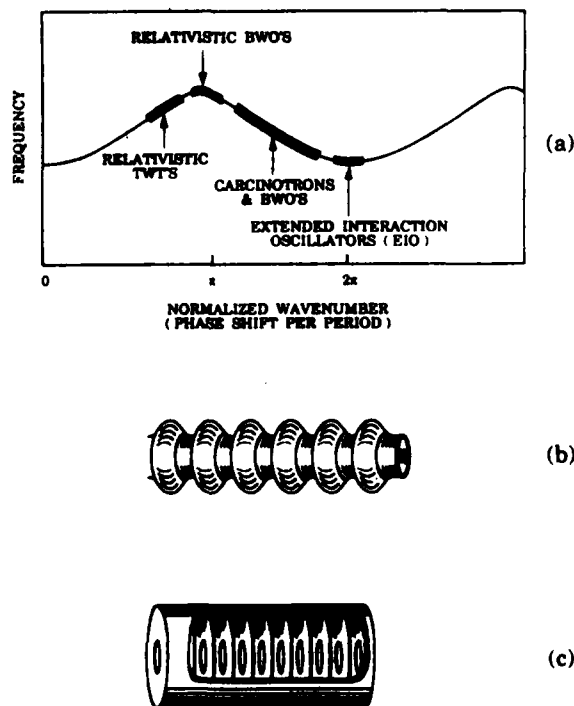

FIG. 1. (a) Regions of operation in the frequency-wavelength domain of various microwave and millimeter wave generators; (b) schematic diagram of a sinusoidally corrugated waveguide; (c) iris loaded waveguide.

TABLE I. Resonance frequencies (GHz) of a sinusoidally corrugated waveguide cavity ($R_0 = 1.5$ cm, $L = 1.67$ cm, $h = 0.273$ cm).

Resonance frequency (GHz)	2-period cavity	4-period cavity
$f_0 = f(\beta L = 0)$	7.404	7.412
$f(\beta L = \pi/4)$	N/A	7.589
$f_{\pi/2} = f(\beta L = \pi/2)$	8.046	8.046
$f(\beta L = 3\pi/4)$	N/A	8.557
$f_\pi = f(\beta L = \pi)$	8.773	8.754

Instead of using a large number of periods to accurately calculate the dispersion relation, we will show that it is sufficient to calculate the short circuit cavity resonant frequencies corresponding to three special normalized wave number values, $\beta L = 0$, $\pi/2$, and π radians by rigorously solving the boundary value problem. With these three frequencies, one can use an analytical expression to produce the complete dispersion curve. Furthermore, we can also analytically calculate the phase and group velocities at any point along the dispersion relation. We have used a two-dimensional electromagnetic code[5] ("Superfish") for the calculation of these three special frequencies for a sinusoidally corrugated waveguide, oriented in the z direction whose radius is described by

$$R = R_0[1 + h\cos(2\pi z/L)],\qquad (1)$$

where R_0 is the average radius, h is the normalized corrugation amplitude, and L is the structure period.

For high-power relativistic BWOs, the main mode of interest is the cylindrically symmetric TM_{01} mode. In our test case, the waveguide average radius was $R_0 = 1.50$ cm, the ripple period was $L = 1.67$ cm, and the normalized corrugation amplitude was $h = 0.273$ cm. Superfish modeling yielded (with proper boundary conditions) the three special resonance frequencies in the lower passband. The results are tabulated in the second column of Table I (two period cavity). The corresponding mode patterns (electric field lines) are shown in Figs. 2(a), 2(b), and 2(c), which pertain to phase shifts per period of 0, $\pi/2$, and π, respectively.

Next, the expression used to calculate the complete dispersion relation is discussed. By using the impedance or $ABCD$ matrix of a four-terminal network, together with Floquet's theorem[6] to describe a periodic slow wave structure, the dispersion relation can be expressed in the nonexplicit form

$$f = f(\cos\beta L, G)\qquad\cdot\qquad (2)$$

where f is the frequency of the electromagnetic radiation and G is a geometric factor related to a specific slow wave structure dimension. Let $A = f_{\pi/2}$, $B = (f_\pi - f_0)/2$, $C = f_{\pi/2} - (f_\pi + f_0)/2$. It can be shown that the dispersion relation of any general periodic structure can be expressed in the following explicit, approximate form:
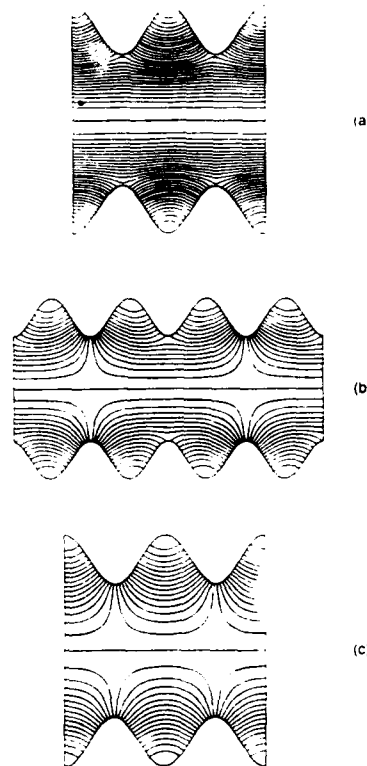
$$f = A - B\cos\beta L - C\cos^2\beta L.\qquad (3)$$

FIG. 2. (a) Mode patterns (electric field lines) corresponding to zero phase shift, (b) $\pi/2$ phase shift, and (c) π phase shift in the TM_{01} lower pass band of a sinusoidally corrugated waveguide.

The three terms in Eq. (3) are sufficient to ensure excellent accuracy for most practical cases, as will be shown later. Notice that the geometrical factor G (as yet unspecified) does not appear in the equation. Rather, it enters indirectly through A, B, C, which are geometry-dependent parameters with simple physical meaning. The first term, A, represents the value of the frequency near the midband. The second is an increment term whose maximum value equals half the difference between the upper and lower cutoff frequencies of the passband. The third term is a correction term. The combination of all three terms exactly satisfied the dispersion relation at the three special wave numbers (0, $\pi/2$, and π) and is an excellent approximation at all other wave numbers, as will be shown later.

Equation (3) enables one to directly calculate the phase and group velocities at any point along the dispersion region. The expressions derived for the velocities are given in Eqs. (4) and (5):

$$v_{\text{phase}} = \frac{[2L\pi f_{\pi/2}(1 + \Delta f/f_{\pi/2})]}{\cos^{-1}([(B^2 - 4C\Delta f)^{1/2} - B]/2C)},\qquad (4)$$

$$v_{\text{group}} = \partial\omega/\partial\beta = 2\pi L(B\sin\beta L + 2C\cos\beta L\sin\beta L),\qquad (5)$$

where $\Delta f = f - f_{\pi/2}$.

The results of our test case are plotted in Fig. 3. It shows the TM_{01} dispersion curve in the lower passband for the sinusoidally corrugated waveguide Fig. 3(a), as well as that of an iris loaded waveguide having the same minimum and maximum radial dimensions. The two are similar with
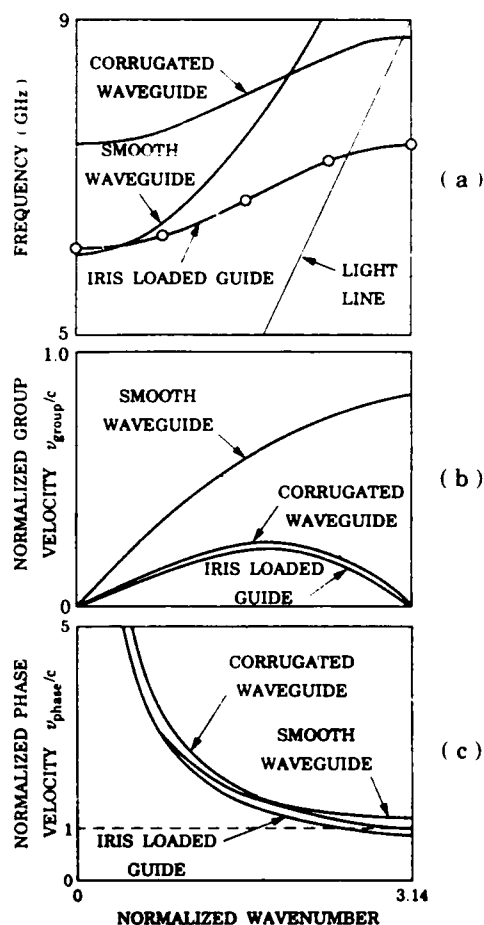
FIG. 3. (a) TM_{01} dispersion curve for a sinusoidally corrugated, iris loaded, and smooth waveguide, (b) normalized group velocities, (c) phase velocities.

FIG. 4. Comparison of the TM_{01} dispersion curve of Ref. 7 (solid line) and this work (dotted line) for a sinusoidally corrugated waveguide.

the iris loaded guide dispersion curve always lower in frequency compared to the corrugated guide. This is expected since the volume of the first is larger than that of the second, driving all the resonant frequencies down. The open circles at $\beta L = 0$, $\pi/2$, and π were calculated by using Superfish and were used in Eq. (3) to calculate the complete dispersion relation. For comparison, the dispersion relation of a smooth waveguide is also given. Figures 3(b) and 3(c) display the phase and group velocities (normalized to the speed of light) for the same cases [Eqs. (4) and (5)].

In order to estimate the accuracy of this technique as applied to the sinusoidally corrugated guide, we first calculate additional resonance points on the dispersion curve, using "Superfish". Four periods of the corrugated guide cavity were modeled, yielding five resonances in the wave number range of 0 to π and the results are given in the third column of Table I (four-period cavity) and are plotted as additional open circles in Fig. 3(a) with very good agreement (eight periods were also successfully modeled). As an independent check, the dispersion relation derived here was compared to the dispersion relation derived elsewhere[7,8] for the same corrugated guide geometry by solving a system of coupled linear differential equations. Figure 4 shows a comparsion between the dispersion curve
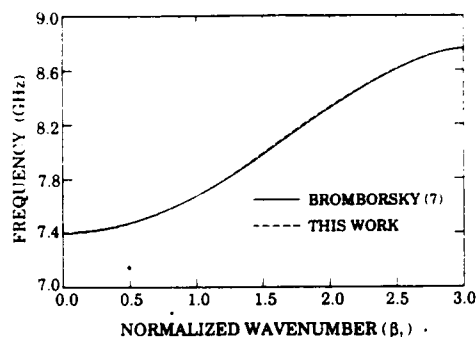
as calculated by these two techniques [Ref. 7 and Eq. (3)] for the same corrugated guide. The results are in excellent agreement (within 0.15%) over the entire wave number range $0 < \beta L < \pi$. Outside this range the dispersion relation is, of course, periodic.

It is expected that this technique will be beneficial for determining the dispersion curve of periodic structures of arbitrary shapes. The three special resonance frequencies which are needed in order to generate the complete, general dispersion curve can be calculated by rigorously solving the boundary problem or measured experimentally.

Corrugated slow wave structures may prove beneficial in prospective applications such as TE mode slow wave cyclotron amplifiers,[9] TM mode relativistic extended interaction oscillators and amplifiers,[10] TE mode CARMs,[11] electromagnetically pumped free-electron lasers,[12,13] and plasma-loaded backward wave oscillators.[14]

[1] J. A. Nation, D. Shiffler, J. D. Ivers, and G. Kerslick, Proc. Int'l. Soc. Opt. Eng. 1061, 17 (1989).
[2] Y. Carmel, J. Ivers, R. E. Kribel, and J. Nation, Phys. Rev. Lett. 33, 1278 (1974).
[3] S. P. Bugaev, V. A. Cherepenin, V. I. Kanavets, A. I. Klinov, A. D. Kopenkin, V. I. Koshelev, V. A. Popov, and A. I. Slepkov, IEEE Trans. Plasma Science 18, 525 (1990).
[4] S. P. Bugaev, V. I. Kanavets, A. I. Klimov, V. I. Koshelev, G. I. Mesyates, and V. A. Cherepenin, Proceedings of the 6th International Conference on High Power Electron Beams, (Laser Society of Japan, Osaka, 1986). p. 584.
[5] K. Halbach and R. Holsinger, Part. Accel. 1, 213 (1976).
[6] C. C. Johnson, Field and Wave Electromagnetics (McGraw-Hill, New York, 1965).
[7] A. Bomborsky and B. Ruth, IEEE Trans. Microwave Theory Tech. MTT-32, 600 (1984).
[8] J. A. Swegle, J. W. Poukey, and G. T. Leifeste, Phys. Fluids 28, 2882 (1985).
[9] H. Guo, L. Chen, H. Keren, J. L. Hirshfield, S. Y. Park, and K. R. Chu, Phys. Rev. Lett. 49, 730 (1982).
[10] A. Staprans, E. W. McCune, and J. A. Ruetz, Proc. IEEE 61, 299 (1973).
[11] D. B. McDermott, H. Cao, and N. C. Luhmann, Int'l. J. Electronics 65, 477 (1988).
[12] Y. Carmel, V. L. Granatstein, and A. Gover, Phys. Rev. Lett. 51, 566 (1983).
[13] R. A. Kehs, Y. Carmel, V. L. Granatstein, and W. W. Destler, Phys. Rev. Lett. 60, 279 (1988).
[14] Y. Carmel, K. Minami, R. A. Kehs, W. W. Destler, V. L. Granatstein, D. Abe, and W. R. Lou, Phys. Rev. Lett. 62, 2389 (1989).

Demonstration of Efficiency Enhancement in a High-Power Backward-Wave Oscillator by Plasma Injection

Y. Carmel, K. Minami,[a] R. A. Kehs,[b] W. W. Destler, V. L. Granatstein, D. Abe, and W. L. Lou

Laboratory for Plasma Research, University of Maryland, College Park, Maryland 20742

(Received 4 November 1988)

An experimental demonstration of a strong enhancement of the interaction efficiency in a high-power relativistic backward-wave oscillator when plasma is injected is presented. Controlled plasma injection enhances the interaction efficiency over the vacuum case by a factor of up to 8 to a value of about 40%. The enhanced interaction is attributed to induced scattering of the electromagnetic radiation of electrons in an electrostatic field produced by the background plasma and a beam space-charge wave in the corrugated interaction region.

Many varieties of high-power microwave (HPM) devices have been studied in recent years, including the well-known magnetron and klystron as well as newer devices such as the gyrotron, free-electron laser, and virtual cathode oscillator.[1] All of these sources have one thing in common—they are driven by an intense, monoenergetic, unneutralized electron beam which unstably interacts in high vacuum with an electromagnetic wave, leading to the conversion of the beam's kinetic energy into electromagnetic radiation. The power levels available from such devices have grown by an order of magnitude every decade since 1940, reaching about 10^{10} W at a wavelength of 3 cm and 10^8 W at 3 mm.[2]

This work demonstrates for the first time a strong efficiency enhancement in a relativistic backward-wave oscillator (BWO) by external plasma injection. Plasma effects in conventional microwave devices can usually be neglected since the plasma frequency of the background gas is much smaller than the plasma frequency of the electron beam $(\omega_p/\omega_{pb} < 10^{-2})$. Recent theoretical studies,[3] however, have predicted that the presence of a plasma in HPM devices may lead to greatly enhanced performance, attracting renewed scientific interest.[4] The presence of a background plasma can serve to increase the space-charge limiting current by a factor of $[1-f]^{-1}$, where $f = n_i/n_e$ represents any neutralization provided by the ions in the background plasma. The space-charge limiting current in the presence of the plasma for a thin hollow beam with a mean radius a and a thickness $\Delta \ll a$ is given by

$$I_l = \frac{17[\gamma_0^{2/3} - 1]^{3/2}}{[2\ln(b/a)][1-f]} \text{ kA}. \tag{1}$$

Here γ_0 is the relativistic mass factor for the beam electrons, and b is the radius of the drift tube. By increasing the beam current through introduction of a background plasma, a new limitation is encountered which is imposed by the onset of beam-plasma instability. This instability will occur at current levels which are larger than the vac-

uum limiting current by the factor[3]

$$\gamma[(1-\gamma^{-2})/(1-\gamma^{-2/3})]^{3/2}. \tag{2}$$

In the case of mildly relativistic electron beams having $\gamma = 3$, the actual current carried by the beam in the presence of plasma may be 7 times larger than the vacuum case. The increased injected current level simply allows operation at higher beam power and associated higher microwave power output without affecting the interaction efficiency or the physical interaction mechanism.

The plasma presence in the device can, however, also completely alter the nature of the interaction mechanism, leading to greatly enhanced device efficiency. The studies reported here are the first which clearly belong to this latter category.

Since BWO's[5] are simple devices, provide fairly effective conversion of electron beam energy into radiation, and can easily be filled with plasma, they are ideal candidates for the evaluation of plasma effects. Initial studies[6,7] utilized background plasmas produced by electron-beam-impact ionization of a low-pressure neutral-gas background, and demonstrated enhanced microwave output powers. Interpretation of the results, however, and identification of the physical mechanisms involved have proven difficult. In some of these earlier studies,[6] the increased output power was attributed to a substantial increase in injected beam current allowed by the increase in the space-charge limit allowed by the plasma. In another,[7] beam current was again increased over the vacuum BWO studies, and identification of the mechanism was complicated by the strong resonant dependence of microwave output on the externally applied magnetic field. In the work presented here, injected beam parameters were carefully held constant for both vacuum and plasma-filled BWO experiments. The resulting enhancement in BWO microwave output power when plasma is present is therefore clearly a result of an improvement in the electronic efficiency of the device. Thus this work unambiguously demonstrates efficiency
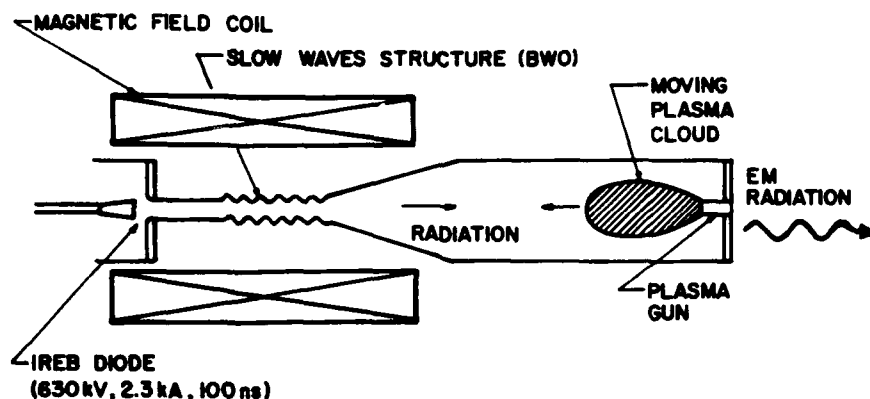
FIG. 1. Schematic diagram of a relativistic backward-wave oscillator with external plasma injection.

enhancement in a high-power microwave tube.

In the experiments, an independently controllable argon plasma source was used to externally inject plasma directly into the BWO structure as shown in Fig. 1. A hollow, relativistic electron beam (630 kV, 2.3 kA, 100 ns) of average radius 0.8 cm and electron density of about 5×10^{11} cm^{-3} was injected into a BWO corrugated-wall slow-wave structure immersed in a uniform axial magnetic field of about 12 kG. A coaxial plasma gun,[8] located about 100 cm downstream in a field-free region, generated an argon plasmoid which crossed magnetic field lines at an average velocity of about 1.2 cm/μs on its way towards the interaction region. The entire system was evacuated to pressure $<4 \times 10^{-5}$ Torr. The plasma column parameters were measured with 35- and 70-GHz microwave interferometers (for density) and Langmuir probes (for velocity, density, and temperature). Initial results indicate that the average plasma density could be varied continuously by changing the gun voltage and gas pressure from zero up to a maximum value estimated at $\sim 10^{13}$ cm^{-3}, which is well above the corresponding beam density $(5 \times 10^{11}$ cm$^{-3})$.

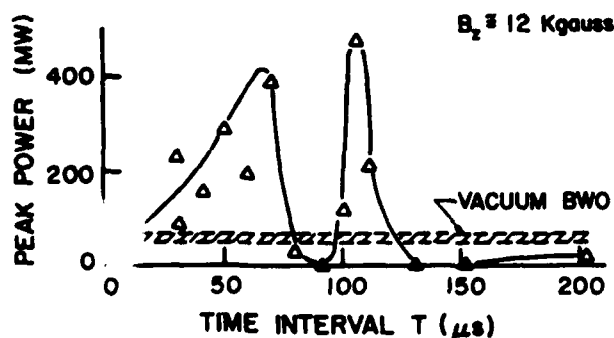Efficiency enhancement was observed over a wide range of injected plasma densities, $0 < n < n_{cr}$, where n_{cr}

is a critical plasma density. This critical plasma density, to be discussed later, occurred at $T \approx 90$ μs on the plasma pulse time scale. The efficiency enhancement factor over vacuum BWO operation was found to be density dependent, and reached a maximum value of 8 when the electron beam was injected into an optimized plasma density. This occurs twice on the plasma pulse time scale, once during density rise $(T \approx 60$ μs) and then again during density decay $(T \approx 100$ μs); see Fig. 2. At these points the interaction efficiency increased to almost 40% compared with about 5% for the vacuum BWO under the s operating conditions.

From c considerations it is possible to estimate the critical plasma density which will overdrive the device and quench the interaction. Figure 3 depicts the approximate dispersion relation of the lowest-order symmetric electromagnetic branches[9] (labeled TM$_{01}$ and TM$_{02}$) as well as the plasma branches (labeled plasma waves) which we shall refer to later. Note that the intersection point of the TM$_{01}$ mode and the electron-beam space-charge wave lies on a portion of the electromagnetic-wave dispersion relation having negative group velocity,

FIG. 2. Peak power output at 8.4 GHz vs the time interval between the plasma gun operation and the electron beam firing.
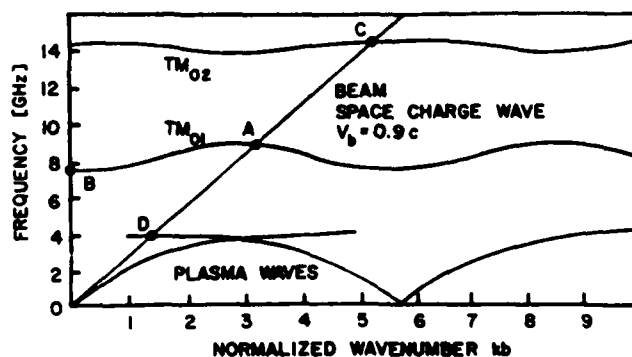

FIG. 3. The dispersion relation of plasma-filled corrugated waveguide including the electromagnetic and plasma branches, with superimposed ideal beam wave added. V_b is the beam velocity, c is the speed of light, and $b = 1.445$ cm is the average radius of the corrugated waveguide, with radius given by $r = b + 0.445 \sin(2\pi z / 1.67)$ cm.

which implies a backward-propagating wave. The backward-propagating wave is reflected by a waveguide beyond cutoff at the injection point and then detected downstream from the structure (Fig. 1). This intersection occurs close to the upper cutoff frequency of the TM_{01} passband at 8.4 GHz (point A in Fig. 3). To first order, the presence of a magnetized plasma in the slow-wave structure will raise its lower cutoff frequency above the vacuum value of 7.5 GHz (point B). If the device is overdriven to the point where the lower cutoff frequency in the presence of plasma is equal to or greater than the upper cutoff frequency in the absence of plasma, no backward-wave interaction is possible.

An approximate expression for the cutoff frequency (TM modes) of a waveguide filled with magnetized plasma is[10,11]

$$f_{\infty} = \frac{c}{2\pi}\left[\left(\frac{P_{nl}}{b}\right)^2 + \left(\frac{\omega_p}{c}\right)^2\right]^{1/2}. \tag{3}$$

In Eq. (3) ω_p is the background plasma frequency, c is the speed of light, P_{nl} are the roots of the Bessel functions corresponding to the mode of interest, and b is the waveguide radius. When solved for the critical background plasma density which would quench the interaction, using our experimental parameters, Eq. (3) yields

$$n_{cr} = 2\times10^{11}\text{ cm}^{-3}. \tag{4}$$

When the backward-wave oscillator was overdriven with plasma above the critical density, the fundamental TM_{01} mode at 8.4 GHz was quenched and strong, higher-frequency emission (12–18 GHz) was observed, possibly indicating mode switching from TM_{01} to TM_{02} (point C in Fig. 3).

The dramatic mode switching is shown in Fig. 4. It shows the amplitude (vertical scale) of different frequency (horizontal scale) components of the backward-wave oscillator using the dispersive line technique (different frequencies are resolved by their different propagation velocities in a dispersive waveguide). Figure 4(a) represents the spectrum emitted by the backward-wave oscillator under the condition of strong plasma enhancement, where the dominant frequency component is near 8.4 GHz. An undispersed, prompt microwave output signal is superimposed on the dispersed signal as a timing reference. Figure 4(b) represents the spectrum for an overdriven device, in which case mode switching occurred and frequency components in the range 10–18 GHz are present (TM_{02} or other high-order modes as well as plasma oscillation). At even larger plasma densities, microwave breakdown within the device will occur.

Strong microwave emission was also detected in the 18–26-GHz band, proportional in amplitude to the fundamental TM_{01} backward-wave oscillations. These high frequencies are believed to be produced by a free-electron laser interaction driven by an electromagnetic pump, as reported previously.[12,13]
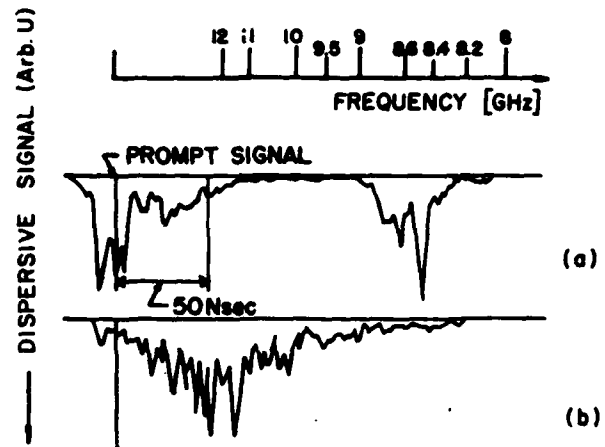

FIG. 4. Spectral results from plasma-enhanced backward-wave oscillator. (a) Maximum enhancement and (b) overdriven device.

As these experiments demonstrate, the controlled presence of a plasma in the corrugated structure strongly enhances the interaction efficiency over a very wide range of plasma densities. To understand the physical mechanism responsible for the enhanced interaction, Fig. 3 also depicts the approximate dispersion relation of a plasma-filled corrugated waveguide. It consists not only of the known slow electromagnetic branches, but the plasma branches as well (labeled plasma waves in Fig. 3). These low-frequency modes are purely plasma waves and vanish in the limit of small background plasma density ($\omega_p \to 0$). They are the corrugated-waveguide version of the Trivelpiece-Gould (TG) modes.[11] Normally, those plasma oscillations are trapped in the plasma and cannot be coupled out efficiently in the form of electromagnetic radiation. However, for the range of values of the plasma density and beam energy relevant to our work, the beam is simultaneously in synchronism (and therefore can exchange energy) with the backward branch of electromagnetic wave (point A) and the backward branch of the plasma wave (point D in Fig. 3). Under these conditions, all three waves involved have the same phase velocity, ω/k, and a strong component of axial electric field, E_z. Therefore, a strong enhancement is expected. It is believed that the greatly enhanced efficiency observed results from this mechanism, namely, induced scattering of the electromagnetic radiation of electrons in an electrostatic field produced by the background plasma in the presence of the corrugated wall.

The introduction of plasma into the device did not affect the diode voltage or current, and the beam current actually entering the slow-wave structure was unaffected by the plasma. No diode shorting due to the injected plasma was observed, and the performance of the plasma BWO with respect to variations in the applied axial magnetic field was similar to the vacuum BWO.[14] No sharp resonance (similar to the one in Ref. 7) is expected for

this mechanism, and none was observed.

An efficient interaction also implies a very broad gain curve with respect to the electron beam energy. This is expected for the present mechanism since the electrons tend to stay in synchronism with both backward branches (points A and D in Fig. 3) even as the beam is losing energy. Although the effect of the plasma on beam transport inside the slow-wave structure could not be directly measured, no evidence of significant beam current striking the structure walls was observed.

It is anticipated that plasma injection may also prove beneficial in other high-power microwave devices such as free-electron laser and gyrotrons, providing frequency tunability,[15] overcoming space-charge limitations,[16] and enhancing interaction efficiencies.[17]

The authors would like to acknowledge the helpful discussions with Dr. B. Levush, Dr. T. Antonsen, and Dr. J. Booske, and the technical assistance of J. Rodgers, D. Cohen, and J. Pyle. This work is supported in part by the Strategic Defense Initiative Organization through a contract administered by the Harry Diamond Laboratory.

[1]See, for example, special issues on high-power microwave sources [IEEE Trans. Plasma Sci. 13, No. 6 (1985); 16, No. 2 (1988)].

[2]V. L. Granatstein, Int. J. Electron. 57, 787 (1984); also S. P. Bugaev et al., Pis'ma Zh. Tekh. Fiz. 9, 26 (1983) [Sov. Tech. Phys. Lett. 9, 11 (1983)].

[3]See, for example, a review paper by M. V. Kuzelev et al., [Sov. J. Plasma Phys. Fiz. Plazmy 13, 1370 (1987) [Sov. J. Plasma Phys. 13, 793 (1987)].

[4]V. I. Kurilko et al., Zh. Tekh. Fiz. 51, 1415 (1981) [Sov. Phys. Tech. Phys. 26, 812 (1981)]; W. W. Destler et al., Proc. SPIE 873, 84 (1988).

[5]Y. Carmel et al., Phys. Rev. Lett. 33, 1278 (1974); N. Kovalev et al., Pis'ma Zh. Eksp. Teor. Fiz. 18, 232 (1983) [JETP Lett. 18, 138 (1973)].

[6]Yu V. Tkach et al., Fiz. Plazmy 1, 81 (1975) [Sov. J. Plasma Phys. 1, 43 (1975)]; Yu V. Tkach et al., Fiz. Plazmy 5, 1012 (1979) [Sov. J. Plasma Phys. 5, 566 (1979)].

[7]K. Minami et al., Appl. Phys. Lett. 53, 7 (1988).

[8]J. Marshall et al., in Proceedings of the Second International Conference on Plasma Physics Controlled Nuclear Fusion Research, Culham, England, 1965 (IAEA, Vienna, 1966), Vol. 2, p. 449.

[9]J. Swegle et al., Phys. Fluids 28, 2882 (1985); A. Bromborsky, IEEE Trans. Microwave Theory Tech. 3, 600 (1984).

[10]M. V. Kuzelev et al., Fiz. Plazmy 4, 433 (1978) [Sov. J. Plasma Phys. 4, 242 (1978)].

[11]A. W. Trivelpiece and R. W. Gould, J. Appl. Phys. 30, 1784 (1959).

[12]R. A. Kehs et al., Phys. Rev. Lett. 60, 279 (1988).

[13]Y. Carmel et al., Phys. Rev. Lett. 51, 566 (1983).

[14]R. A. Kehs et al., IEEE Trans. Plasma Sci. 13, 559 (1985).

[15]L. S. Bugdankevich et al., Usp. Fiz. Nauk 133, 3 (1981) [Sov. Phys. Usp. 24, 1 (1981)].

[16]W. M. Manheimer et al., Bull. Am. Phys. Soc. 33, 1956 (1988).

[17]See, for example, M. B. Reid et al., Int. J. Electronic. 65, 533 (1988); Pei Wen-Bing, Int. J. Electron. 65, 551 (1988).